FIELD-SCALE EVALUATION OF IN SITU COSOLVENT FLUSHING FOR ENHANCED AQUIFER REMEDIATION

By

RANDALL K. SILLAN

A DISSERTATION PRESENTED TO THE GRADUATE SCHOOL
OF THE UNIVERSITY OF FLORIDA IN PARTIAL FULFILLMENT
OF THE REQUIREMENTS FOR THE DEGREE OF
DOCTOR OF PHILOSOPHY

UNIVERSITY OF FLORIDA

1999

ACKNOWLEDGMENTS

My successful adventure through the perils and triumphs of academia and field research was made possible by many people whose numbers are too numerous to list. However, I would like to acknowledge those who were instrumental in helping me achieve my dream of being a Doctor. Suresh Rao, chairman of my graduate committee, was a great mentor who constantly challenged me academically and personally. His energy in the lab and in the field, even at four o'clock in the morning, was key to the successful completion of the work presented in this dissertation.

Mike Annable, cochairman of my committee, provided limitless support and guidance which started with our first class at UF in '92 and service on both of my graduate committees at UF. Mike was an excellent troubleshooter and valued companion during our time in the field.

For their support, assistance and encouragement, I would like to acknowledge the remaining members of my graduate committee, Kirk Hatfield, Wendy Graham, and Dean Rhue. I would also like to thank Kirk for all of the pep talks at the O&B, especially the one several years ago that helped me decide to go on this challenging journey.

Most importantly, I would like to thank my companion for life, Gloria. Always at my side, she too experienced many of the hardships and joys of this work. Finally, I would like to say to all of my family and friends, thanks for your love and support throughout my long stay at UF.

TABLE OF CONTENTS

ACKNOWLEDGMENTS ii

LIST OF TABLES vi

LIST OF FIGURES viii

ABSTRACT xiii

1 INTRODUCTION 1
1.1. Justification 1
1.2. Cosolvent Flushing 5
1.2.1. Theoretical Background 5
1.2.1.1. Residual NAPL mobilization 6
1.2.1.2. NAPL dissolution 8
1.2.1.3. Enhanced desorption 13
1.2.1.4. Dissolution nonequilibrium 14
1.2.2. Technology History 15
1.3. Partitioning Tracers 18
1.3.1. Theoretical Background 18
1.3.2. Technology History 20
1.4. Field Studies 21
1.4.1. Hill Air Force Base 21
1.4.1.1. Project overview 21
1.4.1.2. Site background 23
1.4.1.3. Instrumentation 24
1.4.1.4. Preliminary laboratory investigations: NAPL compositional analysis 26
1.4.1.5. Preliminary laboratory investigations: Partitioning tracer selection 26
1.4.1.6. Preliminary laboratory investigations: NAPL dissolution 28
1.4.1.7. Preliminary laboratory investigations: Cosolvent hydrodynamics 29
1.4.2. Former Sages Dry Cleaning Facility 33
1.4.2.1. Project overview 33
1.4.2.2. Site background 34
1.4.2.3. Instrumentation 35
1.5. Dissertation Research Objectives 36
1.6. Chapters Ahead 37

2 HILL AFB FIELD STUDY 38
2.1. Site Characterization 38
2.1.1. Soil Coring 38
2.1.2. Partitioning Tracer Test 39
2.1.2.1. Methods 39
2.1.2.2. Analysis of EW data 43
2.1.2.3. Analysis of MLS data 46
2.1.2.4. Summary 53
2.2. Cosolvent Flushing 53
2.2.1. Methods 53
2.2.2. Cosolvent Hydrodynamics 57
2.2.2.1. Analysis of MLS data 57
2.2.2.2. Analysis of EW data 65
2.2.2.3. Cosolvent Recovery 66
2.2.3. Dynamics of NAPL Constituent Removal 67
2.2.3.1. Analysis of EW data 68
2.2.3.2. Analysis of MLS data 70
2.2.3.3. Summary 81
2.3. Performance Evaluation 81
2.3.1. Post-Flushing Partitioning Tracer Test 82
2.3.1.1. Analysis of EW data 84
2.3.1.2. Analysis of MLS data 86
2.3.2. Efficiency and Effectiveness 94
2.3.2.1. Method development 95
2.3.2.2. Analysis of field data 100
2.4. Summary 107
2.5. Recommendations 109

3 SAGES SITE STUDY 111
3.1. Flow Configuration Design 111
3.1.1. Flow Modeling Methods 112
3.1.2. Modeling Results 113
3.2. Site Characterization 114
3.2.1. Soil Coring 114
3.2.1.1. Methods 115
3.2.1.2. Results 118
3.2.2. Partitioning and Interfacial Tracers Test 122
3.2.2.1. Determination of partitioning coefficients 123
3.2.2.2. Field methods 124
3.2.2.3. Analysis of RW data 130
3.2.2.4. Analysis of MLS data 132
3.2.3. Summary 138
3.3. Cosolvent Flushing 139
3.3.1. Field Methods 139
3.3.1.1. Cosolvent delivery 139

3.3.1.2. Sample collection and analysis 142
3.3.2. Analysis of RW Data 142
3.3.2.1. PCE dissolution 143
3.3.2.2. Ethanol recovery 146
3.3.3. Analysis of MLS Data 147
3.3.4. Waste Treatment 148
3.4. Performance Evaluation 152
3.4.1. Soil Coring 152
3.4.2. Partitioning Tracer Test 153
3.4.2.1. Field methods 153
3.4.2.2. Analysis of EW data 155
3.4.3. Aqueous PCE Concentrations 157
3.4.4. Efficiency and Effectiveness 157
3.4.4.1. Comparison of RW and MLS efficiency 160
3.5. Costs Analysis 161
3.5.1. Actual Costs 161
3.5.2. Cost Optimization 163
3.6 Summary 167
3.7 Recommendation 168

4 SYNTHESIS 171
4.1. Technology Transferability 171
4.2. Technology Application 173

REFERENCES 175

BIOGRAPHICAL SKETCH 181

LIST OF TABLES

Table 1-1. Target analyte concentrations in an LNAPL sample collected from the test cell 27

Table 1-2. Tracers used in pre- and post-flushing partitioning tracer tests 27

Table 2-1. Swept volume, average NAPL saturation, and NAPL volume for each EW and the test cell 44

Table 2-2. Cosolvency power for six of the NAPL target analytes in ethanol/water and ethanol/pentanol/water systems. 54

Table 2-3. Properties of the injected cosolvent mixtures 56

Table 2-4. Mass of selected NAPL constituents removed during cosolvent flushing (adapted from Rao et al., 1997). Note that the fraction (%) of total constituent mass recovered at each EW is shown in parentheses. 70

Table 2-5. Mass recovery, well swept volume, retardation coefficient, and NAPL saturation estimates for the EWs. 86

Table 2-6. Comparison of NAPL saturation and volume based on PITTs conducted prior to and after the cosolvent flushing. 86

Table 2-7. NAPL saturation S_N and removal effectiveness E_N at the multilevel sampling locations. 90

Table 3-1. NAPL-water partitioning coefficients. 125

Table 3-2. Well flow rates and coefficient of variation. 126

Table 3-3. Tracers used during the test, injected concentrations and duration of the injection. 127

Table 3-4. Moment analysis results for the non-reactive tracer methanol 135

Table 3-5. Retardation coefficients relative to methanol for the three partitioning tracers. 135

Table 3-6. Summary of NAPL saturation and volume estimates (based on e-HEX). 135

Table 3-7. Comparison of partitioning and interfacial tracer results at MLS-4..... 136

Table 3-8. Optimal flow rates based on contact ratio estimates and the actual flow rates during the cosolvent flood. 143

Table 3-9. Mass and volume of PCE extracted at the RWs during cosolvent flushing. 146

Table 3-10. Estimates of ethanol recovery for the raw and extrapolated data. 147

Table 3-11. Tracers and injected concentrations used during the post-flushing tracer test 155

Table 3-12. Average flow rate and coefficient of variation at each well. 155

Table 3-13. NAPL satuartion and swept volume estimates for the post-flushing partitionig tracer test. 157

Table 3-14. Comparison of pre- and post-flushing NAPL volumes based on tracer tests. 159

Table 3-15. Comparison of the pre-flushing NAPL distribution to the volume of PCE removed during the cosolvent flood. 159

Table 3-16. Endpoint efficiency at the RWs. 160

Table 3-17. Costs of Sages site field study 164

LIST OF FIGURES

Figure 1-1. Site treatability and the level of site-specific testing required as a function of contaminant and geologic properties (source: NRC, 1997). Note that "H" indicates high and "L" indicates low 3

Figure 1-2. Ternary phase diagrams for two systems: (a) TBA/PCE/water (from Farley et al., 1993) and (b) ethanol/PCE/water (from LFR, 1998) 9

Figure 1-3. Log solubility (S_m) of 1,2-dichlorobenzene as a function of ethanol volume fraction (f_c) in an ethanol-water solvent mixture (adapted from Dai, 1997) 11

Figure 1-4. Log solubility of 1,2-dichlorobenzene from the Hill AFB multi-component NAPL in an ethanol-water solvent mixture (adapted from Dai, 1997) 13

Figure 1-5. Schematic representation of the hydraulically isolated test cell and instrumentation (adapted from Sillan et al., 1998) 25

Figure 1-6. Schematic of vertical multi-level sampler locations (cross section A-A' of Fig. 1-5; water table location is approximate and based on measurements during cosolvent flushing; adapted from Sillan et al., 1998) 26

Figure 1-7. Cosolvent enhanced extraction of NAPL constituents (a) 1,2-dichlorobenzene and (b) *n*-undecane from a 1-D column packed with contaminated soil (adapted from Dai, 1997) 30

Figure 1-8. Location and shape of miscible displacement fronts during (a) cosolvent flooding and (b) water flooding of the 2-D flow chamber (adapted from Jawitz et al., 1998) 32

Figure 1-9. Site map of well and MLS locations within the approximated extent of the DNAPL source zone at Sages 36

Figure 2-1. NAPL constituent soil concentration distribution with depth prior to cosolvent flushing in the Hill test cell (adapted from Rao et al., 1997) 40

Figure 2-2. Concentration of *n*-decane in soil as a function of DCB soil concentration at all soil core locations in the Hill test cell. 41

Figure 2-3. Schematic representation of the multilevel sampling system (SS = stainless steel, adapted from Sillan et al., 1998). 42

Figure 2-3. Tracer BTCs measured in the extraction fluids during the pre-flushing partitioning tracer test (adapted from Annable et al., 1998)..... 45

Figure 2-4. Tracer BTCs with exponential extrapolation at EW-3..... 46

Figure 2-5. Fluid travel time distribution during the partitioning tracer test. 49

Figure 2-6. Pre-cosolvent flushing conservative (nonreactive) and partitioning tracer breakthrough curves at all depths of MLS-6 (adapted from Sillan et al., 1998)..... 51

Figure 2-7. NAPL saturation (S_N) distribution prior to cosolvent flushing based on partitioning tracer test results (adapted from Sillan et al., 1998). 52

Figure 2-8. Alcohol concentration in the injection fluids. 55

Figure 2-9. Cosolvent concentration breakthrough curves at four depths of MLS-11: (a) ethanol and (b) *n*-pentanol (adapted from Sillan et al., 1998). 59

Figure 2-10. Spatial distribution of (a) fluid residence times along the EW-3 transect during water flooding based on median arrival times of bromide during the partitioning tracer test and (b) the ratio of mean to median arrival times (ND = no data)..... 62

Figure 2-11. Spatial distribution of (a) fluid residence times along the EW-3 transect during cosolvent injection based on median arrival times of ethanol and (b) the difference between local fluid residence times during water flooding (Figure 2-10a) and ethanol injection (ND = no data)..... 63

Figure 2-12. Spatial average of the ethanol concentration in the capillary fringe during water flooding (water flooding began on day 11). 65

Figure 2-13. Cosolvent concentration (% volume fraction) in samples collected from the three extraction. Also shown are the ethanol and n-pentanol concentrations delivered to the injection wells (adapted from (Rao et al., 1997)). 67

Figure 2-14. Concentration of NAPL constituents (a) 1,2-dichlorobenzene and (b) n-undecane in extraction well samples during cosolvent flushing. Also shown are the alcohol flux-averaged concentrations at the EWs (adapted from Rao et al., 1997)..... 71

Figure 2-15. NAPL constituent response to cosolvent flushing at a single depth (4.95-m bgs) for four MLS locations along a line transect. 74

Figure 2-16. NAPL constituent (DCB and *n*-undecane) response to cosolvent breakthrough curves at four depths at a single MLS location: (a) 4.95, (b) 5.33, (c) 5.72, and (d) 6.10 m bgs (adapted from Sillan et al., 1998)..... 75

Figure 2-17. The 80 mg/L concentration isosurfaces for DCB at six times during cosolvent flushing: (a) 1.4, (b) 1.8, (c) 2.2, (d) 2.6, (e) 3.0, and (f) 4.0 days (adapted from Sillan et al., 1998)..... 79

Figure 2-18. The 80 mg/L concentration isosurfaces for *n*-undecane at six times during cosolvent flushing: (a) 2.2, (b) 3.0, (c) 4.2, (d) 5.4, (e) 7.0, and (f) 9.0 days..... 80

Figure 2-19. Post-flushing partitioning tracer test data measured at the EWs (input pulse time was 0.15 d)..... 85

Figure 2-20. Post-cosolvent flushing nonreactive and partitioning tracer BTCs at all depths of MLS-6 (adapted from Sillan et al., 1998)..... 89

Figure 2-21. NAPL saturation (S_N) distribution after cosolvent flushing based on partitioning tracer test results (adapted from Sillan et al., 1998). 91

Figure 2-22. Vertical distribution of NAPL removal effectiveness determined from partitioning tracer tests data and soil cores..... 93

Figure 2-23. NAPL-water partition coefficient (K_{NW}) as a function of the NAPL's equivalent alkane carbon number (EACN) for three alcohol tracers (from Dwarakanath and Pope, 1998)..... 94

Figure 2-24. Concentration BTCs, removal effectiveness and removal efficiency in two systems (a-d: plug flow model, e-h: A-D model) with a two-component NAPL..... 102

Figure 2-25. Removal (a) effectiveness and (b) efficiency for DCB and *n*-undecane as a function of time at the 5.33-m depth of MLS-11..... 104

Figure 2-26. Efficiency as a function of effectiveness for DCB and *n*-undecane at the 5.33-m depth of MLS-11..... 104

Figure 2-27. Endpoint removal effectiveness (DCB) as a function of multilevel sampler height above the clay. 105

Figure 2-28. Maximum removal efficiency (DCB) as a function of multilevel sampler height above the clay. 107

Figure 2-29. Contact ratio variability with height above the clay. 106

Figure 3-1. Approximate horizontal extent of free-phase PCE at the Sages site. 112

Figure 3-2. Pathlines generated by hydraulic modeling of two different well configurations: (a) 2 IWs and 5 RWs, (b) 3 IWs and 6 RWs. 115

Figure 3-3. Laser induced fluorescence of subsurface as a function of depth. 117

Figure 3-4. High frequency soil sub-sampling template and sampled soil core. 117

Figure 3-5. Vertical distribution of PCE concentration in soil samples collected from (a) IW-1, (b) IW-2, (c) IW-3, (d) RW-7, and (e) MLS-1. 121

Figure 3-6. Particle size distribution of soil samples collected at various depths at MLS-1. 122

Figure 3-7. Alcohol tracer NAPL-water partitioning. Slope of line represents tracer partitioning coefficient. 125

Figure 3-8. Comparison of normalized partitioning behavior of 2-ethyl-1-hexanol to ideal behavior (Raoult's law). 126

Figure 3-9. Alcohol tracer BTCs at (a) RW-2, (b) RW-3, and (c) RW-4. 133

Figure 3-10. Alcohol tracer BTCs at (a) RW-5, (b) RW-6, (c) RW-7. 134

Figure 3-11. Alcohol tracer BTCs at the five depths of MLS-4. 137

Figure 3-12. Interfacial tracer (SDBS) retardation relative to the non-reactive tracer iodide at the five depths of MLS-4. 138

Figure 3-13. Flows rate of cosolvent solution delivered to the IWs below the specified packer height. 141

Figure 3-14. Ethanol and PCE BTCs at (a) RW-2, (b) RW-3, and (c) RW-4. Note that the scale of the PCE and etahnol axis change with location. 144

Figure 3-15. Ethanol and PCE BTCs at (a) RW-5, (b) RW-6, and (c) RW-7. Note that the scale of the PCE and etahnol axis change with location. 145

Figure 3-16. Ethanol breakthrough curves with extrapolated tails at (a) RW-3 and (b) RW-7. 149

Figure 3-17. Ethanol and PCE BTCs measured at four depths of MLS-4: (a) 8.69 m, (b) 9.07 m, (c) 9.45 m, and (d) 9.91 m bgs..... 150

Figure 3-18. Trailer mounted macro-porous polymer extraction (MPPE®) system used to separate PCE from the waste stream..... 151

Figure 3-19. Location of the post flushing soil cores relative to the IWs and RWs. 153

Figure 3-20. PCE concentration in soil cores collected after the cosolvent flood. 154

Figure 3-21. Partitioning tracer BTCs and exponential extrapolations at (a) RW-3 and (b) RW-7. 158

Figure 3-22. Efficiency (ε) as a function of time at (a) RW-4 and (b) the 29.25-ft depth of MLS-4. 162

Figure 3-23. Distribution of total and operational costs for the Sages site field study. .. 165

Abstract of Dissertation Presented to the Graduate School
of the University of Florida in Partial Fulfillment of the
Requirements for the Degree of Doctor of Philosophy

FIELD-SCALE EVALUATION OF IN SITU COSOLVENT FLUSHING
FOR ENHANCED AQUIFER REMEDIATION

By

Randall K. Sillan

May 1999

Chairman: Dr. P. Suresh C. Rao
Cochairman: Dr. Michael D. Annable
Major Department: Soil and Water Science

Innovative technologies that are developed to remediate contaminated soil and ground water require extensive field testing in various environmental scenarios in order to establish credibility and determine their applicability, transferability, and eventual commercialization. The objective of the work presented in this dissertation is to evaluate the field-scale performance of an innovative remediation technology, in situ cosolvent flushing, using data collected during field-scale evaluation at two sites. In situ cosolvent flushing is a chemically enhanced pump-and-treat technique where cosolvents, such as alcohols, are flushed through aquifers contaminated with nonaqueous phase liquids (NAPLs). Cosolvents increase the quantity of contaminants transported in the flushing fluid by increasing the solubility, desorption, and mass transfer rate of the NAPL components or by free-phase mobilization through reduction in the NAPL-water interfacial tension, thus reducing the cleanup time and total volume of flushing fluid that

must be extracted to achieve the remediation goals. A secondary objective of this work was to develop measures of remediation effectiveness and efficiency that provide a technique for evaluating the spatial variability in performance of in situ flushing technologies. Data used to accomplish these objectives was collected from research conducted at two field sites: Hill Air Force Base, Utah and the Former Sages Dry Cleaner Site, Jacksonville, Florida.

Two important characteristics that differentiate these sites are: (1) Dense NAPL versus Light NAPL, and (2) contained vs. uncontained flow system. The contaminant at Hill was a weathered multi-component LNAPL that coated most of the soil in the flushed region. Although variability in the NAPL saturation was measured, the data and observation of the soil cores showed that the entire vertical extent of the flow domain was contaminated by NAPL to some degree. In contrast, the Sages site was contaminated with a single-component DNAPL (tetrachloroethylene) that migrated below the water table where it collected at high saturations in thin, discontinuous layers wherever a change in the soil structure prevented downward migration. The NAPL saturations at Hill ranged form 1 to 10%, whereas the Sages site had a much larger range in values from 0 to 35%. An important consequence of the Sages NAPL distribution is the inefficiencies associated with flushing cosolvent through a region where only a small portion in the vertical direction is contaminated. The average maximum efficiency measured at the Hill site was approximately 0.04 L of NAPL/L cosolvent. In comparison the average maximum efficiency at the Sages site was 0.02 L of NAPL/L cosolvent. Thus, the more heterogeneous distribution of the NAPL at the Sages site reduced the removal efficiency in comparison to the more uniformly distributed NAPL at Hill.

In both field studies, an extensive network of multi-level samplers (MLSs) allowed observation of the link between spatial variability in performance and spatial variability in hydrodynamics and NAPL saturation. However, an extensive MLS network is not likely to be cost effective for full-scale remediation systems. Although material and installation costs for MLSs are small compared to other components, sample collection and analysis costs can make the use of MLSs prohibitive.

CHAPTER 1
INTRODUCTION

1.1. Justification

Two recent reports by the National Research Council (NRC, 1994, 1997) highlight the threat to human health and the environment from an estimated 300,000 to 400,000 sites in the United States that have contaminated soil and ground water. An estimated expenditure of $500 billion to $1 trillion to cleanup these sites over the next 20 to 30 years prompted regulators, consultants, and researchers to evaluate the ability of current technologies to restore contaminated aquifers within reasonable time frames and cost. The most common technology in use at these sites for ground water cleanup is pump-and-treat. However, the two NRC reports state that the physical heterogeneity of the subsurface and the complex behavior of contaminants (especially nonaqueous phase liquids) in the subsurface have severely limited the success of pump-and-treat. Thus, the daunting prospect of trying to cleanup the nation's contaminated aquifers with this inefficient and costly remediation technology has prompted great interest in the development of innovative technologies that have the potential to increase the effectiveness and reduce the costs of ground water cleanup. Although several promising technologies have been developed and applied to a limited number of contaminated sites, the commercialization and wide spread use of these technologies has been slowed by technical, institutional, and economic barriers (NRC, 1997; Rao, 1999).

For a new remediation technology to be commercialized, prospective users must be convinced that the technique is cost effective and can solve the problem with minimal risk of failure. One approach to minimizing the risk associated with using an innovative technology is to provide sufficient, quality data that proves its performance under field conditions. Two fundamental questions should be used to determine the data required to verify a technology's performance (NRC, 1997):

1. Is the risk posed by ground water or soil contamination reduced by the technology?
2. How does the technology work to reduce the risk?

Remediation technologies reduce risk by decreasing the mass, concentration, mobility, and/or toxicity of contaminants in the subsurface. Data that show a decrease in one or more of these parameters are essential for answering the first question and proving the performance of a technology. However, these measurements may not be sufficient to prove that the technology was responsible for the observed decrease in contamination. Thus, a cause-and effect relationship between application of the technology and observed decrease in contamination must be established by collecting data that answers the second question.

Typically, technology testing follows a hierarchical process: starting with theoretical concepts, proving these concepts in laboratory experiments and then in field tests, and then demonstrating the technology at full scale in the field. Laboratory testing is useful for identifying the mechanisms of the remediation technology and for estimating the applicability of the technology to specific contaminant and/or hydrogeologic scenarios. At the field-scale, heterogeneity in the physical properties of the porous media

and the complex behavior of contaminants in this media hinders the ability to predict the technology performance from site to site. Thus, the degree of field testing required to determine the performance, applicability, and transferability of a remediation technology depends on the treatability of the site. Figure 1-1 depicts the hydrogeologic and waste treatability factors that influence site cleanup and the need for site-specific testing of remediation technologies.

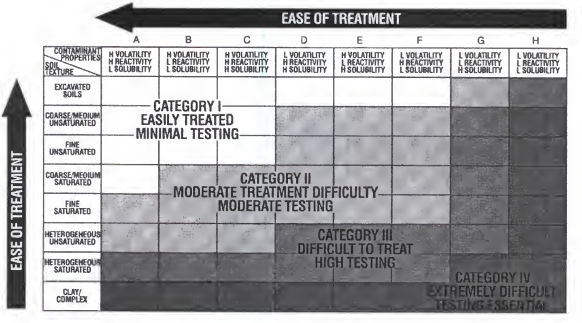

Figure 1-1. Site treatability and the level of site-specific testing required as a function of contaminant and geologic properties (source: NRC, 1997). Note that "H" indicates high and "L" indicates low.

Figure 1-1 divides remediation sites into four categories: (I) highly treatable, (II) moderately difficult to treat, (III) difficult to treat, and (IV) extremely difficult to treat. As the difficulty of treatment increases, so does the amount of site-specific testing required to prove efficacy and applicability. Unfortunately, the majority of identified contamination sites fall under categories III and IV, which implies that the performance of

cleanup technologies applied to these sites is likely to be highly site specific and difficult to transfer or scale-up to full site remediation. Thus, innovative technologies that are developed to remediate these sites require extensive field testing in various environmental scenarios in order to establish credibility and determine its applicability, transferability, and eventual commercialization.

The main objective of the work presented in this dissertation is to evaluate the field-scale performance of an innovative remediation technology, in situ cosolvent flushing, using data collected during field-scale evaluation at two sites. In situ cosolvent flushing is a chemically enhanced pump-and-treat technique where cosolvents, such as alcohols, are flushed through aquifers contaminated with nonaqueous phase liquids (NAPLs) (Augustijn et al., 1997; NRC, 1997). A series of wells are used to deliver the cosolvent solution to the contaminated zone of the aquifer, while extraction or recovery wells are used to pump fluids to the surface for treatment or disposal. In general, cosolvents increase the quantity of contaminants transported in the flushing fluid by increasing the solubility, desorption, and mass transfer rate of the NAPL components or by free-phase mobilization through reduction in the NAPL-water interfacial tension, thus reducing the cleanup time and total volume of flushing fluid that must be extracted to achieve the remediation goals.

An essential element in determining the efficacy of a remediation technology at the field scale is knowing the nature and extent of contamination prior to and after application of the remedial technique. Since in situ cosolvent flushing targets the regions of the contaminated aquifer containing NAPL (source zone), a reliable technique is needed to detect and characterize the distribution of NAPL in the source zone. The most

common technique used for NAPL source zone mapping is soil core sampling, which provides point measurements of NAPL component concentrations. To estimate NAPL mass, the point measurements are spatially interpolated making the estimate subject to considerable uncertainty. A new technique, based on the displacement of a suite of tracers through the NAPL source zone, provides an integrated measure of the average NAPL saturation, or volume, within the zone swept by the tracers. This technique, partitioning interwell tracer test (PITT), was used at both field sites to support the evaluation of in situ cosolvent flushing performance.

Several techniques are available to evaluate the performance of a remedial technology: comparison of contaminant concentrations in the ground water and soil before and after the remedial action, and comparison of NAPL volumes and distributions before and after the remedial flood. These techniques estimate how effectively the contaminant was removed. In order to gain a better understanding of the processes that control the technology performance, quantitative measures of the removal effectiveness and efficiency during the remedial flood are needed. Thus, an objective of this work was to develop measures of remediation effectiveness and efficiency that provide an alternative technique for evaluating the spatial variability in performance of in situ flushing technologies.

1.2. Cosolvent Flushing

1.2.1. Theoretical Background

The advantage of alcohol flooding as a NAPL remediation technology stems from four principles (Augustijn et al., 1997):

1. Cosolvents decrease the interfacial tension between the aqueous phase and the NAPL, inducing mobilization of an immobile NAPL trapped by capillary forces in the porous media.
2. Cosolvents increase the solubility of non-polar organic chemicals by decreasing the polarity of the solvent mixture, thus enhancing the transfer of organic constituents from the immobile NAPL to the mobile cosolvent solution.
3. Cosolvents reduce sorption of non-polar organic compounds to the porous media since sorption is inversely related to solubility, thus facilitating faster transport of dissolved NAPL components.
4. Cosolvents increase the dissolution rate of components from the NAPL since the equilibrium concentration, solubility, of the NAPL components increases.

1.2.1.1. Residual NAPL mobilization

Although mobilization typically removes NAPL from porous media more efficiently than solubilization, remediation techniques that mobilize NAPL risk contaminating regions of the aquifer that where previously uncontaminated by enhancing NAPL migration. This is more of a concern at sites contaminated with dense nonaqueous phase liquids (DNAPLs), which are heavier than water. The focus of the field studies presented in this dissertation was NAPL remediation through enhanced solubilization. However, since the addition of alcohol does reduce the NAPL-water interfacial tension, it is important to consider the potential for NAPL mobilization during a cosolvent flood. Recognizing that NAPL densities are typically different than water, Pennel et al. (1996) presented a method for predicting NAPL displacement using a total trapping number

(N_T), which relates viscous and buoyancy forces to the capillary forces acting to retain the NAPL in the porous medium:

$$N_T = \sqrt{N_{Ca}^2 + 2N_{Ca}N_B \sin\alpha + N_B^2} \tag{1-1}$$

where N_{Ca} is the capillary number, N_B is the bond number and α is the angle the flow makes with the horizontal axis. The capillary number (N_{Ca}) is a dimensionless quantity that relates viscous to capillary forces:

$$N_{Ca} = \frac{q_w \mu_w}{\sigma_{nw} \cos\theta} \tag{1-2}$$

where q_w is the Darcy velocity of the aqueous phase, μ_w is the dynamic viscosity of the aqueous phase, σ_{nw} is the interfacial tension between the NAPL and aqueous phase, and θ is the contact angle at the NAPL-aqueous phase interface. The bond number (N_B) represents the ratio of buoyancy to capillary forces:

$$N_B = \frac{\Delta\rho g k k_{rw}}{\sigma_{nw} \cos\theta} \tag{1-3}$$

where $)\rho = \rho_w - \rho_n$ (density difference between the NAPL, n, and aqueous phase, w), g is the gravitational acceleration constant, k is the intrinsic permeability of the porous medium, and k_{rw} is the relative permeability to the aqueous phase. Pennel et al. (1996) reports that the critical value for the total trapping number (N_T) to initiate tetrachloroethylene (PCE) mobilization fell within the range of 2 x 10^{-5} to 5 x 10^{-5}, while complete displacement of PCE was observed as N_T approached 1 x 10^{-3}.

Cosolvents may also enhance the mobilization of a residual NAPL as a result of preferential partitioning of the cosolvent into the NAPL. When a cosolvent partitions preferentially into the NAPL, discontinuous NAPL globules may swell and coalesce into

a continuous phase that is easier to displace. Swelling also reduces the density of the NAPL thereby making NAPLs more buoyant and less likely to migrate downward (Farley et al., 1993). NAPL swelling is more likely for alcohols with high molecular weight and hydrophobicity, such as t-butanol (TBA). This behavior is indicated by tie lines with positive slopes in a ternary phase diagram (Figure 1-2a). More polar, lower molecular weight alcohols (e.g., such as methanol and ethanol) partition favorably into water, indicted by tie lines with negative slopes (Figure 1-2b), and do not promote mobilization. During the field studies presented here, ethanol was the primary cosolvent; thus, swelling of the NAPL was not a concern and increased solubility was the primary means of enhanced NAPL remediation.

For the more viscous, multi-component NAPLs, such as coal tar, creosote, and crude oils, swelling induced mobilization is unlikely. These types of NAPLs strongly interact with both mineral and organic components of the porous media, and as a result, exist primarily as thin films or coatings that act differently than trapped NAPL ganglia (Luthy et al., 1993). Thus, removal of complex, viscous NAPLs is more likely to occur through the release of their organic constituents by solubilization.

1.2.1.2. NAPL dissolution

By adding a water-miscible organic cosolvent to water, the polarity of the solvent mixture decreases, resulting in a nearly log-linear increase in solubility (S_m) of non-polar organic chemicals in the solvent mixture with increasing volume fraction of cosolvent (f_c).

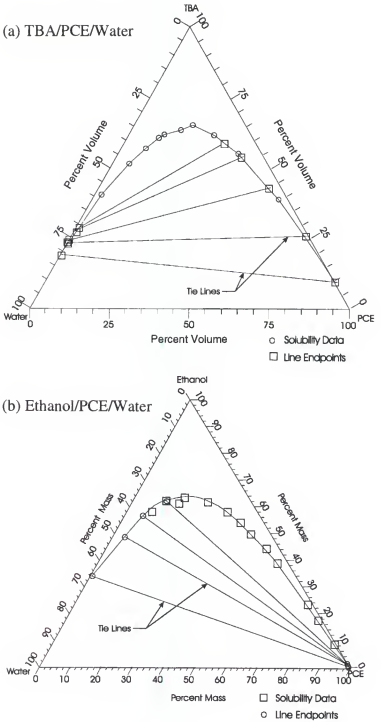

Figure 1-2. Ternary phase diagrams for two systems: (a) TBA/PCE/water (from Farley et al., 1993) and (b) ethanol/PCE/water (from LFR, 1998).

For a mixture of several cosolvents, the generalized expression for cosolvent-enhanced solubility is (Rao et al., 1991):

$$\log S_m = \log S_w + \sum_{i=1}^{N} \beta_i \sigma_i f_{c,i} \tag{1-4}$$

where

$$\sigma_i = \log \frac{S_{c,i}}{S_w} \tag{1-5}$$

the subscript i designates the values for the ith cosolvent, β_i is an empirical coefficient that accounts for water-cosolvent interactions, $S_{c,i}$ is the solubility of the organic solute in the neat cosolvent i, S_w is the solubility of the organic solute in water, σ_i is the cosolvency power of the cosolvent i for the solute of interest, and N is the number of cosolvents in the mixture.

The cosolvency power (σ) is a measure of a cosolvents ability to increase the solubility of an organic solute. For a given cosolvent, σ increases with increasing log K_{ow} of the solute, an index of solute hydrophobicity. The log-linear cosolvency model, shown above (equation 1-4), is adequate for describing the solubility profiles of a number of non-polar organic chemicals in a variety of solvent-water mixtures (Rao et al., 1991). An example of the enhanced solubility of an organic solute, 1,2-dichlorobenzene, in ethanol-water mixtures is presented in Figure 1-3. Deviations from the log-linear cosolvency model are generally caused by non-ideal behavior as a result of water-cosolvent interactions. When these water-cosolvent interactions are significant, more sophisticated methods should be used to predict activity coefficients in the solvent mixture (Pinal et al., 1991). Also, when the NAPL is completely dissolved in the solvent mixture at high

cosolvent contents, the log-linear model approximation needs to be replaced by a more general approach that permits construction of appropriate ternary phase diagrams.

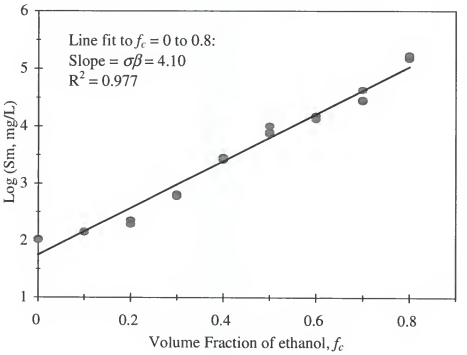

Figure 1-3. Log solubility (S_m) of 1,2-dichlorobenzene as a function of ethanol volume fraction (f_c) in an ethanol-water solvent mixture (adapted from Dai, 1997).

For a cosolvent mixture in contact with a single-component NAPL (as shown in Figure 1-3), the increase in solute solubility or equilibrium concentration is predicted by equation 1-4. For a multi-component NAPL, the equilibrium concentration (C) of component i in a solution can be predicted by (Augustijn, 1993):

$$C_i = \gamma_i X_i S_i \tag{1-6}$$

where γ_i is the activity coefficient of component i in the NAPL, X_i is the mole fraction of component i in the NAPL, and S_i is the aqueous solubility of the pure component. In

many cases the activity coefficient of an organic constituent in the NAPL is assumed to be unity, simplifying equation 1-6 to Raoult's law.

Since the pure component solubility (S_i) increases log-linearly with cosolvent addition, a log-linear increase in solution-phase concentrations (C_i) of organic constituents of the multi-component NAPL can be expected. An example of the increase in solute concentrations when ethanol is added to a solution in contact with a multi-component NAPL is presented in Figure 1-4. Note that the slope of the line fit to the data in Figures 1-3 and 1-4 represents the product $\beta\sigma$. Although the slopes (4.10 for Figure 1-3 and 3.94 for Figure 1-4) in these two figures are similar, differences in the product $\beta\sigma$ obtained for various organic constituent in different systems (single vs. mulit-component NAPL) have ranged up to 1 indicating that the interaction coefficient β is not unity and varies with the NAPL-solvent system (Dai, 1997). Thus, if accurate modeling of the log-linear solubility increase is required at a contaminated site, studies should be conducted with the site-specific NAPL-solvent systems. Note that deviation of the solubility data from the log-linear model at high ethanol fractions in Figure 1-4 has been attributed to depletion of the more-soluble components from the complex NAPL (Dai, 1997). As the more-soluble components are selectively removed from the NAPL, the mole fractions change along with solubility according to equation 1-6. A limited quantity of the component present in the complex NAPL can also cause the data to plateau.

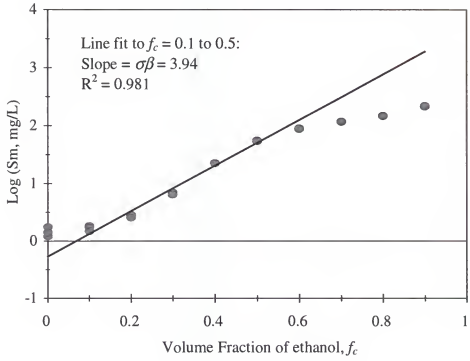

Figure 1-4. Log solubility of 1,2-dichlorobenzene from the Hill AFB multi-component NAPL in an ethanol-water solvent mixture (adapted from Dai, 1997).

1.2.1.3. Enhanced desorption

Sorption of non-polar organic compounds can be described by a linear sorption isotherm, characterized by an equilibrium partition coefficient (K). Since sorption is inversely related to the solubility of the organic solute, a log-linear increase in solubility upon addition of cosolvents results in a proportional decrease in sorption. Thus, the equilibrium sorption coefficient (K_m) in mixed solvents decreases log-linearly with increasing cosolvent content (Rao et al., 1991):

$$\log K_m = \log K_w - \sum_{i=1}^{N} \alpha_i \beta_i \sigma_i f_{c,i} \tag{1-7}$$

where α is an empirical coefficient that accounts for solvent-sorbent interactions, K_w is the sorption coefficient in water, and all other terms are as defined previously. During

remediation of a NAPL contaminated soil using cosolvents, it is likely that the solution containing cosolvent and solubilized organics will contact uncontaminated regions of the aquifer. Because of the log-linear reduction in sorption caused by the cosolvent, transport through uncontaminated regions will show minimal retardation.

1.2.1.4. Dissolution nonequilibrium

Dissolution of organic components from NAPL is generally considered to be limited by diffusion through a boundary layer from the interface into the bulk solution. The rate of dissolution from a NAPL ($M\,m/M\,t$) is often described by a first-order rate law:

$$\frac{\partial m}{\partial t} = -\theta k_1 \left(C_{eq} - C \right) \tag{1-8}$$

where m is the contaminant mass in the NAPL phase, t is time, θ is the volumetric water (or mixed solvent) content, k_1 is the first-order dissolution rate coefficient, and C is the solution phase concentration. C_{eq} is the equilibrium concentration which is the component solubility limit for single-component NAPLs (equation 1-4) or the equilibrium concentration based on Raoult's law for multi-component NAPLs (equations 1-4 and 1-6). Thus, when cosolvent is added to a NAPL contaminated soil, the solubility, and hence C_{eq}, will increase, enhancing the dissolution rate.

Another factor in equation 1-6 that may change during cosolvent flushing is the mass-transfer coefficient (k_1), which has been shown to have positive correlation with pore-water velocity, NAPL saturation, and fluid properties such as vicosity and density (Powers et al., 1994). The mass-transfer coefficient is also proportional to the interfacial area across which the dissolved contaminants are diffusing to reach the mobile phase.

Thus, the distribution in ganglia size and shape, as well as their accessibility to mobile fluids, is a factor determining NAPL dissolution kinetics.

Changes in NAPL properties may also affect the dissolution rate. In viscous, multi-component NAPLs, like coal tar or crude oil, diffusive transport within the organic phase is the most likely mechanism controlling kinetics (Augustijn, 1993). During dissolution, the low molecular weight components will dissolve leaving behind the high molecular weight components, making the NAPL more viscous and diffusive transport slower. However, cosolvents that preferentially partition into the NAPL may prevent this effect to some extent by enhancing the diffusivity of components within the NAPL.

1.2.2. Technology History

In the early 1960s, solvent flushing was investigated by the petroleum industry as a technique to enhance oil recovery from deep reservoirs (Gatlin and Slobod, 1960; Taber et al., 1961; Holm and Csaszar, 1962). Although various alcohols were found capable of enhancing oil displacement, the solvent flushing technique was not widely applied in the oil industry because of the relatively high cost of alcohols compared to the additional oil recovered.

The use of cosolvents for remediation of contaminated soils first appeared in the literature in the mid-80's in studies investigating organic contaminant sorption processes in mixed solvents (Rao et al., 1985, 1991; Nkedi-Kizza et al., 1985, 1987; Fu and Luthy, 1986a, 1986b). Prior to this work, theory on cosolvency was developed in pharmaceutical research (e.g., Yalkowsky and Roseman, 1981). Over the past decade, the concept has been expanded with more recent studies focusing on enhanced removal of sorbed organic contaminants (Augustijn et al., 1994a, 1994b, 1997; Wood, 1995), and

dissolution or mobilization of residual NAPLs (Boyd and Farley, 1992; Luthy et al., 1992; Rixey et al., 1992; Farley et al., 1993; Peters and Luthy, 1993, 1994; Imhoff et al., 1995; Roy et al., 1995). To date, applications of the cosolvent flushing technique have been demonstrated in laboratory-scale column studies. Regulatory approval for cosolvent use in situ has been slow, and this factor has contributed to limited field-scale testing, even though ex situ cosolvent extraction of contaminated soils has been demonstrated at the commercial scale (U.S. EPA, 1990).

Two techniques used on a commercial basis that use solvents to treat excavated soils (solvent washing) are the Basic Extraction Sludge Treatment (BEST) and the CF Systems process (U.S. EPA, 1991). The BEST process uses triethylamine as the solvent to extract organic chemicals from the contaminated soil while the CF system uses propane or carbon dioxide at super-critical conditions (high temperature and pressure). Unfortunately, remediation of contaminated soils using ex situ technologies requires excavation and sophisticated treatment equipment, making it very expensive. In addition, excavation increases the risk of exposure and requires a significant destruction of the landscape. Therefore, treatment of contaminated sites in situ may be preferred.

Prior to the field studies reported in this dissertation, there has been only one field-scale evaluation of in situ cosolvent flushing. Broholm and Cherry (1994) reported the results from the first pilot-scale field testing of in situ cosolvent flushing for enhanced recovery of residual NAPL. They constructed a hydraulically-isolated test cell (4.5 x 5.5 x 2.3 m) in a shallow sandy aquifer, and introduced a small volume (about 5 liters) of a ternary mixture of NAPLs (10% chloroform, 40% TCE, and 50% PCE) at 5-cm below the water table. About 220 days after releasing the NAPL mixture, the test cell was flushed

for 5.5 days with 30% methanol at a pore-velocity of 13 cm/day. This was followed by another 100 days of flushing with water. During this entire period about 30% of the introduced NAPL mixture was recovered, as determined by post-flushing sampling in the test cell. Although their study demonstrated enhanced NAPL dissolution, it was not conducted in an effort to evaluate overall effectiveness of cosolvent flushing for subsurface remediation.

Although laboratory studies prior to the research presented in this dissertation showed the potential for cosolvent flushing to remediate soils in situ, several issues related to field-scale implementation remained unclear: (1) ability to deliver the cosolvent solution to the NAPL, (2) reduced efficacy of the process due to soil heterogeneities and non-uniform distribution of the NAPL, (3) performance metrics for evaluating effectiveness and efficiency, (4) recovery of remedial fluids, (5) waste management, and (6) costs.

As stated previously, an essential element in evaluating the field-scale performance of in situ cosolvent flushing is having a reliable estimate of the amount and distribution of the NAPL prior to and after application of the cosolvent flood. Thus an innovative technique, the partitioning interwell tracer test (PITT), was used at both field sites to provide integrated measures of the NAPL content and distribution. A description of this technique is provided in the following section.

1.3. Partitioning Tracers

1.3.1. Theoretical Background

The PITT involves injecting a mixture of conservative and partitioning tracers in one or more wells and the subsequent recovery of the tracers from one or more nearby extraction wells. The theoretical basis for the use of partitioning tracers, detailed by Jin et al. (1995), is briefly reviewed here. The fundamental relationship in the partitioning tracers technique is the partition coefficient (K_{NW}), which describes the distribution between of the tracer between the NAPL and the aqueous phase:

$$K_{NW} = \frac{C_N}{C_W} \tag{1-9}$$

where C_N is the tracer concentration in the NAPL, and C_W is the tracer concentration in the ground water at local chemical equilibrium. Conservative or non-partitioning tracers have a $K_{NW} = 0$, whereas the partitioning tracers have $K_{NW} > 0$. Thus, in a steady-state flow field, transport of the conservative tracers is not retraded by NAPL in the media pore space, whereas the partitioning tracers undergo retardation by partitioning into and from the NAPL. The chromatographic separation of the tracers due to this partitioning is used to measure the average NAPL saturation, S_N, within the tracer flow field (Pope et al., 1994a; Jin, 1995):

$$R = 1 + \frac{K_{NW} S_N}{\left(1 - S_N\right)} = \frac{t_p}{t_n} \tag{1-10}$$

where R is the retardation factor for the partitioning tracer, which is calculated as the ratio of average travel times for the partitioning tracer pulse (t_p) and the nonpartitioning tracer pulse (t_n) introduced and displaced simultaneously during steady flow. Estimation of the

average travel times (t_p and t_n) are determined using the first temporal moment normalized by the zeroth temporal moment of the breakthrough curves (BTCs) for the partitioning and nonpartitioning tracers measured in the effluent from the extraction well. Since, field tracer experiemnts typically involve injecting a tracer pulse; the first, normalized, temporal moments of the tracers must be corrected for the finite tracer pulse duration.

Equation 1-8 assumes sorption of the partitioning tracer onto the aquifer solids in the swept zone is insignificant. However, if adsorption of the partitioning tracer on the solid matrix is significant, then equation 1-10 should be modified to account for the additional retardation (Nelson and Brusseau, 1996):

$$R = 1 + \frac{K_{NW} S_N}{(1 - S_N)} + \frac{\rho_b K_d}{\varepsilon (1 - S_N)} = \frac{t_p}{t_n} \tag{1-11}$$

where K_d (mL/g) is the soil-water partition coefficient, ρ_b is the soil bulk density (g/cm^3), and ε is the porosity. Note that the product of ε and (1-S_N) is the volumetric water content (θ_w). The soil-water partition coefficient ($K_d = S/C_w$) in equation 1-11 is assumed to be reversible and at equilibrium where S (μg/g) is the adsorbed concentration on the solid matrix.

Using the average travel time of the nonpartitioning tracer (t_n), the effective pore volume swept by the tracers recovered at an extraction well can be determined using

$$V_s = Q\, t_n \tag{1-12}$$

where Q is the steady volumetric flow rate at the extracion well. Since S_N is the average NAPL saturation in the matrix volume swept by the well, the total NAPL volume (V_N) in the swept zone of the well is given by

$$V_N = \frac{S_N V_S}{1 - S_N} \tag{1-13}$$

It should be noted that the NAPL saturation determined using this method represents the average within the tracer-swept volume and is not necessarily equal to the local residual NAPL saturation. Because of the media heterogeneity of typical aquifers, the residual NAPL is likely to be non-uniformly distributed. Within the swept volume of an extraction well, regions may exist in which NAPL is not present. Therefore, the average NAPL saturations determined using this method are typically less than local residual NAPL saturations. This does not affect the estimation of the total volume of NAPL within the swept volume of the well. However, spatial variability in the NAPL distribution does determine how efficiently the NAPL is removed by the remedial flood. This topic is addressed in later sections.

1.3.2. Technology History

Partitioning tracer tests have been widely used in the petroleum industry to estimate residual oil saturation prior to the beginning of enhanced oil recovery operations. The use of the partitioning tracers technique to estimate the amount of residual NAPL and assess remediation performance was first demonstrated in column experiments and in simulations of a hypothetical two-dimensional aquifer contaminated with PCE (Jin, 1995; Jin et al., 1995). The simulations were performed with UTCHEM, a comprehensive three-dimensional, chemical flood compositional simulator developed at the University of Texas.

The use of partitioning interwell tracer tests for characterizing NAPL-contaminated aquifers was first demonstrated at the field scale prior to a cosolvent

flushing study at Hill Air Force Base, Utah (Annable et al., 1994,1998a). The results from this tracer test and subsequent cosolvent flood are presented in chapter 2 of this dissertation (see section 2.1.2).

1.4. Field Studies

As stated previously, the focus of this dissertation is to evaluate the field-scale performance of an innovative remediation technology, in situ cosolvent flushing. Data used to accomplish this objective was collected from research conducted at two field sites: Hill Air Force Base, Utah and the Former Sages Dry Cleaner Site, Jacksonville, Florida. Data from field measurements and experiments, used to support the dissertation research, were collected at the Hill AFB site starting in June of 1994 and ending in July of 1995, while work at the Sages Dry Cleaner site was performed from March through September of 1998.

1.4.1. Hill Air Force Base

1.4.1.1. Project overview

The purpose of the study conducted at Hill Air Force Base (AFB) was a comprehensive investigation of the effectiveness of the in situ cosolvent flushing technique for enhanced remediation of aquifers contaminated with residual NAPLs. An equally important objective of the field study was to identify limitations or difficulties related to larger-scale applications of the in situ cosolvent flushing technique. This study was the first investigation funded by the Strategic Environmental Research and Development Program (SERDP) at Hill AFB. This program was created to evaluate the

performance of several innovative remediation technologies and is a joint effort by the Department of Defense, the Department of Energy, and the EPA.

A brief overview of the tasks completed during this study is provided here. The experiments were conducted in an existing NAPL plume at Hill AFB. A hydraulically-isolated test cell (4.3 m x 3.5 m) was constructed in the surficial sand-gravel-cobble aquifer, which was contaminated with a mixture of JP-4 jet fuel and chlorinated solvents disposed at the site. During installation of wells and sampling points, soil cores and groundwater samples were collected. Laboratory studies were conducted on several soil cores and samples of site LNAPL to aid in partitioning tracer and cosolvent selection. A non-reactive tracer test was first conducted to characterize the hydrodynamic characteristics of the saturated zone within the test cell (Annable et al., 1998b); these data were used to guide the design of other tests in the cell. Prior to cosolvent flushing, the first field demonstration of the partitioning tracers technique was conducted to characterize the volume and distribution of NAPL in the test cell (Annable et al., 1998a; Sillan et al., 1998). During cosolvent flushing, a ternary mixture of water and two water-miscible alcohols was used; ethanol was the primary flushing cosolvent, and *n*-pentanol was added to enhance solubilization of the strongly hydrophobic constituents present in the NAPL. After cosolvent flushing, another partitioning tracer test was conducted along with soil coring. Pre- and post-flushing soil cores and partitioning tracer tests provided a method to evaluate the effectiveness of NAPL removal and compare innovative characterization techniques (Rao et al., 1997; Sillan et al., 1998).

1.4.1.2. Site background

Hill Air Force Base is located in northern Utah, approximately 40 km north of Salt Lake City, on the former Weber River Delta immediately west of the Wasatch Mountain Range. The field site is located at the northeast boundary of the Base within Operable Unit 1 (OU 1). Potential contaminant sources within OU 1 include two landfills, two chemical disposal pits, two fire training areas, and above ground waste-fuel storage tanks. The primary sources of NAPL in the region of the test cell were the chemical disposal pits. An unknown quantity of liquid wastes, primarily fuels and spent solvents, were disposed in the pits from the early 1950's until 1973. The liquid was periodically burned in the pits until 1967. These activities produced a NAPL plume covering about 2.8 ha (7 acres) and an extensive dissolved plume that has traveled past the Hill AFB boundaries. The history and physical characteristics of this Superfund site are reported in detail in Remedial Investigation Reports prepared by James M. Montgomery, Inc. (1992, 1993).

The site geology is characterized by two distinct formations. The Provo Formation is the water-bearing surficial aquifer and consists of inter-fingered sands, gravelly sands, and gravels. This is underlain by a silty clay aquitard (the Alpine Formation, approximately 60 meters thick) containing thin stringers of sand and silt. A complex depositional environment produced an uneven erosional interface between the two formations characterized by interbeds of silt, very fine sand, and clay. In the area where the field study was constructed, the sand and gravel unit is approximately 6.1 m (20 ft) thick, and the water table was located at approximately 5.8 m (19 ft) below ground surface (bgs) at the time of test cell installation.

The contaminant at Hill AFB was a complex, multi-component NAPL with low solubility and low volatility. Using the treatability chart presented in Figure 1-1, the properties of the Hill NAPL place this contaminant in class F or H. The combination of this contaminant classification and the aquifer properties (saturated, heterogeneous course to medium sand) would give it a category III or IV treatability. This implies that remediation of this site would be difficult and would require site specific testing to determine efficacy of the technology.

1.4.1.3. Instrumentation

The test cell constructed at Hill AFB used the Waterloo Sheet Pile design (Starr et al., 1992, 1993), forming a rectangular cell measuring 4.3 by 3.5 meters (14.1 by 11.5 ft) at the ground surface (Figure 1-5). Prior to installation, three monitoring wells were installed and core samples collected to verify the contaminant and clay present in the proposed cell location. These wells, along with several others installed later, were used for monitoring outside of the cell. The constructed sheet pile cell extends to a depth of 9.1 m (30 ft) with a clay layer encountered at approximately 6.1 m (20 ft). The joints connecting each sheet were flushed with water and filled with a custom-designed bentonite/cement/polymer mixture to provide the hydraulic barrier.

The test cell was instrumented with four injection wells (IWs), three extraction wells (EWs), twelve multilevel samplers (MLSs), and four piezometers (Figure 1-5). The injection and extraction wells (IWs and EWs) were fully screened over the entire vertical extent of the saturated zone being flushed. Three rows of MLSs were aligned in groups of four with the extraction wells, with the MLSs evenly spaced between the injection and extraction wells in each row. At each MLS, sampling points were vertically distributed at

an interval of 0.38 m (1.25 ft) starting at 4.6 m (15.0 ft) bgs and extending to 6.1 m (20.0 ft) bgs (Figure 1-6). Seven of the MLSs had an additional sampler placed at 6.5 m (21.3 ft) to investigate migration of tracers and cosolvents into the aquitard. Along the center row of the cell, piezometers were installed with the MLSs.

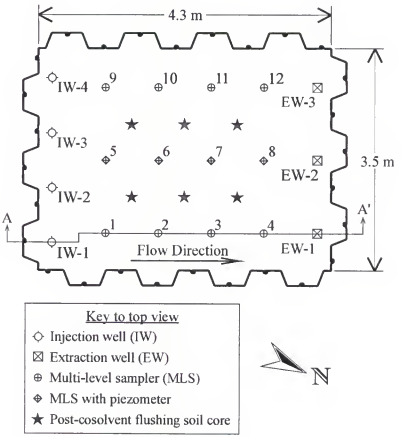

Figure 1-5. Schematic representation of the hydraulically isolated test cell and instrumentation (adapted from Sillan et al., 1998).

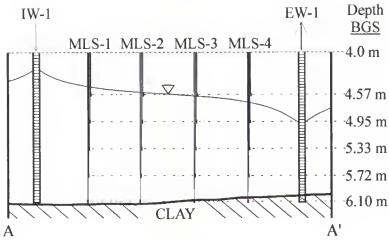

Figure 1-6. Schematic of vertical multi-level sampler locations (cross section A-A' of Fig. 1-5; water table location is approximate and based on measurements during cosolvent flushing; adapted from Sillan et al., 1998).

1.4.1.4. Preliminary laboratory investigations: NAPL compositional analysis

Laboratory (UF) analysis was performed on an LNAPL sample taken from an extraction well (EW-2) within the test cell to identify and quantify constituents. The site NAPL was found to have numerous constituents (>200). Thus, a few target analytes were selected for monitoring during the study, which represent various chemical classes and mass fractions in the NAPL (Table 1-1).

1.4.1.5. Preliminary laboratory investigations: Partitioning tracer selection

The partitioning tracers were chosen based on the partitioning coefficient, K_{NW}, values measured in batch and column tests conducted using the NAPL from the test site (UF Lab; Pope et al., 1994b). Tracers should be selected that are significantly retarded (R > 1.2) to insure reliable estimates of the NAPL saturation. However, a retardation factor less than four is also desirable to limit the duration of the tracer test. Thus, it is recommended that multiple partitioning tracers be used during a test to insure retardation

within these limits for an expected range in NAPL saturations. Table 1-2 lists the tracers used during the Hill AFB study and their measured K_{NW} values. Other desirable tracer characteristics include: (1) non-hazardous; (2) non-toxic; (3) non-degrading; (4) low volatility; (5) reasonable cost and availability; and (6) easily quantifiable, especially in the presence of numerous NAPL constituents (Annable et al., 1998a).

Table 1-1. Target analyte concentrations in an LNAPL sample collected from the test cell.

Target Analyte	Mass Fraction (mg/g)	Log K_{ow}	Aqueous Solubility (mg/L)
1,1,1-trichloroethane	0.016	2.49	44,000
Toluene	0.074	2.59	515
p-,*m*-xylene	0.17	3.09	200
1,2-dichlorobenzene	6.10	3.40	100
1,3,5-trimethylbenzene	0.83	3.55	...
1,2,4-trimethylbenzene	0.71	3.55	...
Naphthalene	0.11	3.59	20
1,2,4-trichlorobenzene	11.81	4.10	...
n-decane	5.20	6.00	0.009
n-undecane	16.00	6.35	...
n-tridecane	2.93	7.15	...

Table 1-2. Tracers used in pre- and post-flushing partitioning tracer tests.

Tracer	K_{NW}
Bromide	0.0
Ethanol	0.1
Methanol	0.1
n-pentanol	3.6
n-hexanol	5.1
2,2-dimethyl-3-pentanol (DMP)	12.9
6-methyl-2-heptanol (HEPT)	40.0

1.4.1.6. Preliminary laboratory investigations: NAPL dissolution

Several batch and column studies were performed in the laboratory (UF) in order to study the dissolution behavior of the NAPL constituents in various cosolvent mixtures (Dai, 1997). Batch experiments provided estimates of NAPL constituent solubility in ethanol/water and ethanol/pentanol/water solutions. In a 70/30-ethanol/water solution, the solubility of DCB was 118 mg/L, which is 84 times greater than the measured aqueous solubility of 1.4 mg/L. Note that the measured aqueous solubility of DCB from the multi-component NAPL is less than the 100 mg/L for the neat chemical in water. This behavior is expected and can be approximated with Raoult's law. Adding 10% pentanol to the ethanol/water solution increases the DCB solubility to 207 mg/L, which is 148 times greater than the aqueous solubility.

The more hydrophobic constituent *n*-undecane is practically insoluble in water. An estimate of aqueous solubility was determined from the log-solubility curve to be approximately 0.002 mg/L (Dai, 1997). In the 70/30-ethanol/water solution, the *n*-undecane concentration was 79 mg/L, which increased to approximately 300 mg/L with the addition of 10% pentanol. These values are 4×10^4 and 1.5×10^5 times larger than the estimated aqueous solubility for *n*-undecane. This data suggests that the addition of pentanol greatly increases the solubility of the more hydrophobic compounds in the NAPL such as *n*-undecane.

Based on information obtained from the batch studies, two cosolvent mixtures (70/30 ethanol/water and 70/10/20 ethanol/pentanol/water) were chosen to flush contaminated soils from the test cell in one-dimensional column experiments. Figure 1-7 shows the flux-averaged concentrations for two target analytes (DCB and *n*-undecane)

measured in the effluent of soil columns flushed with the two different cosolvent mixtures. Both analytes were more efficiently removed by the ethanol/pentanol/water mix than with the ethanol/water cosolvent mix due to the higher solubility limits in the presence of pentanol. This difference in removal rate was much larger for the more hydrophobic constituent (*n*-undecane). Also, note that the maximum concentration of DCB during the flood with the ethanol/pentanol/water solution did not reach the solubility limit determined from the batch experiments. This behavior is likely due to a combination of hydrodynamic dispersion and the limited amount of DCB available for removal from the NAPL contaminated soil. Thus, the mass of DCB in the NAPL was depleted before the solubility limit in the solution could be reached. This behavior is likely to be more prevalent at the field scale for similar reasons plus the likelihood of increasing heterogeneity in the NAPL distribution at the field scale.

Based on the results from the batch and column experiments, the decision was made to include *n*-pentanol in the cosolvent mixture used in the field experiment in order to improve the removal efficiency of the more hydrophobic compounds in the complex NAPL.

1.4.1.7. Preliminary laboratory investigations: Cosolvent hydrodynamics

Miscible displacement technologies such as cosolvent flushing rely on the stability of the interface between the resident and displacing fluids for efficient removal of the contaminants. Contrasts in density and viscosity between the resident and displacing fluids can adversely affect the stability of the displacement front. The purpose of a laboratory study conducted by Jawitz et al. (1998) was to investigate how density and

viscosity contrasts affected cosolvent displacements in unconfined porous media characterized by the presence of a capillary fringe.

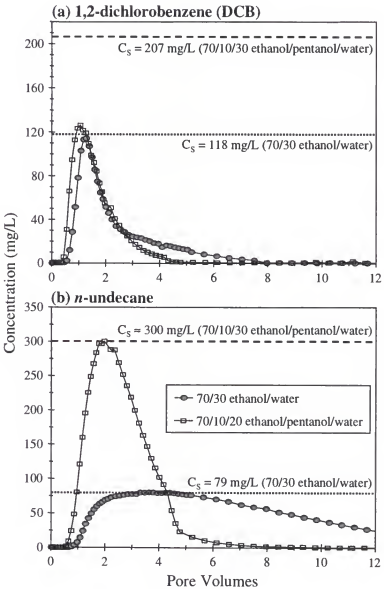

Figure 1-7. Cosolvent enhanced extraction of NAPL constituents (a) 1,2-dichlorobenzene and (b) *n*-undecane from a 1-D column packed with contaminated soil (adapted from Dai, 1997).

Scaled two-dimensional flow experiments were conducted in the laboratory to determine potential implications of flow instabilities in homogeneous sand packs. Descriptions of the experimental materials and methods can be found in Jawitz et al. (Jawitz et al., 1998). For the cosolvent displacements studied, the gravity forces were expected to dominate the viscous forces; thus, the experiments focused on flow instabilities induced by density differences.

To investigate displacement of the resident water by a less-dense cosolvent, a two-dimensional sand-packed box was flushed with a cosolvent mixture. In order to simulate the fluid dynamics of the field-scale cosolvent flood in a lab-scale flow chamber, Jawitz et al. (1998) scaled appropriate system variables to provide similarity. Thus, the cosolvent mixture strength (which determines the fluid property contrasts), the chamber dimensions, and the flow rate were scaled to maintain a ratio of viscous to gravitational forces expected at the field scale.

The advance of the cosolvent displacement front is shown in Figure 1-8a. The flow patterns show that the less-dense cosolvent mixture tended to override the water. Another important characteristic of the flow pattern was the collapse of the capillary fringe. The capillary fringe collapse was caused by a reduction in the air-liquid interfacial tension as the cosolvent front advanced into the capillary fringe.

The advance of the displacement front for water displacing the cosolvent mixture is presented in Figure 1-8b. A comparison with Figure 1-8a shows that the gravity underride during water flooding was more severe than the override during the cosolvent flood. It was also observed that the increase in the capillary fringe height expected as water displaced the cosolvent mixture took much longer than the previously noted

capillary fringe collapse. Thus, during water flooding, buoyant forces effectively trapped the cosolvent mixture in the capillary fringe above the denser water (Jawitz et al., 1998).

The results from these experiments indicated that the presence of a capillary fringe was an important factor in the displacement efficiency. Buoyant forces can act to carry a lighter-than-water cosolvent preferentially into the capillary fringe during displacement of the resident groundwater. During subsequent water flooding, buoyancy forces can act to effectively trap the cosolvent in the capillary fringe, contributing to the inefficient removal of cosolvent from the aquifer.

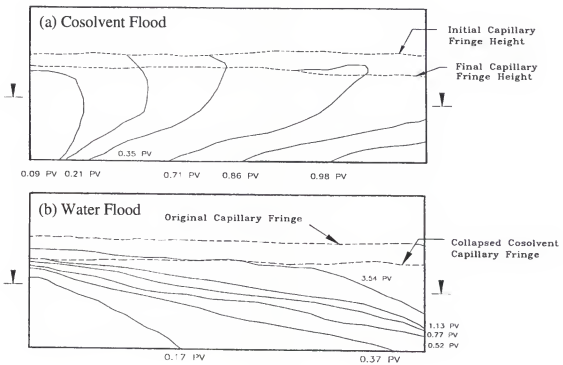

Figure 1-8. Location and shape of miscible displacement fronts during (a) cosolvent flooding and (b) water flooding of the 2-D flow chamber (adapted from Jawitz et al., 1998).

1.4.2. Former Sages Dry Cleaning Facility

1.4.2.1. Project overview

The main objective of the study conducted at the Sages site was to evaluate the feasibility and effectiveness of in situ cosolvent flushing at this and other Florida Department of Environmental Protection (FDEP) Dry Cleaner Site Program (DCSP) facilities. This project was the first field test of the cosolvent flushing technology at a site with DNAPL. This study was also the first use of the in situ cosolvent flushing technique in a system without physical barriers. Another important objective was to demonstrate the use of the partitioning interwell tracer test for characterizing DNAPL distributions at a FDEP DCSP facility.

An overview of the work conducted during this study is provided here. The first step was to determine the approximate extent of the free-phase tetrachloroethylene (PCE) contamination at the site. Methods used were soil coring and in situ measurement techniques including cone penetrometer tests with a resistivity module and direct push laser induced fluorescence (LIF). Once the approximate extent and geometry of the DNAPL was determined, hydrodynamic modeling was conducted to determine the number and location of the wells required to ensure coverage of the contaminated region. During installation of the wells and multi-level sampling points, soil cores were collected to obtain local estimates of PCE soil concentration. A partitioning and interfacial tracer test was conducted next to characterize the hydrodynamics and NAPL properties of the well swept zones. Cosolvent flushing with a 95% ethanol solution was followed by another tracer test to determine the amount and distribution of the PCE not removed. Soil

cores were collected after the post-flushing tracer test to provide an alternate method to tracers for evaluating the performance of the cosolvent flood.

1.4.2.2. Site background

The Former Sages Dry Cleaner site is located at 5800 Fort Caroline Road in Jacksonville, Florida. The soil and ground water at this site are contaminated with tetrachloroethylene (PCE), a common ground water contaminant detected at sites in proximity to operating or closed dry-cleaning facilities. Information on when and the amount of PCE released at the Sages site is not available. Buildings that housed the dry-cleaning facility at the Sages site were removed before the study, leaving the asphalt and concrete foundation in place.

Characteristics of the subsurface matrix and a contamination assessment are provided in a report prepared by Levine-Fricke-Recon (1997). The following details are provided:

1. Fine to very fine sand occurred at the site from ground surface to approximately 30 feet bgs. From 30 feet to 35 feet bgs, very fine to silty sand was encountered. A thin clay layer (0.5 to 1 foot thick) was detected at approximately 35 feet bgs in most soil borings, but was not found in the southwest corner of the site. Beneath the clay layer, very fine sand to silty fine sand was observed.
2. The depth to ground water is approximately 10 feet bgs. The natural ground water flow direction is toward the west and has a hydraulic gradient of approximately 0.0025 (ft/ft).
3. The hydraulic conductivity (estimated from slug test data) averaged about 20 ft/day in the upper sand unit and 10 ft/day in the lower sand to silty sand zone.

4. High aqueous concentrations of PCE (75 % of solubility limit) were detected in ground water samples collected during the contamination assessment. Six inches of free-phase PCE (DNAPL) were detected in the former Sages supply well; and high PCE dissolved-phase concentrations were detected in ground water samples from existing monitoring wells.

The high hydraulic conductivity along with the high volatility of PCE (contaminant class B) would give this site a category II treatability according to Figure 1-1. This ranking implies that remediation of this site would be moderately difficult and require some site specific testing. However, the treatability of this site could become increasingly difficult due to changes in soil texture with depth, making the porous media more heterogeneous. Another factor making these types of sites difficult to treat is the problem with reliably delineating the extent of DNAPL contamination. Because DNAPLs are heavier than water, they can travel to great depths in the porous media and spread horizontally in thin layers wherever there is a slight change in soil texture (permeability). This site reflects conditions common to dry-cleaning-related sites contaminated with PCE in Florida; and thus, data from the study presented here should be applicable to other FDEP DSCP sites in Florida.

1.4.2.3. Instrumentation

To flush the contaminated region of the aquifer at the site, three injection wells screened from 7.6 to 9.9 m (25 to 32.5 feet) bgs were encompassed by six recovery/extraction wells screened from 7.9 to 9.6 m (26 to 31.5 feet) bgs (Figure 1-9). These wells were constructed of polyvinyl chloride (PVC) and had a diameter of four inches. Within the swept volumes of these wells, seven multi-level samplers were

installed with five sampling depths at each location. The MLS sample depths were approximately 8.1, 8.7, 9.1, 9.4, and 9.9 m (26.5, 28.5, 29.75, 31.0, and 32.5 feet) bgs.

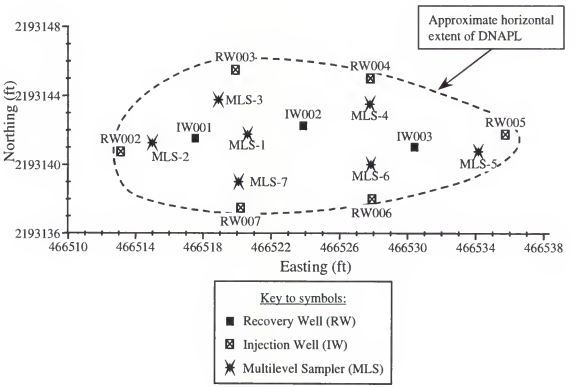

Figure 1-9. Site map of well and MLS locations within the approximated extent of the DNAPL source zone at Sages.

1.5. Dissertation Research Objectives

The overall objective of the research presented in this dissertation is to evaluate the field-scale performance of in situ cosolvent flushing at the two field sites. In order to accomplish this objective, the following task were completed:

1. Demonstrate the use of the partitioning tracers technique to characterize the volume and distribution of NAPL at the two sites.

2. Identify difficulties related to field-scale application of in situ cosolvent flushing.
3. Develop and apply measures of remediation effectiveness and efficiency that provide an alternative technique for evaluating the spatial variability in performance of in situ flushing technologies.
4. Evaluate the costs of field-scale in situ cosolvent flushing.

1.6. Chapters Ahead

This chapter is followed by three additional chapters. The next chapter presents results from the field study at Hill Air Force Base. This includes evaluation of the NAPL distribution prior to and after cosolvent flooding, cosolvent hydrodynamics, and NAPL dissolution behavior during the cosolvent flood. Chapter 3 presents the results from the study conducted at the Sages site. Unlike the Hill AFB study, methods and materials used during the Sages site study have not been presented elsewhere; thus, chapter 3 includes summaries of the methods and materials used at all phases of the study. The final chapter provides a summary and comparison of the field studies and presents a discussion of issues related to the transferability and application of in situ cosolvent flushing.

CHAPTER 2
HILL AFB FIELD STUDY

2.1. Site Characterization

This section provides data from soil coring and a partitioning tracer test to characterize the initial NAPL volume and distribution within the Hill AFB test cell. Equally important was the characterization of the hydrodynamic variability within the test cell during the flushing experiments.

2.1.1. Soil Coring

Soil cores were collected from the Hill AFB test cell during the installation of the three extraction wells, four injection wells and MLS locations 5 through 8 (Figure 1-5). Analysis of up to 120 methylene chloride extracts of soils sub-sampled from all of the cores was used to quantify the initial NAPL constituent mass present in the test cell. By integrating the contaminant mass in each soil core, Rao et al. (1997) reported the constituent mass per unit area for 1,2-dichlorobenzene (DCB) as 88 g/m^2 and for *n*-decane as 130 g/m^2. The statistical distributions of concentrations at specified depths are shown in Figure 2-1 for DCB and *n*-decane. The vertical distribution of the individual NAPL constituents, as shown by the mean values, was consistent, suggesting that the composition of the NAPL was relatively constant within the test cell.

Uniformity of the NAPL composition within the test cell is an important issue since the partitioning tracers technique, used to estimate NAPL volume, currently

assumes that the NAPL-water partition coefficient is constant in space. Thus, *n*-decane soil concentrations were plotted against DCB soil concentrations in Figure 2-2 to estimate NAPL compositional uniformity. The linear trend in the data in Figure 2-2 indicates that the NAPL composition is uniform with respect to these two constituents. This is significant because *n*-decane is from JP-4 while DCB is from spent solvents disposed at the site. Constituents of two different wastes are present more or less uniformily, suggesting that the spent solvents are well mixed with the JP-4.

In general, analysis of soil cores indicated the following: (1) the NAPL was located in a 1.5-meter (5-ft) smear zone immediately above the clay confining unit; (2) the largest amounts of NAPL (based on constituent analysis) were near the water-table position prior to test cell installation (5.8 m bgs); and (3) NAPL penetrated about 0.5 m into the confining unit via sand stringers near the aquifer-aquitard interface (Rao et al., 1997). The vertical extent of the NAPL (≈1.5 m above the clay) determined the height of the water table in the cell during the subsequent tracer and cosolvent floods.

2.1.2. Partitioning Tracer Test

2.1.2.1. Methods

The tracers used in this experiment were bromide (non-reactive tracer applied as KBr), ethanol, *n*-pentanol, *n*-hexanol, and 2,2-dimethyl-3-pentanol. The partitioning tracer test was conducted over an eight-day period in October 1994, during which water samples were collected at frequent intervals from the extraction wells (EWs) and multi-level samplers (MLSs). An approximate 0.1 pore volume pulse of a mixture of the tracers was introduced over a 3.3-hour period after steady flow had been established for approximately three pore volumes. The average flow rate during the tracer study was 3.2

liters/min (0.85 gpm), equivalent to an average Darcy velocity of about 0.03 m/hr, or an average hydraulic residence time in the test cell of about 1 day. Additional details of the equipment and methods used during the tracer test are contained in Annable et al. (1998).

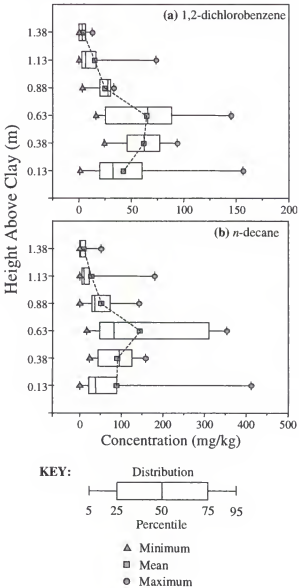

Figure 2-1. NAPL constituent soil concentration distribution with depth prior to cosolvent flushing in the Hill test cell (adapted from Rao et al., 1997).

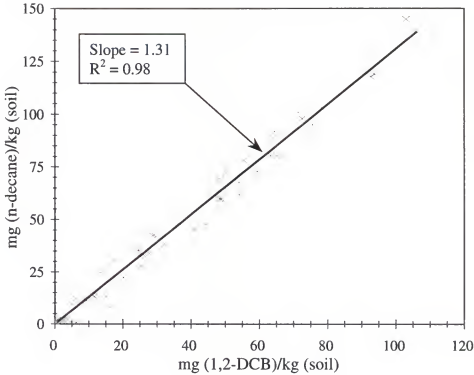

Figure 2-2. Concentration of *n*-decane in soil as a function of DCB soil concentration at all soil core locations in the Hill test cell.

A schematic (Figure 2-3) and brief description of the MLS sampling procedure is provided. At each MLS, a vacuum of approximately 700 millibars was used to draw sample through a 20-µm stainless steel filter and 0.32-cm stainless steel tubing into a 20-mL VOA vial. The initial 20 mL of sample drawn was discarded as purge. A 10-20 mL sample was then collected and transferred to a 5-mL glass vial with Teflon-backed septa. Samples were immediately cooled and shipped in quantity by overnight freight to the University of Florida (UF) and the National Risk Management Research Laboratory (NRMRL) in Ada, OK for analysis. At the laboratories, samples were stored at 5°C until analyzed.

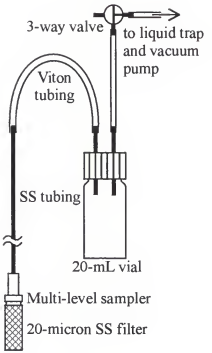

Figure 2-3. Schematic representation of the multilevel sampling system (SS = stainless steel, adapted from Sillan et al., 1998).

Gas chromatographic techniques were used to quantify the concentrations of tracers in the EW and MLS samples. Details of analytical equipment used in this study are provided by (Annable et al., 1998). Analytical methods are provided in Standard Operating Procedures (SOPs) on file with the USEPA's National Risk Management Research Laboratory in Ada, OK.

Although several tracers were used in this test, data analysis focused on the non-reactive tracer, bromide, and the partitioning tracer, 1,2-dimethyl-3-pentanol (DMP). This tracer combination was chosen based on favorable mass recovery estimates (>90%) and partitioning coefficient (Table 1-2) for the partitioning tracer (DMP).

2.1.2.2. Analysis of EW data

The results presented here focus on the samples collected from the three extraction wells. The data were used to estimate the average NAPL saturation (S_N) and the total NAPL volume (V_N) within the swept zones for each of the three extraction wells. Retardation of the partitioning tracers compared to bromide is taken as evidence for the presence of residual NAPL. The field data for bromide and 2,2-dimethyl-3-pentanol, which had the best mass recovery (102% and 92% respectively) and temporal separation, are presented in Figure 2-3.

Temporal moment estimates of the BTCs were used in Equations 1-10, 1-12, and 1-13 to determine average NAPL saturation, swept volumes, and NAPL volume for each extraction well. The tracer BTCs appear to be truncated, which can produce moments that underestimate the NAPL present. To improve the estimated NAPL saturation in the test cell, an exponential extrapolation of the tracer data was performed. The exponential extrapolations were generated by regressing a linear function through the linear portion of the natural-log transformed data in the tails of the breakthrough curves. The results of the exponential extrapolation of the tracer data from EW-3 is shown in Figure 2-4. The extrapolated results along with analysis of the unextrapolated data are also presented in Table 2-1. A comparison of the moment analysis for the extrapolated data with results based on non-extrapolated moments shows a small increase in the calculated NAPL saturation. Using the total estimates for the swept volume (5.32 m^3) and NAPL volume (309.8 L) from the extrapolated data, the overall average NAPL saturation in the test cell was 5.5%.

Comparison of S_N estimates based on data for the individual extraction wells indicates a general trend of increasing NAPL content from the EW-1 side to the EW-3 side of the cell. The total swept volume of 5.32 m^3 (1405 gal) yields a cell-average mobile water content of 0.21, which compares well with the value of 0.2 estimated based on hydraulic testing of the cell. Note also that of the total swept volume, approximately 40% is captured by one well (EW-1) with the other wells at approximately 30% each. These data suggest that the EW-1 side of the test cell contains less permeable regions, when compared to the EW-3 side.

Table 2-1. Swept volume, average NAPL saturation, and NAPL volume for each EW and the test cell.

Well	Bromide Swept Volume (m^3)		S_N		V_N (L)
	Data	Extrapolated	Data	Extrapolated	Extrapolated
EW-1	2.03	2.11	0.029	0.031	67.5
EW-2	1.43	1.48	0.050	0.049	76.3
EW-3	1.50	1.72	0.065	0.088	166.0
Total	4.96	5.32	0.046	0.054	309.8

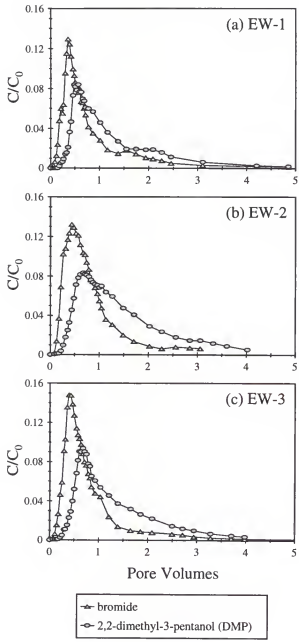

Figure 2-3. Tracer BTCs measured in the extraction fluids during the pre-flushing partitioning tracer test (adapted from Annable et al., 1998).

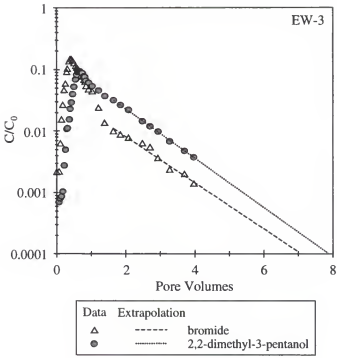

Figure 2-4. Tracer BTCs with exponential extrapolation at EW-3.

2.1.2.3. Analysis of MLS data

Data analysis methods. Tracer concentration breakthrough curves (BTCs) measured at the MLSs were used to determine average NAPL saturations (S_N) in the tracer flow paths between the injection wells and the sampling locations, or MLSs. The pulse-corrected, first, normalized, temporal moment of the non-reactive and partitioning tracer resident concentration BTCs were calculated and used to estimate S_N. Breakthrough curves for the non-reactive (bromide) and partitioning (DMP) tracers were measured at 41 MLS locations. Zeroth and first temporal moments were determined at each MLS location using trapezoidal rule integration, integration with exponential extrapolation of the BTC tail data, and non-linear regression estimation (Helms, 1997). These techniques were evaluated for determining reliable estimates of moments for

observed field data that are imperfect. Many of the observed tracer BTCs were truncated or noisy, or contained large intervals of missing data. In general, numerical integration provided satisfactory estimates when tracer BTCs were relatively complete; exponential extrapolation improved moment estimates when the BTC tail was truncated; and nonlinear regression exhibited a significant advantage compared to the other methods when rising or peak data were missing (Helms, 1997).

Since the exact flow path of the tracers from the injection wells to a given MLS is unknown, the calculated S_N is viewed as a representative value for the zone between the injection wells and each sampling point. The volume of the porous medium that any given multi-level sampling point represents depends on the flow domain geometry and the spatial density of monitoring points available. Thus, our ability to characterize the spatial NAPL distribution improves with higher density sampling, and knowledge of the general flow direction. A simple approach, defined here as "differential retardation," was used to estimate the spatial distribution of NAPL within the test cell based on S_N estimates from the MLS data. This method assumes that tracers arriving at sequential MLS monitoring points, located approximately down gradient from one another, encounter media representative of each zone traversed. In other words, the retardation attributed to a given segment of the tracer flow path is expected to combine with the tracer responses from all other segments (upstream and/or downstream) to produce the measured BTC at a down gradient MLS. If each segment of the tracer flow path is generally representative of the block of medium between MLSs, then estimating NAPL saturations between monitoring locations, based on the "differential retardation" observed, will provide an approximation of the NAPL distribution within the test cell.

Conservative tracer. The bromide BTC data at the MLSs was used to investigate the variability of flow within the test cell. Variability in tracer arrival time at different depths was evident from the MLS BTCs. Sampling points located below the clay confining unit (6.1-m and 6.5-m depth) showed little or no tracer response during the period of sample collection indicating very low advective velocities. Also evident in the uppermost sampling points were the delayed breakthrough due to the presence of longer flow paths associated with the capillary fringe. The bromide BTC at each MLS was evaluated using temporal moment analysis to provide fluid residence times of the region between the injection wells and the measurement points. Plots of travel time distributions in three transects that coincide with the MLSs are presented in Figure 2-5. The presence of a higher velocity zone in the center of the flow domain and the location of the capillary fringe can be inferred from the distribution map. The travel time distribution in the center transect reveals a relatively low fluid velocity zone near the clay (bottom) and MLS-5, 6, and 7. Because of this low fluid flux, it was expected that it would be difficult to deliver remedial fluids to this region (evidence of this is shown in following sections).

NAPL distribution. Bromide and DMP breakthrough curves from all five depths at the MLS-6 location during the pre-flushing partitioning tracer test are presented in Figure 2-6. The variability of NAPL saturation with depth can be inferred from the retardation of DMP compared to that of bromide at each monitoring location. The general trend within the test cell, lower NAPL saturation in the upper portion of the test cell and the highest saturations near the clay-confining unit, is reflected in the MLS-6 tracer data. This NAPL distribution is the result of historical fluctuations of the water

table just above the confining unit and is in general agreement with analysis of soil core samples collected during installation of the MLSs.

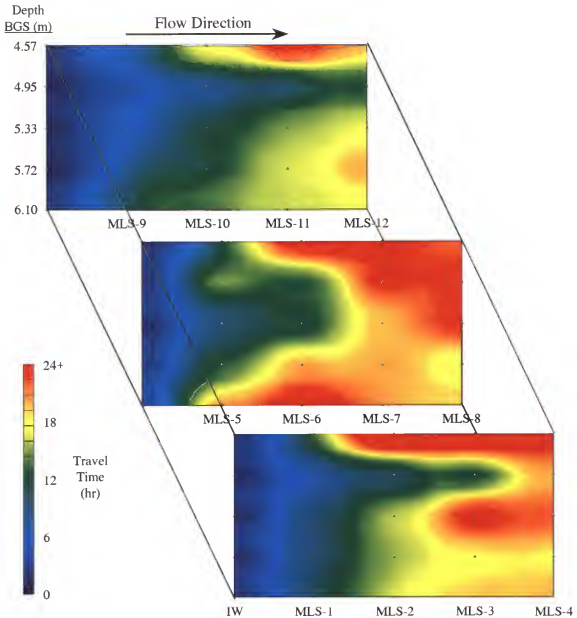

Figure 2-5. Fluid travel time distribution during the partitioning tracer test.

Spatial trends in the NAPL distribution obtained from the "differential retardation" approach were visualized using the Department of Defense's Groundwater Modeling System (GMS) (Owen et al., 1996). The simplest form of inverse distance weighted interpolation, Shepard's method, was used to interpolate the estimates of NAPL saturation to a uniform grid within the network of MLSs. Since the S_N estimates from the tracer test represents averages over the interval between sampling points, the S_N values were assigned to points located at the center of each interval. The interpolation weights were determined using the six nearest points after the vertical scale was expanded by a factor of two (Z-Scale Factor=2). Thus, points in the horizontal plane were given a higher relative weight than points along the vertical plane. This approach was chosen to improve accuracy since the horizontal correlation length is expected to be greater than the vertical correlation length based on an understanding of the NAPL plume, hydrogeologic characteristics, and the line-drive forced-gradient experiment. The objective of the visualization process was to observe the spatial trends in the data, but not to perform a complete geostatistical analysis.

Enclosed within the iso-surface in Figure 2-7b is the volume of the porous media within the test cell that had a NAPL saturation equal to or greater than the average S_N of 5%. Figure 2-7 shows that the highest NAPL saturations in the test cell are located near the clay on the east side (EW-1) and in a large portion of the flow domain of the west side (EW-3).

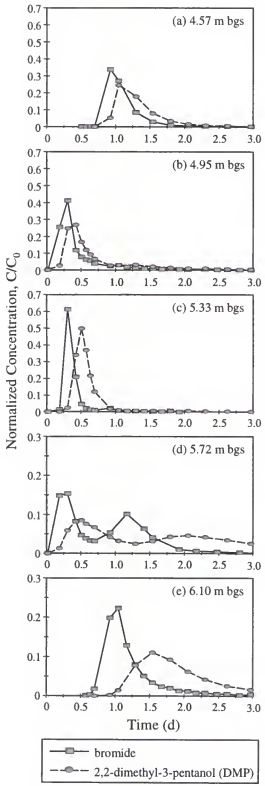

Figure 2-6. Pre-cosolvent flushing conservative (nonreactive) and partitioning tracer breakthrough curves at all depths of MLS-6 (adapted from Sillan et al., 1998).

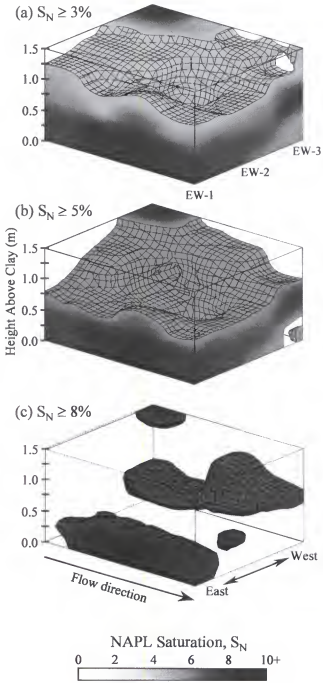

Figure 2-7. NAPL saturation (S_N) distribution prior to cosolvent flushing based on partitioning tracer test results (adapted from Sillan et al., 1998).

2.1.2.4. Summary

The spatial distribution of S_N shown in Figure 2-7 agrees with the values determined from the EW data (Table 2-1). Both data sets show that the majority of the NAPL (≈50%) prior to the cosolvent flood was within the swept volume of EW-3. Travel time distributions (Figure 2-5) also show that this region (EW-3 swept zone) had relatively shorter tracer travel times or faster fluid velocity. Thus, it is expected that EW-3 will recover the majority of the NAPL mass and have an overall higher effective removal of this mass.

The vertical distribution of the NAPL, as determined from the soil cores and from the MLS tracer data, show that the majority of the NAPL is in the region from 0 to 1 meter above the clay. The MLS tracer data also confirms that the highest NAPL saturations are located approximately 0.3 m (1 ft) above the clay, which was the water table height prior to test cell installation.

2.2. Cosolvent Flushing

2.2.1. Methods

During cosolvent flushing, a ternary mixture of water and two alcohols was used. The slope ($\beta\sigma$) of the log-linear solubility enhancement for six of the Hill NAPL target analytes as a function of ethanol and pentanol fraction are shown in Table 2-2. Ethanol was the primary flushing cosolvent, and *n*-pentanol was added to enhance solubilization of the strongly hydrophobic constituents present in the NAPL such as *n*-decane and *n*-undecane (Table 2-2).

Table 2-2. Cosolvency power for six of the NAPL target analytes in ethanol/water and ethanol/pentanol/water systems.

Target Analyte	[a]$\beta\sigma$ for ethanol	[a]$\beta\sigma$ for pentanol at 0.6 f_c ethanol
1,2-dichlorobenzene	4.10	3.94
1,3,5-trimethylbenzene	4.77	6.65
1,2,4-trimethylbenzene	4.24	6.02
1,2,4-trichlorobenzene	4.93	3.61
n-decane	6.56	8.87
n-undecane	7.50	9.13

[a] Slope values are from Dai (1997).

An ethanol-water binary mixture was introduced into the test cell first using a gradient ethanol injection during which the ethanol content was increased from 0 to 72% over a period of 1 day (Figure 2-8). After an additional 0.82 day flood with mixture #1 (Table 2-3), two ternary mixtures (mixtures #2 and #3) of ethanol, *n*-pentanol, and water were injected for 7.5 days representing approximately seven test cell pore volumes. Cosolvent mixture #2 was introduced only after the initial ethanol/water flood (mixture #1) to avoid phase separation of *n*-pentanol since its aqueous solubility is approximately 2.2% by weight. One pore volume of the fourth cosolvent mixture was introduced to displace the bulk of the cosolvent containing *n*-pentanol before water flooding began.

Flow instabilities were a concern during both cosolvent flushing and subsequent water flushing because of bulk fluid property contrasts between the cosolvent mixture and water (Farley et al., 1993; Grubb and Sitar, 1994; Wood, 1995; Jawitz et al., 1998). In order to minimize such flow instabilities, the ethanol fraction in the injection fluid was programmed to increase linearly for approximately one pore volume to a final value of 72% (mix #1). This type of gradient injection of the cosolvent mixture creates a gradual,

rather than abrupt (step), change in fluid properties in the aquifer, and has been shown to improve the displacement efficiency of unstable displacements (Slobod and Lestz, 1960; Kyle and Perrine, 1965; Claridge, 1978; Jawitz et al., 1998). The same gradient-injection technique was also used during the water flood to displace the cosolvent mixture from the test cell.

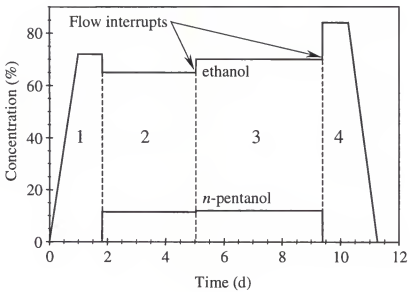

Figure 2-8. Alcohol concentration in the injection fluids.

During cosolvent flushing, two flow interruptions were implemented: one for 40 hours at 5 pore volumes, and another for 18 hours at 9.4 pore volumes. These flow interruption periods were intended to allow for mass transfer equilibration in the heterogeneous flow domain.

The 10-day cosolvent flood was followed by a 20-day period of flushing with water. Throughout the test, the fluid injection and extraction rates (about 3.1 L/min) were equivalent to approximately one pore volume per day displacement. During cosolvent

flushing, this flow rate produced water-table mounding, above the static condition, of 0.35 m (1.15 ft) at the IWs and drawdowns of 0.43 m (1.4 ft) at the EWs (Figure 1-6). The hydraulic gradient and the mounding or drawdown effects were magnified during cosolvent flushing since the cosolvent mixtures were more viscous compared to water (Table 2-3). Fluid storage, fluid delivery and waste management are described in detail by Rao et al. (1997).

Table 2-3. Properties of the injected cosolvent mixtures.

Cosolvent Mixture Number	Ethanol Fraction % Volume	*n*-pentanol Fraction % Volume	Water Fraction % Volume	Density (g/cm^3)[a] (22°C)	Viscosity (cP)[a] (22°C)
1	72	0	28	0.874	2.27
2	65	11.5	13.5	0.862	2.26
3	70	12	18	0.847	2.06
4	85	0	15	0.838	1.81

a - Laboratory analysis at the University of Florida

During the cosolvent flushing study, samples of the extraction fluids were collected from the three extraction wells. Fluid samples from the MLSs were also collected at selected time intervals to provide synoptic snapshots of target analyte and alcohol concentration distributions in the test cell. A total of approximately 525 extraction well samples and 3500 MLS samples were taken during the flushing experiment. A limited number of samples were analyzed at the field site for rapid evaluation of alcohol and target analyte concentrations. All samples collected from the EWs and the MLSs were preserved on ice, and sent via overnight freight to laboratories at UF (Gainesville), EPA (Ada), and Hill AFB for target analyte analysis. Materials and

methods for fluid delivery and handling, EW and MLS sampling, chemical analysis, and waste management are detailed by Rao et al. (1997) and Sillan et al. (1998).

2.2.2. Cosolvent Hydrodynamics

In order for in situ cosolvent flushing to effectively dissolve and extract the NAPL from the contaminated zone, sufficient amounts of cosolvent must contact the NAPL. Thus, evaluation of the technology must include a description of the cosolvent hydrodynamics and the factors that control cosolvent delivery to the NAPL.

2.2.2.1. Analysis of MLS data

In Figure 2-9, ethanol and *n*-pentanol BTCs at four depths at the MLS-11 location are shown as representative of similar depth-variations observed at other MLS locations. Note that the cosolvent injection program is shown and the time axes for the BTCs in Figure 2-9 are scaled to the start of ethanol/water injection. At the MLS-11 location, ethanol began to appear at the various depths within 0.4 days from ethanol injection. Likewise, *n*-pentanol detection at MLS-11 began at approximately 0.4 days after injection of the second cosolvent mixture. The later arrival of *n*-pentanol on the frontal side, and the earlier drop on the distal portions, is the result of the cosolvent injection program (Figure 2-8). For both ethanol and *n*-pentanol, resident concentrations of cosolvents measured at the MLS-11 location are essentially equal to that in the injected fluids after about 2 to 2.5 days.

The variability of cosolvent arrival at a MLS location is controlled by two processes: 1) variations in local flux resulting from permeability and NAPL heterogeneity, and 2) flow instabilities induced by density and viscosity differences between injected and resident fluids. Fluid density differentials tend to cause flow over-

riding or under-riding of the resident fluid by the injected fluid whereas displacement of the resident fluid by a less-viscous fluid can enhance viscous fingering. A preliminary evaluation of the gradient cosolvent introduction by Jawitz (1995) indicated that no flow instabilities were present.

Several factors may have acted in concert to diminish the impact of density-induced flow instabilities during cosolvent flooding. First, the gradient introduction of cosolvent along with mechanical dispersion caused by media heterogeneity produced a buffer zone of mixing in which the viscosity and density gradually changed from that of the resident fluid to that of the displacing fluid. Second, favorable viscous forces, caused by a more viscous cosolvent mixture compared to the resident groundwater (Table 2-3), could have minimized the impacts of the heterogeneities in effective permeability. Finally, the capillary fringe collapsed during cosolvent flushing due to a reduction of the air-liquid interfacial tension as the ethanol content increased. The net effect of this collapse was to reduce the thickness of the capillary fringe relative to the height of the water table (1.5 m above the clay), thus reducing the influence of the capillary fringe on the hydrodynamics of cosolvent introduction.

In order to observe the effect of fluid property contrasts on the displacement behavior during cosolvent injection, the fluid residence times during cosolvent injection were estimated and compared to fluid residence times during the pre-flushing tracer test. Typically, the normalized first temporal moment of a non-reactive solute's BTC is used to estimate the mean arrival time of the solute and thus fluid residence time.

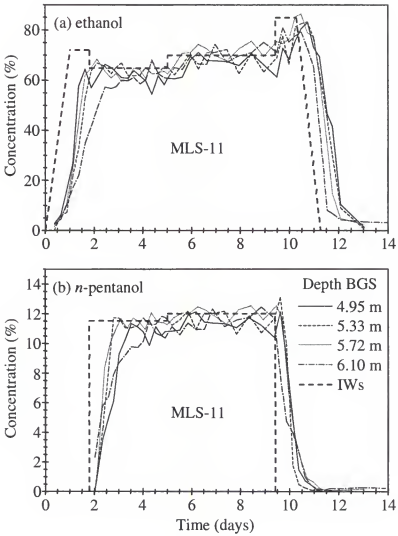

Figure 2-9. Cosolvent concentration breakthrough curves at four depths of MLS-11: (a) ethanol and (b) *n*-pentanol (adapted from Sillan et al., 1998).

Since the fluid residence times change during cosolvent flushing because of fluid property contrast, moment analysis of the ethanol BTCs would provide the average fluid residence time during the entire flood from cosolvent introduction to cosolvent elution. However, only the fluid residence times during cosolvent introduction are needed. Thus, estimates of fluid residence times during cosolvent introduction were determined by estimating the difference in the time at which 35% ethanol was detected at a sampler and the time at

which 35% ethanol was injected. This ethanol concentration was chosen because it is approximately 50% of the ethanol concentration injected at the end of the ramp. The fluid residence time using this method is essentially the median arrival time of the ethanol front since it is the temporal difference between the time of injection and the inflection point of the ethanol response curve at the MLS.

Because median and mean arrival times can be different due to skewed BTCs, the median arrival times of the non-reactive tracer bromide at each MLS were determined and used as an estimate of fluid residence time during water flooding. The median arrival time of the tracer at an MLS was estimated by the temporal difference between the time at which 50% of the tracer mass broke through and the time at which 50% of the tracer was injected. Figure 2-10a shows the spatial map of bromide median arrival time in a transect that coincides with MLSs-9, 10, 11, and 12 (EW-3 transect). This transect was chosen because a more complete ethanol data set was developed compared to the EW-1 and EW-2 transects. However, the overall trends in the hydrodynamics during cosolvent flushing (discussed below for the EW-3 transect) were similar in the EW-1 and EW-2 transects.

The distribution in fluid residence times as determined by median arrival times is compared in Figure 2-10b to the fluid residence times presented earlier (Figure 2-5) based on mean arrival time. As expected, the ratio of mean to median arrival time should be ≥ 1 at all locations within the transect because of the positively skewed BTCs. Although the overall spatial trend in residence times in Figure 2-10 matches well with the data in Figure 2-5, the arrival time ratio near the clay interface shows that this region is characterized by extensive tailing in the BTCs most likely due to higher hydrodynamic dispersion (higher media heterogeneity).

The spatial distribution of the ethanol median arrival time in the EW-3 transect is shown in Figure 2-11a. These data provide a spatial analysis of the fluid residence times or, inversely, the fluid flux during ethanol injection. Likewise, the median arrival time of the non-reactive tracer (Figure 2-10a) during the partitioning tracer test presents the spatial distribution of fluid residence times during a stable miscible displacement; thus, showing the effect of permeability heterogeneity on the distribution of local flux. By subtracting the ethanol arrival time from the tracer arrival time at each MLS, spatial variations in local fluid flux caused by fluid property contrasts are visualized (Figure 2-11b).

In Figure 2-11, shades that represent negative values indicate regions within the MLS-9 through 12 transect where the ethanol front took longer to reach than the non-reactive tracer front. Since, travel time or residence time is inversely proportional to velocity, negative values in Figure 2-11 represent areas of the flow domain where the local flux was slower during cosolvent introduction in comparison to the local flux during water flooding. Likewise, positive values in Figure 2-11 show areas where the local flux was faster during cosolvent introduction.

For the majority of the flow domain (represented by shades of green in Figure 2-11), the ethanol arrival time was not much different than the tracer arrival time indicating the change in local flux during cosolvent introduction was minimal.

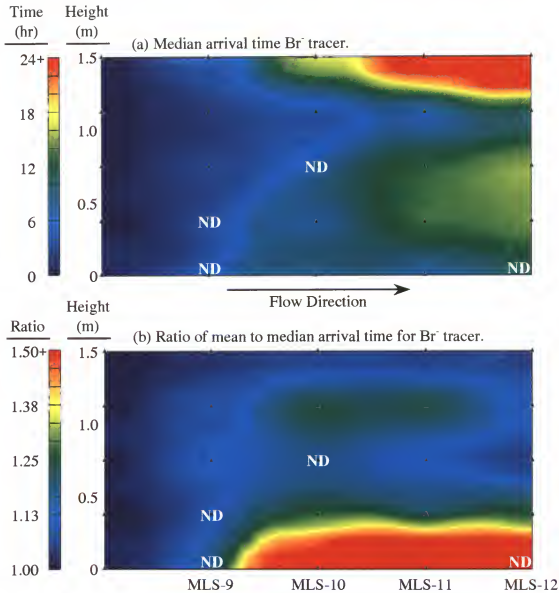

Figure 2-10. Spatial distribution of (a) fluid residence times along the EW-3 transect during water flooding based on median arrival times of bromide during the partitioning tracer test and (b) the ratio of mean to median arrival times (ND = no data).

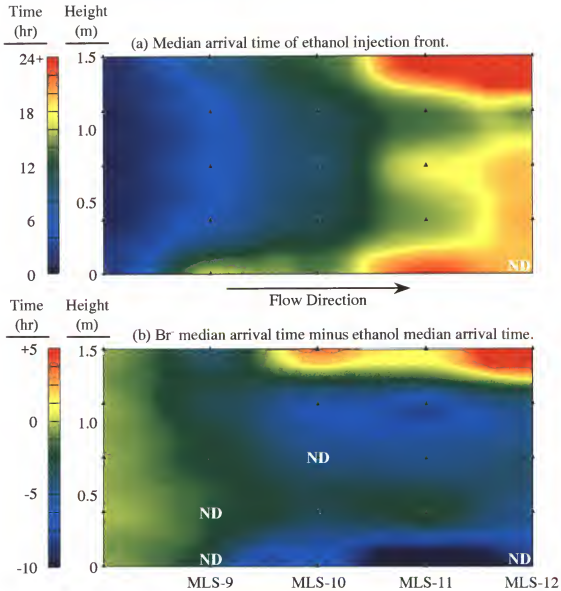

Figure 2-11. Spatial distribution of (a) fluid residence times along the EW-3 transect during cosolvent injection based on median arrival times of ethanol and (b) the difference between local fluid residence times during water flooding (Figure 2-10a) and ethanol injection (ND = no data).

However, two zones of significantly differential flux are shown at the top and bottom of the latter half of the flow domain. The MLSs located in the latter half of the upper portion of the flow domain are in the capillary fringe. Figure 2-11 shows that during cosolvent introduction the local flux in the capillary fringe increased. This increase in flux is likely the result of two effects: (1) buoyancy forces that can cause the less-dense cosolvent mixture to preferentially flow into the capillary fringe, and (2) the collapse of the capillary fringe. Likewise the preferential flow of the ethanol into the capillary fringe reduced the flux of the cosolvent solution through the bottom portion of the flow domain. In general, the analysis shown in Figure 2-11 indicates that only a small portion of the flow domain showed significant variations in local flux caused by fluid property contrasts. However, the slower flux through the portion of the domain near the bottom can reduce the overall effectiveness of the cosolvent flood especially if this region has a high NAPL content.

During the water flood, which started at approximately day 11, water tended to underride the less-dense cosolvent mixture in the capillary fringe, essentially trapping the cosolvent there for several days after water flooding began. This phenomenon is evidenced in Figure 2-12 which shows the spatial average of the ethanol concentration measured at the uppermost sampler of all of the MLSs at selected times after water flooding began. Even after 12 days of water flooding (t = 23 d), the average ethanol concentration in the capillary fringe is approximately 20% whereas the ethanol concentration in samples taken from MLSs below the water table are less than 0.1%. Note that the ethanol concentrations in Figure 2-12 decrease exponentially with time with the exception of the last point which appears to have decreased at a faster rate. Thus, the

capillary fringe acted as a cosolvent trap during water flooding and significantly increased the time over which remedial fluids were recovered from the test cell.

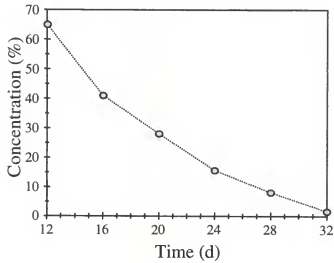

Figure 2-12. Spatial average of the ethanol concentration in the capillary fringe during water flooding (water flooding began on day 11).

2.2.2.2. Analysis of EW data

The measured changes in the alcohol concentrations in the extraction wells are compared in Figure 2-13. In all three wells, the ethanol breakthrough occurred just prior to displacement of approximately one pore volume (i.e., swept volume for that well). The initial sharp rise in alcohol concentrations was followed by an extended period of tailing for each of the cosolvent mixtures introduced. On the distal portion of the ethanol breakthrough curve, measured during water flooding of the resident cosolvent mixture, a sharp drop was followed by prolonged tailing of the ethanol concentrations. After displacing more than eight pore volumes of water through the test cell, ethanol concentrations were approximately 1% (volume basis). Similar patterns observed in the

ethanol elution were also evident for the *n*-pentanol breakthrough in all three wells (Figure 2-13b).

Extensive tailing during the injection and displacement of the cosolvent observed in extraction well fluids was attributed to a wide distribution of fluid travel times within the test cell (Rao et al., 1997). Factors that contributed to this distribution include the spatial heterogeneity of the porous media permeability; longer flow paths associated with the presence of a capillary fringe and the corrugations in the sheet pile wall design (Figure 1-5); and unstable flow effects resulting from differences in the density and viscosity of the resident and injected fluids.

2.2.2.3. Cosolvent Recovery

The total volume of ethanol recovered from the test cell was >99%, based on the data for ethanol breakthrough curves for the three extraction wells. After about three weeks of water flooding through the test cell, ethanol concentrations in the extraction well fluids were 200-300 mg/L, and the total volume of ethanol still remaining in the test cell was estimated to be about 60-80 L, which is <0.3% of the injected volume (about 33,000 L). In summary, the MLS and EW data illustrate the significance of the capillary fringe in prolonging the period over which the solubilized analytes and the injected remedial fluids are recovered. In confined systems or systems with a flow configuration that deliver cosolvents to regions well below the capillary fringe in an unconfined system, cosolvent hydrodynamics are not affected by travel through the capillary fringe. Thus, flow configuration, media heterogeneity, and fluid property contrasts determine cosolvent hydrodynamics.

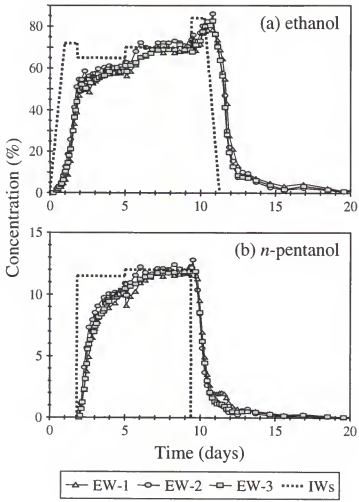

Figure 2-13. Cosolvent concentration (% volume fraction) in samples collected from the three extraction. Also shown are the ethanol and n-pentanol concentrations delivered to the injection wells (adapted from (Rao et al., 1997)).

2.2.3. Dynamics of NAPL Constituent Removal

The effect of cosolvent flushing on NAPL constituent dissolution over time and space was studied during the field experiment. Analyte breakthrough curves were generated at the extraction wells (EWs) and selected multi-level samplers (MLSs) for discussion. In order to describe the spatial behavior of the solubilized NAPL constituents during the cosolvent flood, data analysis was conducted on the chemical analytical results

for 1,2-dichlorobenzene and *n*-undecane in samples collected from the MLSs. These two constituents were present at larger mass fractions (0.006 for DCB and 0.016 for *n*-undecane) in the multi-component NAPL (Rao et al., 1997). DCB (Log K_{ow}=3.4) is representative of chlorinated solvents disposed at the site, while *n*-undecane (Log K_{ow}=6.0), the more hydrophobic of the two, is representative of *n*-alkanes found in JP-4 jet fuels, also disposed at the site. Analyte data from the spatial network of MLSs were used to produce three-dimensional snapshots of concentration distributions within the test cell at selected times. The measured data sets were interpolated to a uniform grid within the network of MLSs and visualized using GMS. The interpolation technique used was the same that was used to visualize the NAPL saturation data described earlier (Sect. 2.1.2.3).

2.2.3.1. Analysis of EW data

The breakthrough curve data for DCB and *n*-undecane monitored in the extraction fluids are presented in Figure 2-14. Significant solubility enhancement of the monitored NAPL constituents during cosolvent flushing is evident when compared to water flushing. For most target constituents, the concentrations in the effluent fluids are elevated by 2 or 3 orders of magnitude over corresponding values for resident groundwater before cosolvent flushing (Rao et al., 1997). The sharp increase in analyte concentrations was coincident with the breakthrough of ethanol for the less-hydrophobic constituents (e.g., DCB), whereas for the more-hydrophobic constituents (e.g., *n*-alkanes) the rise in concentration was delayed until the breakthrough of *n*-pentanol (Figure 2-14b). These field results are consistent with the general trends expected based on the corresponding cosolvency powers (see Table 2-2) for these solute-solvent combinations,

and demonstrates the need for addition of a stronger cosolvent (such as *n*-pentanol) to achieve sufficiently high solubility enhancement for this complex NAPL containing small amounts of a large number of diverse constituents. This distinction between remediation of sites contaminated with single-component NAPLs (e.g., PCE or TCE) and multi-component NAPLs (e.g., hydrocarbon fuels, coal tars) must be considered in designing site remediation strategies.

The breakthrough concentration profile for each NAPL constituent was integrated over the cumulative effluent volume (i.e., zero-th moment) to determine the total NAPL constituent mass removed during the experiment from each of the three extraction wells (Table 2-4). A general trend showing higher constituent mass removed from EW-3 than EW-1 and EW-2 was evident. This is in agreement with partitioning tracer test results that estimated NAPL volumes within the EW-3 swept volume were larger (Table 2-1). This trend was also observed in the MLS data which showed larger solubilized mass on the EW-3 side during cosolvent flushing (Sillan et al., 1998). The data in Table 2-4 also shows that EW-1 and EW-2 recovered approximately 30% each of the total mass extracted. EW-3 recovered 40% of the total mass extracted which is below the initial estimate of 50% of the NAPL in its swept volume based on the tracer test. This suggests that incomplete removal of the NAPL in the swept volume of EW-3 occurred and/or the swept volumes of the wells changed during cosolvent flushing.

An estimate of the NAPL volume present in the region, which was hydrodynamically-contacted during cosolvent flooding, can be estimated by dividing the total mass of a given constituent recovered in the extraction wells by the appropriate mass fraction and density of the NAPL (0.85 kg/L). Such a calculation yields NAPL volume

estimates of 256 L using DCB and 266 L using *n*-undecane. These values agree well with a NAPL volume of about 310 L in the test cell estimated from the pre-flushing partitioning test data (Table 2-1).

Table 2-4. Mass of selected NAPL constituents removed during cosolvent flushing (adapted from Rao et al., 1997). Note that the fraction (%) of total constituent mass recovered at each EW is shown in parentheses.

Target Analyte	EW-1 (kg)	EW-2 (kg)	EW-3 (kg)	Total (kg)
1,1,1-trichloroethane	0.0032 (25)	0.0043 (34)	0.0052 (41)	0.0127
p-,m-xylene	0.061 (30)	0.059 (29)	0.083 (41)	0.203
1,3,5-trimethylbenzene	0.121 (31)	0.110 (29)	0.154 (40)	0.385
1,2-dichlorobenzene	0.424 (32)	0.357 (27)	0.545 (41)	1.326
n-decane	0.596 (32)	0.534 (29)	0.733 (39)	1.863
n-undecane	1.14 (32)	1.06 (29)	1.42 (39)	3.62

2.2.3.2. Analysis of MLS data

Significant spatial variations in media properties, NAPL content, and flow dynamics are reflected in the analyte BTCs presented in Figures 2-15 and 2-16. BTC data are shown for several MLS locations along a transect at a single depth (Figure 2-15), and for different depths at a single MLS location (Figure 2-16). In both cases, data for sampling locations within the swept zone of EW-3 are shown. This region of the test cell is characterized by short travel times and high NAPL saturations (Sections 2.1.2.2 and 2.1.2.3). Also shown in Figure 2-15 are the zero-th temporal moments of the BTCs to assist the comparison of the dissolution behavior relative to location.

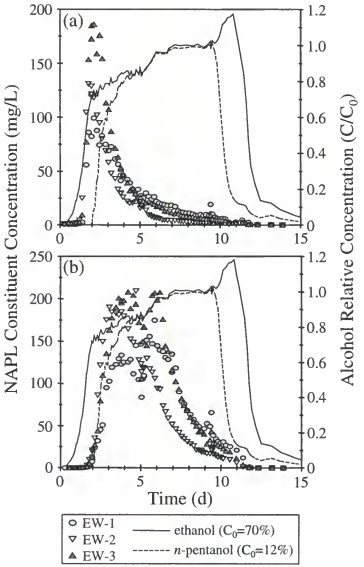

Figure 2-14. Concentration of NAPL constituents (a) 1,2-dichlorobenzene and (b) n-undecane in extraction well samples during cosolvent flushing. Also shown are the alcohol flux-averaged concentrations at the EWs (adapted from Rao et al., 1997).

NAPL analyte breakthrough at different MLS positions along a flow transect (Figure 2-14) do not necessarily follow the expected order based on their distance from the injection wells. While the analyte breakthrough does occur first at the closest location (MLS-9) for both analytes, breakthrough of *n*-undecane at the farthest location (MLS-12)

occurs prior to that at MLS-11 and nearly coincident with that for MLS-10 (Figure 2-15d). Also note that the breakthrough time for DCB was very close at all four locations. This was likely due to the short travel times for ethanol at this depth shown in Figure 2-11a. The zero-th moment data shown in Figure 2-15 is an indication of the cumulative analyte mass transported with time through the region sampled by the MLS. As expected the final value for the cumulative zero-th moment increased with distance along the transect as more NAPL was contacted by the cosolvent. However, the final zero-th moment for DCB was larger at MLS-11 than MLS-12. This indicates that the flux through the media sampled by these two samplers was significantly different and/or these two samplers could have sampled two significantly different paths taken by the analytes. It is important to note that the zero-th moment analysis presented here does not include estimates of the local flux; thus, comparison of the moments only allow comparison of cumulative mass flux between locations if the local fluid flux is similar between these locations.

The analyte BTC data in Figure 2-16 show the significant solubility enhancement of the NAPL constituents in response to the cosolvent arrival. The aqueous phase concentration of DCB began to increase sharply after the ethanol volume fraction in the resident fluid reached approximately 35%, while the more hydrophobic *n*-undecane did not begin to show significant solubility enhancement until the ethanol fraction was over 50%. The maximum DCB concentration at MLS-11 occurred in the 4.95, 5.33, and 5.72-m depths when the ethanol fraction was approximately 65%. With the arrival of *n*-pentanol from the second cosolvent mixture, the DCB concentration quickly decreased

after peaking, indicating that DCB in the flushed zone was being depleted via solubilization.

The solubility of *n*-undecane in the second cosolvent mixture (≈ 300 mg/L) was approximately 2.5 times greater than that in the first mixture resulting in a large increase in concentration coincident with *n*-pentanol breakthrough. Measured *n*-undecane concentrations at MLS-11 reached a maximum of approximately 250 mg/L in the second cosolvent mixture in the BTCs at the 5.33 and 5.72-m depths. The lower solubility limit of *n*-undecane (compared to DCB) coupled with a larger mass fraction in the NAPL caused elevated *n*-undecane concentrations to be sustained over a longer period. Higher concentrations of both analytes monitored at the 5.33 and 5.72-m depths were expected because of greater measured NAPL saturations at these depths compared to the 4.95 and 6.10-m depths (Figure 2-7).

A feature of the BTCs at the 6.10-m depth worth noting is the coincident reduction in analyte concentration as the *n*-pentanol and then ethanol were flushed from the test cell by water (at approximately 11 days). This indicates that the volume of cosolvent flushed through this region was insufficient to remove all of the DCB and *n*-undecane present. Exponential extrapolations of the BTCs at the 6.10-m depth (Figure 2-16d) show that continued flushing with cosolvent mixture #3 would have removed 4% more of the DCB and 16% more of the *n*-undecane mass. The extrapolations also show that approximately fourteen days of cosolvent mixture #3 delivery beyond the cutoff (9.3 days) would have been required to remove this additional mass.

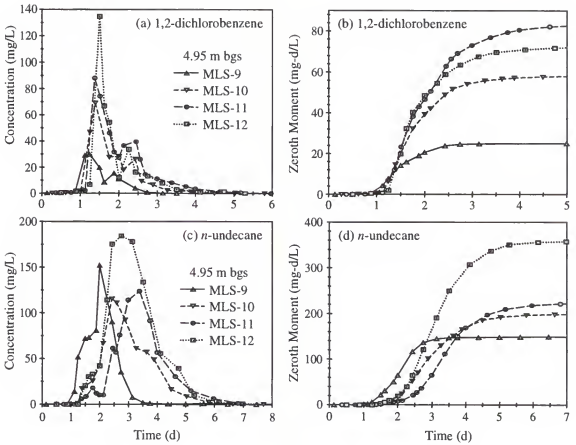

Figure 2-15. NAPL constituent response to cosolvent flushing at a single depth (4.95-m bgs) for four MLS locations along a line transect.

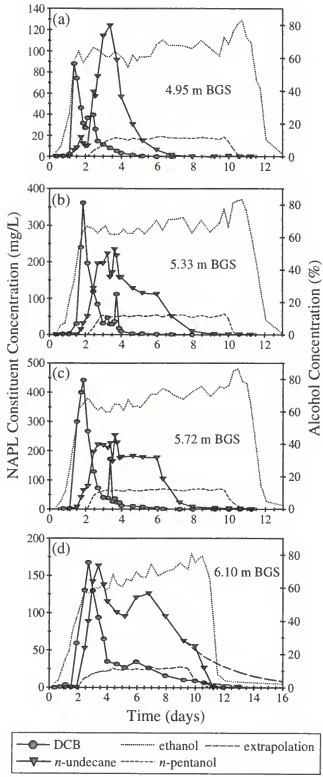

Figure 2-16. NAPL constituent (DCB and *n*-undecane) response to cosolvent breakthrough curves at four depths at a single MLS location: (a) 4.95, (b) 5.33, (c) 5.72, and (d) 6.10 m bgs (adapted from Sillan et al., 1998).

A feature of the BTCs at the 6.10-m depth worth noting is the coincident reduction in analyte concentration as the *n*-pentanol and then ethanol were flushed from the test cell by water (at approximately 11 days). This indicates that the volume of cosolvent flushed through this region was insufficient to remove all of the DCB and *n*-undecane present. Exponential extrapolations of the BTCs at the 6.10-m depth (Figure 2-16d) show that continued flushing with cosolvent mixture #3 would have removed 4% more of the DCB and 16% more of the *n*-undecane mass. The extrapolations also show that approximately fourteen days of cosolvent mixture #3 delivery beyond the cutoff (9.3 days) would have been required to remove this additional mass.

Thus, poor NAPL contact by the cosolvent observed in the lower depths near the clay unit led to lower removal effectiveness of the constituents. At the upper depths, the reduction in the analyte concentration to low levels (<1 mg/L) before water flooding began indicates that sufficient cosolvent volumes were flushed through these regions. This behavior translates to larger values of NAPL removal effectiveness, but also suggests that continued flushing of cosolvents at these depths would be economically inefficient.

Response to flow interruption. Two intentional flow interruptions were conducted during the cosolvent flushing experiment: a 40-hour period on day 5, and an 18-hour period on day 9. These interrupts were employed to detect non-equilibrium NAPL dissolution as evidenced by the occurrence of concentration spikes after flow is resumed (Brusseau et al., 1989; Pennell et al., 1994). No response in DCB concentrations was observed since at most MLS depths, much of the DCB mass had already been solubilized and flushed out before the first flow interruption. At the 5.72-m depth of

MLS-11, the resident *n*-undecane concentration was already near the solubility limit and no further increase was detected (Figure 2-16c). However, at the 6.10-m depth, a gradual rise in the *n*-undecane concentration for approximately 2 days was observed (Figure 2-16d). Detection of non-equilibrium dissolution effects at the aquifer-clay interface indicates that access of the cosolvent to the non-uniformly distributed NAPL may be hindered by the complex nature of the interface. Thus, low effective permeability in zones with high-NAPL content may enhance non-equilibrium NAPL dissolution.

A constituent concentration response, similar to the first flow interrupt, was observed in the extraction well fluids (Rao et al., 1997). However, the magnitude of the *n*-undecane response (peak concentration of 210 mg/L at EW-3) was too large to be entirely due to non-equilibrium effects observed near the clay interface (6.1 m bgs) because of the relatively low effective permeability of this region. Low effective permeability, as evidenced by later arrival of the cosolvent, implies lower cosolvent flux and a smaller contribution of analyte mass from this region to the flux-averaged concentrations measured in the extraction fluids. Thus, other factors discussed by Rao et al. (1997) (such as NAPL solubilized from the desaturated portion of the cone of depression around each extraction well, which is filled with cosolvent during the flow interrupt) may help explain the substantial concentration responses in the extraction well fluids.

Spatial trends in NAPL constituent solubilization. Analyte BTCs measured at all MLS locations were used to produce three-dimensional synoptic views of solubilization and transport of DCB and *n*-undecane during the cosolvent flood. Shown in Figures 2-17 and 2-18 are solid concentration iso-surfaces that enclose the regions

within the test cell where the constituent concentrations are >80 mg/L during the cosolvent flood.

Figure 2-17a and 2-18a indicate an initial northwesterly direction of NAPL removal (from IW-3 & 4 towards EW-3). This trend agrees with the data that show relatively shorter travel times (Figure 2-5) and higher NAPL mass (Table 2-1 and Figure 2-7) in this region (EW-3 transect) of the test cell. Shortly after the analytes breakthrough at the EWs (Figures 2-17b and 2-18b), the majority of the solubilized mass is within the region 0.2 to 0.8 meters above the clay and near EW-3. The upper portions of the flushed zone did show elevated analyte concentrations early in the flood but only on the EW-3 side. This agrees with the partitioning tracer data that shows NAPL located in the upper portions of the flushed zone on the EW-3 side (Figures 2-7a and 2-7b). These observations also support the data in Table 2-4, which show the largest constituent mass removal occurred at EW-3.

Evidence that the cosolvent took longer to flood the region near the clay interface is given by the gradual shift in the concentration iso-surface towards the bottom with time. This shift in the location of the solubilized mass at later times is also towards the EW-1 side of the test cell (Figures 2-17c-f and 2-18c-f) where high NAPL saturations are shown to exist near the clay interface in Figure 2-7c. Thus, larger constituent concentration tailing in the EW-1 fluids is expected and reported by Rao et al. (1997).

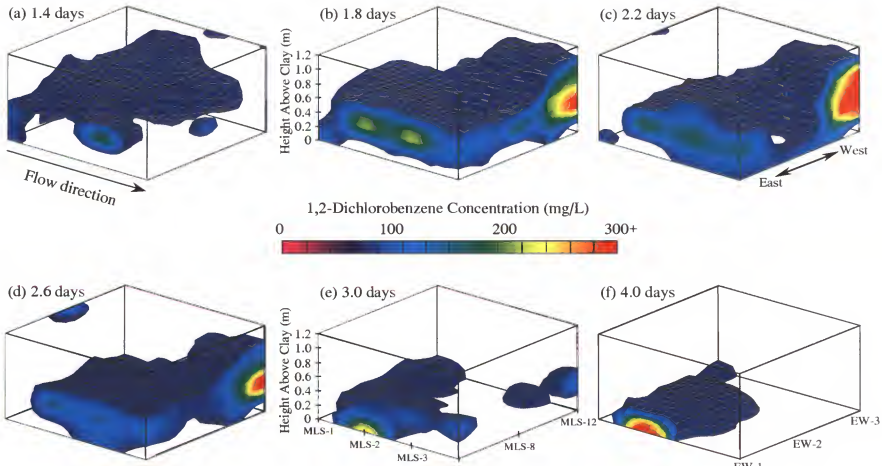

Figure 2-17. The 80 mg/L concentration isosurfaces for DCB at six times during cosolvent flushing: (a) 1.4, (b) 1.8, (c) 2.2, (d) 2.6, (e) 3.0, and (f) 4.0 days (adapted from Sillan et al., 1998).

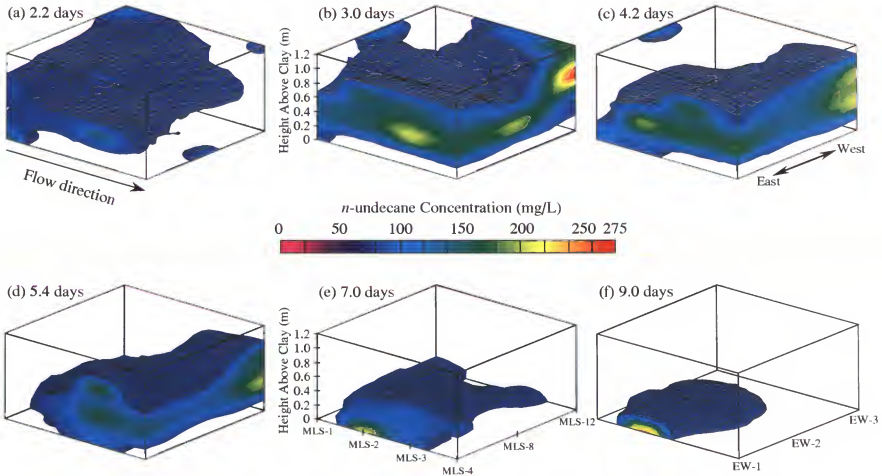

Figure 2-18. The 80 mg/L concentration isosurfaces for *n*-undecane at six times during cosolvent flushing: (a) 2.2, (b) 3.0, (c) 4.2, (d) 5.4, (e) 7.0, and (f) 9.0 days.

2.2.3.3. Summary

In summary, the NAPL constituent dissolution data showed that the mass removal effectiveness was greater in the upper zones than near the clay interface. Thus, less cosolvent contacted the large quantities of NAPL near the clay interface. It is likely that comparable NAPL removal effectiveness could have been obtained near the clay interface with continued flushing of cosolvent. However, this would have also flushed cosolvent through the relatively clean upper zones and reduced the overall efficiency of the technique when considering waste handling and costs. Thus, the data provides a strong argument for monitoring the progress of NAPL constituent removal during the cosolvent flood using strategically located multi-level samplers so adjustments can be made to focus delivery of the cosolvent to regions with low permeability and significant NAPL mass.

2.3. Performance Evaluation

The performance of in situ cosolvent flushing was evaluated using several methods. Comparison of NAPL constituent concentrations in ground water samples and soil cores taken prior to and after cosolvent flushing were reported by Rao et al. (1997) and indicated 90 to 99+% removal of selected constituents in the upper 1 m of the flow domain. However, these data also show that the NAPL constituent mass removal was significantly less, ranging from 50 to 75%, in the region immediately above the clay confining unit. Note that these removal effectiveness values are for individual constituents of the NAPL and are not easily converted to total NAPL mass or volume removed. The reason for this is due to the complexity of the NAPL composition and the

variability in solubility limits for the NAPL components in the cosolvent solution. This variation in solubility limits causes the constituents to be selectively dissolved from the NAPL. NAPL constituents with lower solubility limits in the cosolvent solution will be less effectively removed compared to constituents like DCB, which has a significant solubility enhancement. Thus, estimation of total NAPL mass removal using ground water and soil core samples would require that a large number of the NAPL constituents in the samples be identified and quantified. For NAPLs with many components like the Hill NAPL, this is usually not feasible. However, many sites exist that have single-component NAPLs, such as PCE, which would make the direct comparison of concentrations to evaluate the overall performance more reliable.

Another factor that adds uncertainty to performance evaluation using soil cores is the soil coring method, which provides point measurements of contaminant concentrations and requires spatial interpolation of sparsely-distributed data to estimate total NAPL volumes. In contrast, the partition tracers technique provides a spatially-integrated measure of the residual NAPL volume within the tracer flow domain. The combination of this spatial integration and the non-destructive nature of the test make the partitioning tracer test a valuable tool for performance assessment of in situ remediation technologies as well as for source zone characterization.

2.3.1. Post-Flushing Partitioning Tracer Test

After the cosolvent flood, a partitioning tracer test was conducted, using the same methods applied in the pre-remediation test (Annable et al., 1998), to produce a comparative data set for quantifying NAPL removal. Rao et al. (1997) presented the data from EW-2 and estimates of the total NAPL saturation reduction using the EW data.

Whereas, data from the multilevel samplers was presented by Sillan et al. (1998) and used to estimate the post-flushing NAPL distribution and the spatial variability in NAPL removal effectiveness.

Removal effectiveness is defined as the fraction of NAPL removed due to application of the remediation technology. The removal effectiveness can be determined using estimates of the NAPL volume as follows:

$$E_N = \frac{V_{N,pre} - V_{N,post}}{V_{N,pre}} \tag{2-1}$$

where $V_{N,pre}$ is the NAPL volume prior to cosolvent flushing and $V_{N,post}$ is the NAPL volume after cosolvent flushing. Substituting equation 1-13 into equation 2-1 and assuming that the tracer swept volume does not change, the NAPL removal effectiveness can be determined from NAPL saturation estimates at the multilevel samplers using:

$$E_N = \frac{\dfrac{S_{N,pre}}{1 - S_{N,pre}} - \dfrac{S_{N,post}}{1 - S_{N,post}}}{\dfrac{S_{N,pre}}{1 - S_{N,pre}}} \tag{2-2}$$

For NAPL saturation estimates below 1%, equation 2-2 can be approximated with the following expression:

$$E_N \approx \frac{S_{N,pre} - S_{N,post}}{S_{N,pre}} \tag{2-3}$$

The definition of NAPL removal effectiveness presented here (equation 2-1) differs from a previous definition presented in Sillan et al. (1998) where equation 2-3 was used to estimate the removal effectiveness at the MLSs.

2.3.1.1. Analysis of EW data

Post-flushing NAPL saturations were estimated using the BTC data for bromide and DMP at the three extraction wells (Figure 2-19). Prior to calculating the moments, the BTCs were extrapolated to account for tail truncation caused by ending the test before detection limits were reached. Extrapolations were performed by fitting a log-linear function to the data in the tail of the BTCs until normalized concentrations were reduced to 10^{-4} (Figure 2-19). A summary of the resulting moments and NAPL saturation estimates are presented in Table 2-5. The results indicate that the test cell average NAPL saturation after cosolvent flushing was 1%. This is the same value reported by Rao et al. (1997) that was based on the moments for the unextrapolated data.

The total reduction in NAPL volume based on pre- and post-flushing partitioning tracer tests results was approximately 260 L, which represents a removal effectiveness of 83% (Table 2-6). The lowest post-flushing NAPL saturation was detected in the swept volume of EW-2, which had the highest removal effectiveness of 87%. However, the extrapolation at EW-2 is also the most uncertain. The bromide data at EW-2 shows a second peak or bimodal distribution (Figure 2-19). This hump is not seen in the DMP data because of truncation. Thus, by not capturing the bimodal behavior in the DMP data, the moments and NAPL volume are under predicted at EW-2. The relatively lower recovery of DMP mass at EW-2 indicates this (Table 2-5).

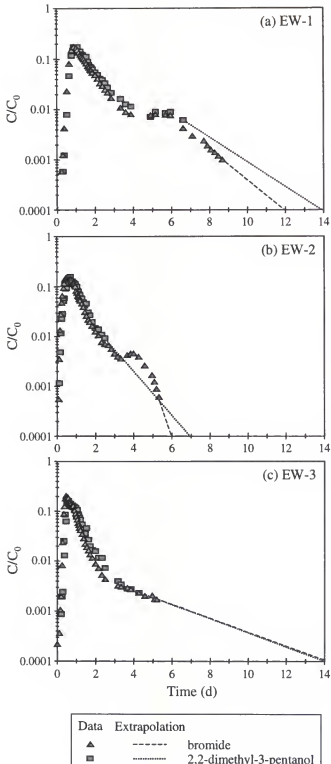

Figure 2-19. Post-flushing partitioning tracer test data measured at the EWs (input pulse time was 0.15 d).

Table 2-5. Mass recovery, well swept volume, retardation coefficient, and NAPL saturation estimates for the EWs.

Well	Bromide Mass[a] Recovery (%)	DMP Mass[a] Recovery (%)	Bromide V_S (m^3)	R	S_N
EW-1	31.6	32.9	1.87	1.14	0.010
EW-2	32.5	28.9	1.52	1.08	0.006
EW-3	31.2	29.7	1.75	1.17	0.013
Total	95.6	91.5	5.14		0.010

Note: DMP is 2,2-dimethyl-3-pentanol.
[a] Mass recoveries estimates are for unextrapolated BTCs.

As stated previously in Section 2.3, the composition of the NAPL is likely to change as a result of selective dissolution during cosolvent flushing. Since, the NAPL-water partition coefficient of the tracers is dependent on the NAPL composition, it is likely that the K_{NW} used to estimate the initial volume of NAPL in the test cell has changed; thus, using the same K_{NW} for both partitioning tracer tests would increase uncertainty in the post-flushing NAPL estimates and evaluation of the removal effectiveness.

Table 2-6. Comparison of NAPL saturation and volume based on PITTs conducted prior to and after the cosolvent flushing.

Well	Pre-flushing PITT		Post-flushing PITT		
	S_N	V_N (L)	S_N	V_N (L)	E_N
EW-1	0.031	67.5	0.010	19.6	0.71
EW-2	0.049	76.3	0.006	9.6	0.87
EW-3	0.088	166.0	0.013	23.0	0.86
Total	0.054	309.8	0.010	52.2	0.83

2.3.1.2. Analysis of MLS data

The BTCs from the post-flushing PITT (Figure 2-20) were used to evaluate the distribution of NAPL saturation within the test cell. Decreased retardation is evident in

the BTCs by comparing the partitioning tracer DMP to methanol, which was used along with bromide as a non-reactive tracer in the post flushing PITT. Methanol was compared to bromide and determined to be non-reactive based on first moments. The 6-methyl-2-heptanol (HEPT), used in the post-flushing IWPT, had retardation comparable to the DMP used in the pre-flushing PITT (Figure 2-6). Since the HEPT partitioning coefficient is three times larger than DMP this suggests a significant amount of NAPL was removed from the test cell. However, near the clay confining unit (Figure 2-20e), the retardation of DMP as well as HEPT is greater than at the upper depths indicating relatively higher NAPL saturations still remain near the clay.

Using average NAPL saturations measured before and after cosolvent flushing, NAPL removal effectiveness values were calculated using equation 2-2 and are reported in Table 2-7. The E_N results in this table should be viewed recognizing that each value represents a zone swept by the tracers between the injection wells and each individual multi-level sampling point. Thus, the "differential retardation" approach was not applied to the NAPL saturation values used to estimate S_N in Table 2-7. The resulting removal effectiveness values reported in Table 2-7 have a large range (19 to 93%). These values are approximately 1 to 2 % higher than those reported earlier by Sillan et al. (1998) because of the new definition for E_N (equation 2-2). Recognizing that these values represent an average removal along the integrated flow path from the IWs to the MLSs, the last row of samplers (MLS-4, 8, and 12) prior to the EWs provide an average removal for the test cell of 79%, which is not significantly different than a removal effectiveness of 82% determined by applying equation 2-2 to the S_N from the EWs in Table 2-6.

After applying the "differential retardation" approach to S_N estimates from the MLS data, the spatial distribution of the NAPL saturation was visualized using GMS and the technique described in Section 2.1.2.3 (Figure 2-21). The post-flushing S_N distribution shown in Figure 2-21 indicates that regions of the flushed zone that had the highest initial NAPL saturations ($S_N \geq 8\%$) in Figure 2-7 still contain NAPL but at significantly lower saturations ($S_N \approx 2\%$). The location of the highest post-flushing NAPL saturations shown in Figure 2-21b (near the clay interface and MLS-6) agrees with the concentration data shown in Figure 2-20e. This suggests that the longer travel times or slower cosolvent flux through this region of the flow domain (shown in Figure 2-5 and indicated by the non-reactive tracer BTCs in Figure 2-6e and 2-20e) reduced the amount of cosolvent available to solubilize the NAPL.

The vertical distribution in NAPL removal effectiveness was also reported by Rao et al. (1997) based on calculations using pre- and post-flushing soil cores. These values are compared to the removal effectiveness estimates in Table 2-7 from the partitioning tracer tests (Figure 2-22). The core data indicate higher removal effectiveness than the partitioning tracers. The core data was based on a single analyte (DCB) which had likely been preferentially removed by the cosolvent flushing process. Using this as a measure of remaining NAPL could be misleading as discussed in Section 2.3. The tracers had been sorbed by something remaining in the soil; however, it was likely that the composition of the NAPL had changed and therefore the partitioning coefficient may be different. Using the original NAPL-water partition coefficient may misrepresent the NAPL content.

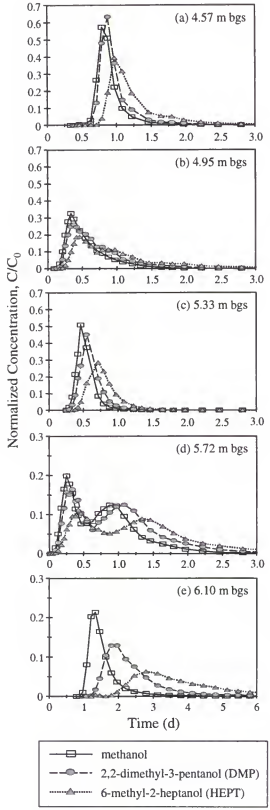

Figure 2-20. Post-cosolvent flushing nonreactive and partitioning tracer BTCs at all depths of MLS-6 (adapted from Sillan et al., 1998).

Table 2-7. NAPL saturation S_N and removal effectiveness E_N at the multilevel sampling locations.

Location	Depth bgs (m)	$S_{N,pre}$	$S_{N,post}$	E_N
MLS-1	4.57	…	0.003	…
	4.95	0.044	0.011	0.76
	5.33	0.047	0.008	0.84
	5.72	0.083	0.031	0.64
	6.10	…	0.014	…
MLS-2	4.57	0.005	0.004	0.19
	4.95	0.035	0.006	0.82
	5.33	0.036	0.013	0.65
	5.72	0.103	0.032	0.71
	6.10	…	0.004	…
MLS-3	4.57	0.004	…	…
	4.95	0.034	0.006	0.83
	5.33	0.048	0.006	0.87
	5.72	0.108	0.014	0.88
MLS-4	4.57	…	0.006	…
	4.95	0.028	0.007	0.77
	5.33	0.046	0.009	0.82
	5.72	0.104	0.018	0.84
MLS-5	4.57	…	0.013	…
	4.95	0.062	0.016	0.76
	5.33	0.068	0.018	0.75
	5.72	0.079	0.020	0.76
	6.10	0.048	0.008	0.85
MLS-6	4.57	0.015	0.010	0.34
	4.95	0.057	0.019	0.68
	5.33	0.050	0.012	0.77
	5.72	0.080	0.020	0.77
	6.10	0.046	0.032	0.32
MLS-7	4.57	…	0.004	…
	4.95	0.040	0.016	0.60
	5.33	…	0.014	…
	5.72	0.059	0.014	0.78
MLS-8	4.57	…	0.010	…
	4.95	0.032	…	…
	5.33	0.053	…	…
	5.72	0.068	…	…
MLS-9	4.57	0.108	0.029	0.75
	4.95	0.072	…	…
	5.33	0.080	0.023	0.73
	5.72	0.098	0.024	0.78
	6.10	0.064	0.005	0.93
MLS-10	4.57	0.074	0.016	0.80
	4.95	0.076	0.023	0.71
	5.33	0.026	0.018	0.30
	5.72	0.100	0.025	0.77
	6.10	0.072	0.014	0.82
MLS-11	4.57	0.042	0.015	0.64
	4.95	0.080	0.015	0.82
	5.33	0.082	0.021	0.76
	5.72	0.104	0.027	0.76
	6.10	0.029	0.015	0.50
MLS-12	4.57	…	0.009	…
	4.95	0.055	0.017	0.71
	5.33	0.088	0.016	0.83
	5.72	0.083	0.019	0.78

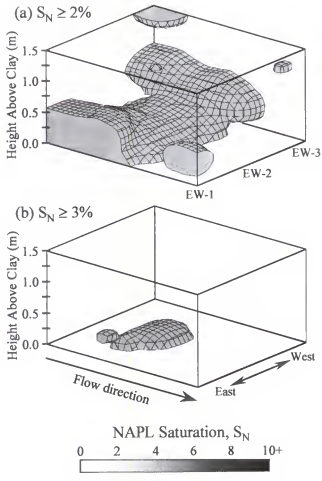

Figure 2-21. NAPL saturation (S_N) distribution after cosolvent flushing based on partitioning tracer test results (adapted from Sillan et al., 1998).

In the past year, two studies have shown how NAPL compositional changes influence the NAPL-water partitioning coefficients (Dwarakanath and Pope, 1998; Lee et al., 1998). Using the equivalent alkane carbon number (EACN) concept, Dwarakanath and Pope (1998) reported a decrease in the NAPL-water partition coefficient for DMP with increasing EACN of the NAPL (Figure 2-23). This behavior suggests, that by selectively dissolving the more-soluble, low-molecular weight compounds from the NAPL during a cosolvent flood, partitioning of the alcohol tracers into the NAPL would

decrease because of an increase in the fraction of higher molecular weight (higher EACN) components in the NAPL. This trend was confirmed by Lee et al. (1998) in batch and column experiments that showed a decrease in K_N after selectively dissolving constituents (using a cosolvent solution) from a NAPL collected at Hill AFB. Data reported by Lee et al. (1998) for three alcohol tracers showed an average decrease in K_{NW} of 20% after washing the Hill NAPL several times with a 60% *t*-butanol solution. This reduction in the K_{NW} would result in an over-prediction of S_N by approximately 20% for most retardation (R) coefficients. The implication of these observations is that the post-flushing partitioning tracer data presented here likely overestimated the NAPL removal effectiveness because of an unknown decrease in the NAPL-water partition coefficient. In contrast, Dai (1997) reported a 6.5 times increase in DMP partitioning in a coal tar contaminated soil after flushing with 200 pore volumes of methanol. This behavior was attributed to an increase in the exposure of the coal-tar NAPL to the tracer based on the likelihood that the methanol wash removed an interfacial film known to form quickly in coal tar-water and crude oil-water systems (Dai, 1997).

Thus, the change in NAPL-water partition coefficients as a results of remedial activities can reduce the reliability of using the partitioning tracers technique to evaluate the NAPL removal unless (1) the NAPL is primarily composed of a single component or (2) the partition coefficient of the tracer into the remaining treated NAPL can be measured or reliably predicted. Unfortunately, the complexity of the Hill NAPL did not allow prediction of K_{NW} using the EACN concept, and the reliability of the technique for measuring changes in K_{NW} using treated or washed NAPL in the laboratory is unknown because of its recent development. Another factor that may influence the reliability of the

post-flushing tracer study is the fact that soil surfaces are increasingly exposed to the mobile ground water as the NAPL is removed by the remedial flood. Thus, background adsorption of the tracers onto the soil surfaces becomes increasingly important and may cause an over-prediction of the remaining NAPL (or underestimate removal effectiveness). Thus, knowledge of the tracer sorption coefficients onto the soil and the organic carbon content of the soil also becomes increasingly important.

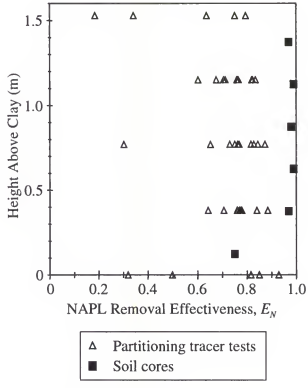

Figure 2-22. Vertical distribution of NAPL removal effectiveness determined from partitioning tracer tests data and soil cores.

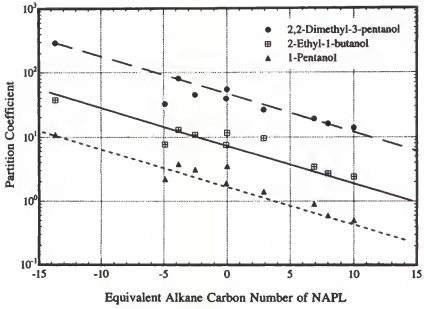

Figure 2-23. NAPL-water partition coefficient (K_{NW}) as a function of the NAPL's equivalent alkane carbon number (EACN) for three alcohol tracers (from Dwarakanath and Pope, 1998).

2.3.2. Efficiency and Effectiveness

Remediation efficiency typically refers to the rate at which the contaminants can be extracted from the contaminated media. More specifically, efficiency is defined as the amount of contaminant removed per amount of treatment applied. Whereas remediation effectiveness refers to the fraction of initial mass of the contaminant removed. In this section, quantitative definitions are derived for remediation effectiveness and efficiency in order to provide an alternative technique for evaluating the spatial variability in performance of in situ flushing technologies. Previously, Jawitz et al. (1997) presented techniques to evaluate remediation effectiveness and efficiency for the entire flow domain using spatially integrated data from soil cores and fully-screened extraction wells. In this section, data from the MLSs, which provides information at smaller spatial scales, is used

to estimate spatial variability in NAPL removal effectiveness and efficiency during the cosolvent flood.

2.3.2.1. Method development

Removal effectiveness. As stated previously in section 2.3.1, removal effectiveness is the fraction of the initial NAPL mass that is removed by cosolvent flushing. Here, estimates of initial and removed NAPL quantities are in terms of NAPL constituent mass, not NAPL volume as in equation 2-1. The amount of mass removed during the cosolvent flood is estimated from the NAPL constituent concentration data whereas the initial constituent mass present is determined from the pre-flushing partitioning tracer test. Thus, the following expression was derived to determine removal effectiveness (E) at a given time, t_1, during the flood:

$$E(\mathbf{x},t_1) = \frac{\textbf{Cumulative mass removed at } t_1 \textbf{ and } \mathbf{x}}{\textbf{Initial mass in flow path sampled at } \mathbf{x}} = \frac{Q_{aq}(\mathbf{x})\int_0^{t_1} c_i(\mathbf{x},t)dt}{V_{void}(\mathbf{x})S_N(\mathbf{x})\chi_i\rho_N} \qquad (2\text{-}4)$$

where Q_{aq}, V_{void}, and S_N are the aqueous volumetric flow rate, volume of void space, and average NAPL saturation in the flow path between the injection wells and a monitoring location with a coordinate $\mathbf{x}$ = (x,y,z). The expression in the numerator is the mass of constituent i solubilized from the NAPL by the remedial fluids in the flow path sampled at $\mathbf{x}$ at time t_1. When t_1 is the time at the end of the flood, the integral of the NAPL constituent concentration, c_i, is known as the zero-th temporal moment. The expression in the denominator is the initial mass of constituent i in the NAPL prior to remedial activities based on the initial NAPL saturation (as determined from the PITT), the mass fraction χ_i of constituent i in the NAPL, and the NAPL density (ρ_N).

In a two fluid phase system (water and NAPL) with no gas present, the volume of the void space in equation 2-4 is replaced with $V_{aq}/(1-S_N)$, where V_{aq} is the water-filled fraction of the pore space:

$$E(\mathbf{x},t_1)=\frac{Q_{aq}(\mathbf{x})}{V_{aq}(\mathbf{x})}\frac{\left[\int_0^{t_1} c_i(\mathbf{x},t)dt\right]\left[1-S_N(\mathbf{x})\right]}{S_N(\mathbf{x})\chi_i\rho_N} \tag{2-5}$$

The ratio Q_{aq}/V_{aq} can be replaced with the reciprocal of the fluid residence time to get the following dimensionless expression for the NAPL constituent removal effectiveness:

$$E(\mathbf{x},t_1)=\frac{\left[\int_0^{t_1} c_i(\mathbf{x},t)dt\right]\left[1-S_N(\mathbf{x})\right]}{S_N(\mathbf{x})\chi_i\rho_N\bar{t}(\mathbf{x})} \tag{2-6}$$

where $\bar{t}$ is the average aqueous-phase fluid residence time for the flow path between the injection wells and a MLS monitoring location with a coordinate $\mathbf{x}$ = (x,y,z). This substitution is made with the assumption that the change in V_{aq} during the remedial flood is insignificant. This is reasonable for systems with small initial S_N or in cases where the constituent of interest is removed while the bulk of the NAPL remains in the system. Also implied by this substitution is that the steady-state hydrodynamic conditions (e.g. head distribution and constant volumetric flow rate) are the same for both the pre-flushing partitioning tracer test and the remedial flood. These equations also assume that the initial constituent mass fraction and the NAPL density are spatially uniform. Note that equation 2-6 can be alternatively defined as the mass of NAPL removed per initial NAPL mass present based on constituent dissolution. In this case, the mass fraction (χ_i) is initially associated with the numerator in equation 2-4.

Removal efficiency. Removal efficiency has been previously defined as the amount of contaminant removed per amount of applied treatment (Jawitz et al., 1997). For enhanced dissolution of NAPL by in situ flushing, the definition used here for estimating local removal efficiency, ε, is the volume of NAPL solubilized per volume of remedial fluids applied:

$$\varepsilon(\mathbf{x},t_1) = \frac{\textbf{Volume of NAPL removed at } t_1}{\textbf{Volume of cosolvent applied at } t_1} = \frac{Q_{aq}(\mathbf{x})\left(\int_0^{t_1} c_i(\mathbf{x},t)dt\right)\left(\chi_i \rho_N\right)^{-1}}{Q_{aq}(\mathbf{x})\int_0^{t_1} f_r(\mathbf{x},t)dt} \tag{2-7}$$

where f_r is the volume fraction of remedial fluids (e.g. cosolvent fraction) at time t measured at a monitoring location, $\mathbf{x}$. In the numerator, the volume of NAPL solubilized is estimated from the NAPL constituent concentration breakthrough curve. Since Q_{aq} represents the volumetric flow rate through the monitored flow path in both the numerator and the denominator, equation 2-7 can be reduced to the following:

$$\varepsilon(\mathbf{x},t_1) = \frac{\int_0^{t_1} c_i(\mathbf{x},t)dt}{\chi_i \rho_N \int_0^{t_1} f_r(\mathbf{x},t)dt} \tag{2-8}$$

If the remedial treatment is a water flood (e.g. pump-and-treat), f_r is one and the integral in the denominator becomes t_1, elapsed time of the applied treatment. Equation 2-8 assumes that the NAPL density and constituent mass fraction are spatially uniform and independent of time. Thus, in situ flushing techniques that selectively dissolve constituents from the NAPL will cause estimates of the removal efficiency to differ

among constituents at the same monitoring location because of the temporally-varying mass fraction.

Contact ratio. The contact ratio is a measure of an in situ flushing technique's ability to deliver remedial fluids to the NAPL. Spatial variability in measured contact ratios indicate heterogeneous flow hydrodynamics and nonuniform NAPL distribution. The contact ratio (C_R) is defined below as the ratio of cumulative aqueous volume to initial NAPL volume in a flow path at time, t, after the start of the flood:

$$C_R(\mathbf{x},t) = \frac{Q_{aq}(\mathbf{x})t}{\dfrac{V_{aq}(\mathbf{x})}{\left[1 - S_N(\mathbf{x})\right]} S_N(\mathbf{x})} \tag{2-9}$$

As in equation 2-5, the expression Q_{aq}/V_{aq} is replaced with the reciprocal of the fluid residence time of the flow path monitored at $\mathbf{x}$:

$$C_R(\mathbf{x},t) = \frac{\left[1 - S_N(\mathbf{x})\right]}{S_N(\mathbf{x})} \frac{t}{\bar{t}(\mathbf{x})} \tag{2-10}$$

The contact ratio is estimated using NAPL saturations and non-reactive tracer residence times measured during a partitioning tracer test conducted prior to an in situ remedial flush. Spatial variations in C_R estimates can reveal locations within the flow domain where accessibility of the NAPL to the remedial fluids may be limited, thus prompting modifications to the remedial design in order to optimize fluid delivery and performance.

An alternate measure of C_R can be estimated by taking the ratio of removal effectiveness to removal efficiency (E/ε). This estimate of the contact ratio differs from

that defined in equation 2-10 because E/ε only accounts for the volume of the remedial fluids instead of the cumulative aqueous volume.

Application of the methods to hypothetical BTCs. In order to gain insight into the factors that determine the performance of in situ flushing, the performance metrics described above were applied to BTCs generated using two hypothetical models: (1) a plug flow assumption, which gives uniform BTCs, and (2) an advection-dispersion (A-D) model. In both cases, breakthrough of a remedial fluid is followed by the dissolution of a hypothetical NAPL with two components at equal mass fractions. The solubility of the second component in the remedial fluid is assumed to be approximately half that of the first component (Figure 2-24a and 2-24e). The simulations were done such that the remedial fluid injection was terminated soon after complete removal of both components.

Figures 2-24b and 2-24f show that the slope of the effectiveness function decreases with decreasing solubility limit. This is expected since it takes longer to remove components that are less soluble in the remedial fluid. Figure 2-24f also shows the long times required for complete removal caused by BTC tailing as a result of medium heterogeneities or nonequilibrium processes. Figures 2-24c and g show that the maximum removal efficiency of a component decreases with its solubility limit in the remedial fluid. The lag in the second component breakthrough in Figure 2-24e is similar to the field data presented earlier, which showed that the more-hydrophobic NAPL constituents (such as *n*-undecane) did not show significant solubility enhancement until the later arrival of *n*-pentanol. A comparison of the efficiency function between the two models also verifies the concept that hydrodynamic dispersion reduces the remediation efficiency achieved during in situ flushing.

Since remediation efficiency is defined as the NAPL volume removed per remedial fluid volume, the curves for the individual components in Figures 2-24c and 2-24g should eventually coincide because the total NAPL volume determined from component BTCs is the same for each component. However, incorrect estimates of the initial component mass fraction, which is used to convert component mass to NAPL mass, or incomplete removal of one component relative to the other will cause an offset in the efficiency curves. Another behavior of the efficiency curves worth noting is the endpoint constant value obtained once remedial fluids are no longer present. If delivery of remedial fluids continues after complete recovery of the components, the removal efficiency decreases with time as shown in Figure 2-24c between the time interval from 11 to 15. A comparison of Figures 2-24d and 2-24h shows how dispersion, characteristic of natural systems, reduces the efficiency during removal of the last fraction of NAPL remaining.

2.3.2.2. Analysis of field data

The measures of remediation performance metrics defined above were applied to the BTC data collected from the network of MLSs during the field experiments at the Hill AFB test site. Analysis of data from the cosolvent flushing experiment was limited to two constituents of the NAPL (1,2-dichlorobenzene (DCB) and *n*-undecane) present in large mass fractions.

An example of the method application to data from the 5.33-m depth of MLS-11 (Figure 2-16b) is presented in Figure 2-25. The removal effectiveness and efficiency as a function of time were estimated with equations 2-6 and 2-8 for both NAPL constituents (Figure 2-25). The average NAPL saturation and fluid residence time of the flow path

represented in Figure 2-25 were determined from the pre-flushing partitioning tracer test (Section 2.1.2.3). The density of the NAPL was 0.85 kg L^{-1}. Mass fractions for DCB (0.0061) and *n*-undecane (0.016) were reported by Rao et al. (1997).

The shapes of the effectiveness and efficiency curves obtained at the other MLS locations are similar to those shown in Figure 2-25. The time lag of the effectiveness and efficiency curves for *n*-undecane compared to DCB is a result of the later arrival of *n*-pentanol, different initial constituent masses, and different solubility limits of the constituents in the cosolvent mixture. Figure 2-25b shows that the NAPL removal efficiency based on *n*-undecane data was much less than that for DCB. This is a result of the lower solubility limit of *n*-undecane in the initial cosolvent mixture prior to *n*-pentanol arrival. Thus, a larger volume of cosolvent was flushed through the flow path before significant enhanced dissolution of *n*-undecane, which caused the removal of *n*-undecane to be less efficient.

The endpoint efficiency in Figure 2-25b indicates that approximately 8 mL of NAPL were removed per liter of cosolvent flushed through the region sampled by the 5.33-n depth of MLS-11. At maximum efficiency, the rate of NAPL removal using the data from both constituents ranged from 13 to 50 mL of NAPL per liter of cosolvent. This is much greater than a maximum removal rate during water flooding of 0.1 mL of NAPL per liter of water based on the measured aqueous solubility of DCB ($\approx$ 0.5 mg/L) from the multi-component NAPL.

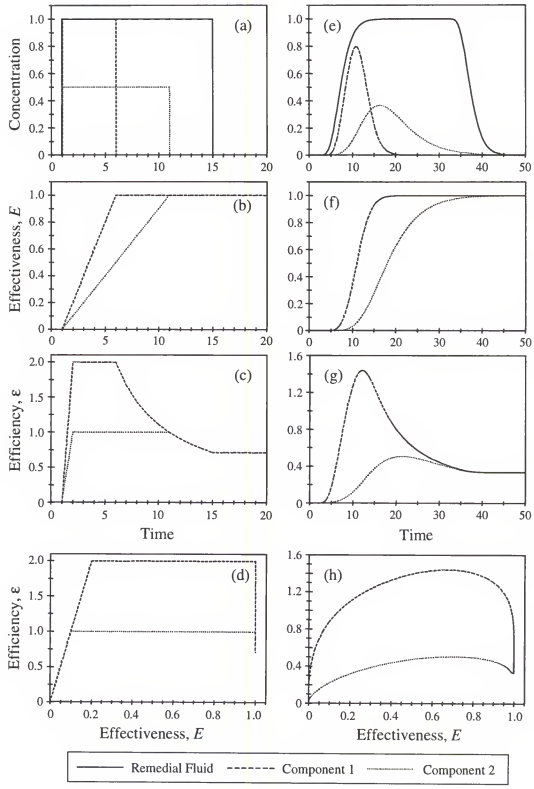

Figure 2-24. Concentration BTCs, removal effectiveness and removal efficiency in two systems (a-d: plug flow model, e-h: A-D model) with a two-component NAPL.

A plot of remediation efficiency as a function of effectiveness for the data in Figure 2-25 shows that the maximum efficiency occurred when approximately 50-60% of the constituent mass was removed from the NAPL (Figure 2-26). Although continued flushing beyond this level of effectiveness will remove more constituent mass, Figure 2-26 shows that the efficiency of the process quickly decreases. This demonstrates the difficulty and high cost of removing small amounts of NAPL mass that may have significant mass transfer rate limitations due to pore scale accessibility and larger scale heterogeneities in permeability and NAPL distribution. Techniques that may increase the efficiency by optimizing the amount of contaminant removed per cosolvent delivered are (1) flow interruptions to allow time for rate limited mass transfer processes to occur and (2) focused flooding, which targets larger quantities of cosolvent to locations where the NAPL is present. Although cosolvent recirculation can reduce the initial amount of cosolvent purchased, this technique would not improve the efficiency of the NAPL removal using the current definition for efficiency unless one or both of the two techniques described in the preceding sentence were implemented.

The removal effectiveness of the constituents at the end of the cosolvent flood, estimated from the data at each MLS location, is denoted here as the "endpoint removal effectiveness." Figure 2-27 shows that the endpoint removal effectiveness for DCB increased with depth. This trend does not agree with those observed in previous sections, which show a significant decrease in removal effectiveness at the clay interface based on analysis of pre- and post-flushing soil core and partitioning tracer data.

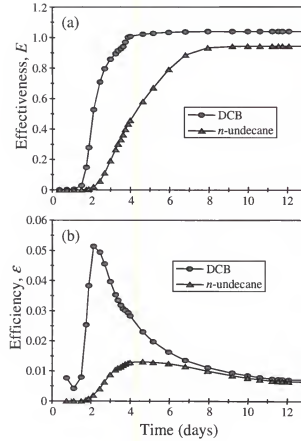

Figure 2-25. Removal (a) effectiveness and (b) efficiency for DCB and *n*-undecane as a function of time at the 5.33-m depth of MLS-11.

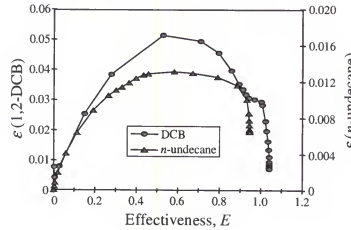

Figure 2-26. Efficiency as a function of effectiveness for DCB and *n*-undecane at the 5.33-m depth of MLS-11.

This observed difference could be caused by a number of factors. In equation 2-6, the most significant assumption was that the flow field during the partitioning tracer test was the same as that during the cosolvent flood. Fluid property contrasts in density and viscosity during cosolvent injection were shown to have slightly altered the local travel times especially near the bottom of the test cell (see Section 2.2.2.1 and Figure 2-11). Other terms in equation 2-6, such as constant χ_i and the value of S_N based on partitioning tracers, could also have an impact on the observed trend.

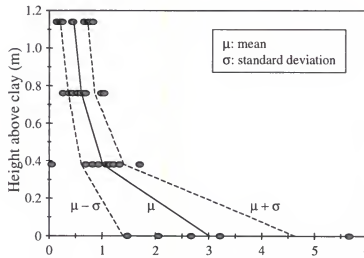

Figure 2-27. Endpoint removal effectiveness (DCB) as a function of multilevel sampler height above the clay.

The maximum removal efficiency, observed during the in situ cosolvent flushing test, was estimated at each MLS and is shown for DCB in Figure 2-28 as a function of height above the clay confining unit. An increase in maximum removal efficiency is noted with increasing depth. Cosolvent flushing through the region near the clay had higher maximum efficiency because of the presence of higher initial NAPL saturation and

longer cosolvent contact time (lower cosolvent flux). In contrast, in the upper zone, the initial NAPL saturation was lower and the cosolvent contact time was shorter. The resulting trend in maximum efficiency with depth may be caused by variability in initial NAPL saturation or the presence of non-equilibrium conditions during the cosolvent flood. Figure 2-29 supports the observed trend in efficiency, showing that the contact ratio decreased with depth, which indicates less cosolvent volume per NAPL volume. As a consequence, insufficient volumes of cosolvent were delivered and suggesting the NAPL removal would be less effective near the clay confining unit, which was observed in soil core and partitioning tracer data presented earlier. In summary, measures of the removal efficiency showed correlation with the contact ratio suggesting that the contact ratio may be used as a tool to determine optimal delivery of the cosolvent in order to maximize the removal efficiency of the NAPL.

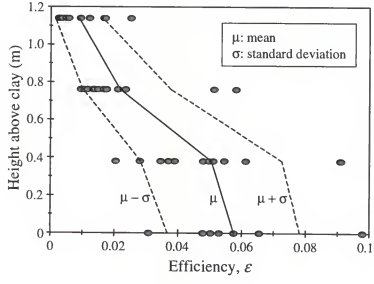

Figure 2-28. Maximum removal efficiency (DCB) as a function of multilevel sampler height above the clay.

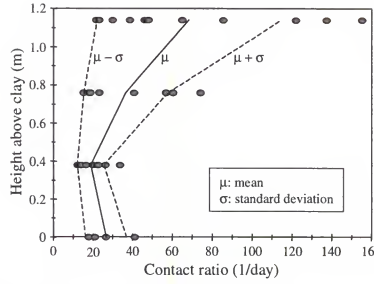

Figure 2-29. Contact ratio variability with height above the clay.

2.4. Summary

Although initial NAPL distributions within the test cell determined from soil coring and a partitioning tracer test agreed, the use of the partitioning tracers technique proved more advantageous by providing a spatially-integrated measure of NAPL volume accessible to flushing solutions. Another advantage of the tracers technique is the characterization of the hydrodynamic properties of the porous media, which can be used to assess the deliverability of treatment fluids to areas within the target flow domain.

In general, 50% of the NAPL volume was within the swept volume of one well (EW-3). Data from the MLSs and soil cores also show that most of the NAPL lies within the 1-m depth interval above the clay with the highest saturations located at 0.3 m within this zone. However, estimates of fluid residence times within this region indicate a relatively lower fluid flux near the clay, which suggests delivery of treatment fluids to this region may be difficult.

An evaluation of hydrodynamics during cosolvent introduction showed a decrease in fluid flux near the clay due to local flow instability effects. The data also showed the slow release of cosolvent trapped in the capillary fringe during water flooding, which substantially increased the time required to operate the system in order to reduce the cosolvent to low levels. Observations of NAPL constituent dissolution behavior agreed with the distributions in the NAPL saturation and fluid flux. Near the end of the cosolvent flood, high constituent concentrations near the clay indicated insufficient delivery of cosolvent to this region.

Post-flushing characterization with soil cores and partitioning tracers provided data to allow evaluation of the spatial distribution of the performance of cosolvent floods. The data showed that approximately 83% of the initial NAPL volume was removed. The removal effectiveness determined by soil coring shows that the upper 1 m of the flow domain had the greatest (90-99+%) removal whereas 70-85% removal near the clay was observed. The post-flushing NAPL saturation distribution agrees with this trend showing saturations >3% near the clay at MLS-6. Application of performance measures to the data provided a technique to quantify the ability to deliver the remedial fluid to the NAPL (contact ratio). In general, low permeability coupled with relatively high NAPL saturations in the region near the clay reduced the volume of cosolvent delivered to this region thereby removing less quantities of NAPL. However, a higher measure of efficiency in this region suggests that techniques to focus delivery of the cosolvent to this region and away from the upper cleaner zones would have been a valuable tool for optimizing the overall NAPL removed per cosolvent used. One technique that could have been used to focus delivery of cosolvent to the lower portion of the flow domain is the

use of well packers. By placing a well packer near the bottom of the flow domain, cosolvent could have been delivered below the packer forcing more cosolvent through this region, thus allowing the use of cosolvent to be optimized. This technique was used during the Sages site field study presented in chapter 3.

2.5. Recommendations

As described throughout this chapter, delivery of the remedial fluids to the NAPL is a factor controlling the performance of this and other technologies based on in situ flushing. Another problem encountered in technologies that deliver treatment fluids to the subsurface is the requirement (regulatory or technical) to remove the treatment fluid. When dealing with treatment solutions that have a density and viscosity different from water (such as cosolvent solutions), flow instabilities have shown to hinder delivery and recovery of the treatment fluid. To minimize this effect, the study presented in this chapter used gradient injections, which reduces the density and viscosity contrasts at the displacement interface in the subsurface. Unfortunately, gradient injection of the remedial fluids uses valuable time and cosolvent. Several researchers have shown that media heterogeneity can also act to reduce fluid property contrasts between two miscible fluids by increasing the length of the mixing zone between the two fluids in the subsurface, thus possibly negating the requirement for gradient injections (Waggoner et al., 1992; Tchelepi and Orr, 1994). Unknown, however, are the levels of media heterogeneity for specific fluid property contrast that determine the necessity for using gradients in the remedial design.

Thus, a recommendation for addressing these issues is offered here. One proposed course of action would be to investigate cosolvent flushing hydrodynamics in porous media with varying degrees of media heterogeneity. This investigation could be conducted primarily through numerical simulation of three-dimensional systems. The numerical model most likely suited for this study would be UTCHEM (Brown et al., 1994), which is a chemical flood simulator developed by the enhanced oil recovery industry. This code has been shown by Jawitz et al. (1998) to adequately model the affects of density and viscosity changes as a function of cosolvent fraction in two-dimensional miscible displacement floods.

Media heterogeneity can be characterized by two parameters: variability and correlation length. Simulations should investigate various heterogeneous structures to determine the sensitivity of the process to these two measures. An increase in media variability alone would likely increase the dispersion in the cosolvent displacement front thus reducing the occurrence of flow instability effects. However, large correlation lengths are indicative of media layering which could lead to viscous fingering.

In section 2.3.2.1, a measure that links the spatial variability of NAPL content to the hydrodynamic variability was presented as the contact ratio, C_R. This measure is obtained from the partitioning tracer test. Thus, the potential exist to use this measure to optimize delivery of cosolvents in situ provided a partitioning tracer test is used to characterize the contaminated region. Thus, the objective would be to focus and optimize the flow rates in order to reduce the spatial variability of the contact ratio. This concept was applied to the field study presented in the next chapter.

CHAPTER 3
SAGES SITE STUDY

3.1. Flow Configuration Design

Preliminary characterization work reported by LFR (Levine-Fricke-Recon, 1998b) was conducted using direct push technologies in order to estimate the extent of the free-phase PCE contamination at the Sages site. These data showed that the source area had an oblong shape that was approximately 7.3 m by 2.7 m (24 ft by 9 ft) (Figure 3-1). Also shown in Figure 3-1 is the suspected location of PCE release into the subsurface through a sump opened directly to the subsurface. In the area near the sump, the vertical extent of the DNAPL was reported to be in the 7.9 m (26 ft) to 9.4 m (31 ft) range bgs. Data from this work also confirmed the discontinuity of the clay, which was encountered at 10.7 m (35 ft) bgs in DP500 but not at DP-501 through DP-503, which were sampled to a depth of 11.3 m (37 ft) bgs (Figure 3-1).

Based on the shape of the DNAPL source area, an initial plan was proposed to install two, four-spot well patterns that share one recovery well (RW), which gives a total of two injection wells (IWs) and five recovery wells (RWs) (Figuer 3-1). The odd shape of both the source area and the well pattern prompted concerns of the design's ability to (1) hydraulically contain injected fluids, and (2) provide adequate coverage of the source area. To address these concerns, numerical simulations of the hydraulics for several well

patterns were investigated using MODFLOW and MODPATH coupled within the Department of Defense Groundwater Modeling System (GMS) (Owen et al., 1996).

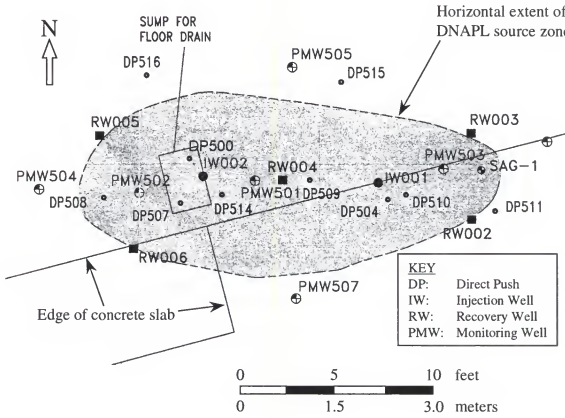

Figure 3-1. Approximate horizontal extent of free-phase PCE at the Sages site.

3.1.1. Flow Modeling Methods

The goal of the hydraulic simulations was to generate pathlines for different well configurations in order to observe coverage of the source area. Thus, an image of the source area shape was imported to GMS so simulation results could be displayed directly on the source area. A 58 x 32 x 1 grid was generated with a variable element size in the x and y directions (15 cm x 15 cm in the source area) and a uniform thickness of 1.5 m (5 ft). A constant head was assigned to the grid boundaries which were located

approximately 1.5 m (5 ft) outside the recovery wells. Thus, the regional gradient in the ground water table was not included in the model. The elements of the grid were assigned a porosity of 0.3 and a transmissivity of 9.3 m^2/d based on slug test data (Levine-Fricke-Recon, 1998c). The total rate of injection was set at 15.1 L/min (4 gpm), while the total extraction rate was 30.3 L/min (8 gpm). This 2:1 extraction ratio was required by the Florida Department of Environmental Protection (FDEP) to insure hydraulic containment of the injected fluids. The injection rate was equally distributed to the number of injection wells used in each model, whereas the extraction rates were distributed based on the number of wells and the geometry of the well pattern. Once the well configuration and flow rates were defined, steady-state hydraulic simulations were performed using MODFLOW, followed by the generation of pathlines using MODPATH.

3.1.2. Modeling Results

As stated previously, the initial well design was a double four-spot pattern with one shared recovery well. The total extraction rate from each four-spot pattern was 15.1 L/min (4 gpm), which was equally split to the three recovery wells. Because one of the wells is shared by each four-spot pattern (center well in Figure 3-2a), the extraction rate in that well was 10.1 L/min (2.67 gpm) compared to 5.0 L/min (1.33 gpm) in each of the other 4 recovery wells. The pathlines for this pattern (shown in Figure 3-2a) indicate that a large portion (≈30 to 40%) of the source zone would likely not be flushed by the remedial fluids. Thus, an alternate design was proposed to provide more uniform and complete coverage of the source area by adding one injection well and one recovery well (Figure 3-2b). A total of 15.1 L/min (4 gpm) was equally distributed to the three IWs arranged along the center of the source area. The six RWs were placed at the edges of the

source area to form 4:5:4 well pattern or 2 four-spots on either side of a five-spot pattern. The four RWs in the center five-spot pattern each had an extraction rate of 5.9 L/min (1.55 gpm), while the two RWs on the ends of the source area were assigned an extraction rate of 3.4 L/min (0.89 gpm). As indicated by the pathlines in Figure 3-2b, this well configuration provided better coverage of the source area than the original design. Thus, the well pattern shown in Figure 3-2b was chosen and implemented during site instrumentation. The "as-built" location of the wells and a description of materials and screened lengths were presented in section 1.4.2.3 and Figure 1-9. Note that this well pattern appears to create two locations within the source zone located between each pair of IWs where stagnation points may occur during the field experiments.

3.2. Site Characterization

3.2.1. Soil Coring

Figure 3-3 shows data obtained during a demonstration at the Sages site of a direct push technique to measure laser-induced fluorescence (LIF) of the subsurface. The spikes in the 8.5 to 8.8-m (28 to 29-ft) range indicate the presence of free-phase PCE (the LIF data were provided by Dakota Technologies Inc., Randy St. Germain). The sharpness of these spikes also indicates that the PCE likely exists as thin layers within the subsurface. Based on this information, a high frequency sub-sampling technique was developed to detect the presence of PCE in soil cores collected during installation of the wells and multi-level samplers.

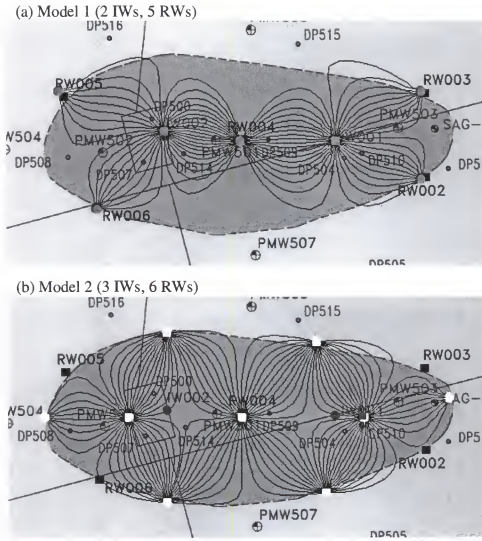

Figure 3-2. Pathlines generated by hydraulic modeling of two different well configurations: (a) 2 IWs and 5 RWs, (b) 3 IWs and 6 RWs.

3.2.1.1. Methods

Soil cores were collected at the site using two methods. During installation of the injection and recovery wells with a 10-in diameter hollow stem auger, a 2-ft long split spoon barrel with a diameter of 2 inches was hammered 2 feet below the bottom of the drill bit. At the surface, the core barrel was split in half leaving the soil cylinder intact. The other soil coring method involved the use of a cone penetrometer rig to push a 1.5-in

diameter, 20-inch long core barrel that was opened once the tip was at the sample depth. Soil cores were collected every two feet using both methods until the desired depth was reached for placement of a well or MLS. Sixteen locations (3 IWs, 6 RWs, and 7 MLSs) were cored. The location of these cores (recovery and injection wells and MLSs) is shown in Figure 1-9.

Once the soil cylinder was brought to the surface, aluminum foil was immediately placed over the soil to minimize volatile loss of PCE. Next, a PVC template with holes drilled every 0.1 feet was placed over the soil to guide sub-sampling efforts (Figure 3-4). Using 5-mL disposable syringes, which had been altered to allow collection of soil, approximately 3-mL of soil sample was extracted from the core at each template position. The sub-sample was immediately placed into 20-mL VOA vials containing 5-mL of methylene chloride and 5-mL of acidified water. The vials were stored on ice until delivery to the laboratory at UF for analysis of PCE content. The remaining soil core sample was placed in 20-mL scintillation vials and 1-pint mason jars.

Sample analysis. Laboratory analyses of PCE in the methylene chloride extracts was completed at UF using a Shimadzu 17-A GC equipped with a flame ionization detector (FID) and J. & W. Scientific DB624 (30m long, 0.53mm ID, 3um film thickness) capillary column. Carrier gas was high purity (99.999%) nitrogen. An initial column temperature of 60 °C was held for 3 minutes, then ramped up at 40 °C/minute to a final temperature of 200 °C. GC temperature zones were set at 150 °C for the injection ports and 220 °C for the detectors.

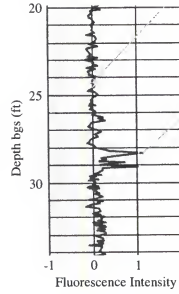

Figure 3-3. Laser induced fluorescence of subsurface as a function of depth.

Figure 3-4. High frequency soil sub-sampling template and sampled soil core.

Particle size distribution. The particle size distribution of six soil samples collected from MLS-1 were determined at UF using the American Society for Testing and Materials (ASTM) Method D422. The organic carbon and water content of these soils were also evaluated. Gravimetric techniques and overnight oven-drying at 110 °C were

used to determine water content. The Walkley-Black method (ASTM Method F1647-98) was used to determine the organic carbon content of the soil samples.

Water-solids partition coefficient for PCE. The soil-water partition coefficient for PCE was estimated using ASTM Method E1195. This analysis was performed at UF on soils collected from MLSs-5, 6 ,and 7. Methylene chloride extracts of soil subsamples collected at these locations showed little or no PCE present. The organic carbon content of the soils used in this analysis was estimated using gravimetric techniques and combustion in a muffle furnace at 450 °C. The organic carbon content of the soils using this method ranged from 0.9 to 3.7% and had a mean of 2.2%; whereas, the organic carbon content of a different set of Sages soil obtained from the Walkley-Black method ranged from 0.9 to 2.4% and had a mean of 1.7%. Although the organic carbon content determined though ignition had a larger maximum (3.7% compared to 2.4%) than that determined using the Walkley-Black method, the mean values were not significantly different.

3.2.1.2. Results

PCE soil concentrations. Soil concentrations of PCE indicative of free-phase presence were detected in soil cores collected from all three IW locations, RW-7, and MLS-1 (Figure 3-5). The high frequency sub-sampling technique delineated thin layers of PCE-DNAPL that did not appear to be horizontally continuous over the extent of the source zone. Although soil cores were collected over the entire vertical extent from 7.9 to 9.8 m (26 to 32 ft) bgs at the IWs and 7.6 to 9.4 m (25 to 31 ft) bgs at the RWs, several gaps exist in the data because of poor soil recovery during coring and collection of soil not representative of the depth cored caused by poor drilling techniques.

By assuming a particle density of 2.65 g/cm^3, a DNAPL density of 1.6 g/cm^3, and a porosity of 0.3; the PCE soil concentrations were converted to local estimates of NAPL saturation (S_N). These S_N values ranged from 12 to 35% for the high concentration layers detected at the three IWs and from 2 to 8% at RW-7 and MLS-1. Thus, PCE concentrations detected in soil cores using a high resolution sub-sampling technique show locally-high DNAPL saturations located in thin layers (5 to 8 cm thick) from 7.6 to 9.4 m (25 to 31 ft) bgs. An important consequence of this distribution is that a large fraction of the nearly uncontaminated aquifer must be flushed in order to contact the DNAPL present in a few thin layers. Thus, large volumes of tracer and cosolvent solutions are likely to completely bypass the DNAPL, making detection difficult and in situ flushing remediation an inefficient process.

Data from the soil core extracts shown in Figure 3-5 was used to estimate the volume of PCE within a volume of soil represented by the IWs and MLS-1. The approximate dimensions of this soil volume (5 m long, 1 m wide, and 2 m deep) represents an estimated 16,000 kg of soil based on an assumed bulk density of 1.6 g/cm^3. Two techniques were used to provide an average PCE soil concentration for this soil volume. The first technique estimated the average concentration in each core by integrating the mass over the length of the core and then dividing by the total length of the core (2 m). This technique assumes that locations in the core where no data is available have PCE concentrations of zero, and thus provides a lower bound to the mass estimate. The same mass integration from the first technique is used in the second but then divided by the length over which data was available. This technique assumes that available data (shown in Figure 3-5) is representative of PCE concentrations in the core

where no data was obtained. Thus, the volume of PCE in the source zone estimated from the PCE concentrations in the soil cores ranges from 15 to 40 liters. Assuming a porosity of 0.3, 40 liters of PCE in the soil volume of 10 m^3 provides an average S_N of 1.3 %.

Particle size distribution. The particle size distribution of soils collected during installation of MLS-1 is shown in Figure 3-6. On average 80% of the soil is classified as a fine sand with the next largest fraction (10%) being very fine sand. The distributions also show an increasing trend in fines (very fine sand to clay) content with depth to a maximum value of 19% at 8.8 m bgs. Below this depth, the fines content decreased with depth. When compared to the soil PCE concentrations in Figure 3-5e for MLS-1, the relative increase in fines content at the 8.8-m depth appears to have delayed the downward migration of DNAPL causing a thin layer to develop at this depth. The average water content of these soil samples was 19.7%, whereas the average organic carbon content was 1.7%.

Water-solids partition coefficient for PCE. Duplicate analysis of PCE sorption onto 12 soil samples provided an estimate for K_d of 0.33 mL/g with a 95% confidence interval of ± 0.04 mL/g. This value is significantly less than a range of 2.7 to 5.9 mL/g reported by (Roberts et al., 1986) in a fine to medium sand. Normalizing K_d with organic carbon content produced a K_{oc} of 15.7 mL/g with a 95% confidence interval of 2.9 mL/g. Assuming a soil particle density of 2.65 g/mL and a porosity of 0.3, a K_d of 0.33 mL/g predicts that 2.3 kg or 1.4 L of PCE are sorbed to the soil within the source area based on a well swept volume of 19,000 L (5000 gal) and an average aqueous concentration of 60 mg/L detected at the site.

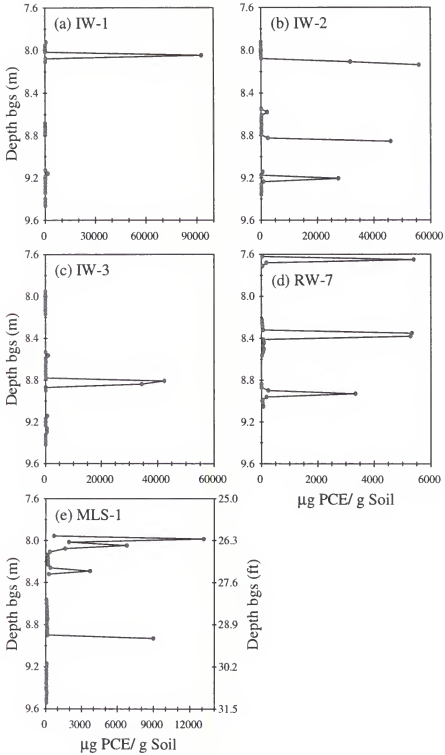

Figure 3-5. Vertical distribution of PCE concentration in soil samples collected from (a) IW-1, (b) IW-2, (c) IW-3, (d) RW-7, and (e) MLS-1.

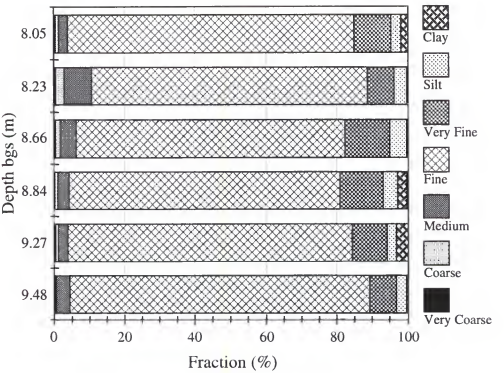

Figure 3-6. Particle size distribution of soil samples collected at various depths at MLS-1.

3.2.2. Partitioning and Interfacial Tracers Test

A partitioning and interfacial tracers test (see Saripalli et al., 1997, Annable et al., 1998, Rao et al., 1998) was conducted prior to cosolvent flushing in order to determine the quantity and distribution of DNAPL in the source area. In order to evaluate the field data, estimates of the NAPL-water partitioning coefficients (K_{NW}) for the tracers were determined in batch experiments.

3.2.2.1. Determination of partitioning coefficients

Methods. Batch experiments were conducted at UF with DNAPL collected from the site and a set of four alcohol tracers. The tracers used, listed in order of increasing hydrophobicity, were methanol, n-hexanol, 2,4-dimethyl-3-pentanol (DMP), and 2-ethyl-1-hexanol (e-HEX). Water to NAPL volume ratios of 45:1 and 5:1 were prepared in 20-mL and 5-mL vials with five different tracer solutions. These tracer solutions were made by diluting an initial concentration (2000 mg/L of methanol, 800 mg/L of hexanol, 400 mg/L of DMP, and 450 mg/L of e-HEX) of tracers 2.5, 5, 10, and 50 times. Each tracer solution was mixed with the DNAPL at a specified volume ratio in triplicate and allowed to mix overnight on a shaker table before analysis. A second set of batch experiments was conducted soon after the first by combining the initial tracer solution in vials at three different water to NAPL volume ratios (18:1, 25:1, and 33:1). This study was also conducted with triplicate batches at each tracer-NAPL combination. The analytical technique used to determine the equilibrium concentration of the tracers in the aqueous solution is described in section 3.2.2.2.

Results. The equilibrium concentration of the three partitioning tracers in the NAPL as a function of their aqueous phase concentration is shown in Figure 3-7. All three tracers show deviation from a linear partition coefficient at high concentrations. This non-linear behavior was observed by Dai (1997) for several alcohol tracers and NAPLs. At high concentrations, Dai (1997) showed that tracer isotherms approach Raoult's law behavior or ideal behavior. By plotting the tracer mole fraction in the NAPL against the equilibrium aqueous concentration divided by its solubility limit (Figure 3-8), the data is shown to be significantly different from ideal behavior (1:1 line) at the tracer

concentrations used in this study. Thus, the design of the field experiment should account for isotherm non-linearity by injecting a tracer solution that produces resident concentrations within the linear range of the partitioning data ($C_0 < 50$ mg/L for 2-ethyl-1-hexanol). Otherwise, an alternate method must be developed that allows for changes in the partition coefficient as a function of the aqueous tracer concentration. Partitioning coefficients for the tracer data in Figure 3-7 are presented in Table 3-1 along with the concentration range in which the value for K_{NW} is valid.

3.2.2.2. Field methods

After establishing steady-state flow using the average flow rate distribution listed in Table 3-2, three separate tracer injection programs were initiated: (1) a common suite of alcohol tracers delivered to all three IWs, (2) three sets of unique alcohol tracer pairs delivered individually to a single IW, and (3) an interfacial and conservative tracer pair delivered to all three injection wells (Table 3-3). The sequence and length of the tracer injections are also provided in Table 3-3. During tracer injections and the subsequent water flood to displace the tracers, the flow rates were maintained at the values listed in Table 3-2.

Table 3-1. NAPL-water partitioning coefficients.

Tracer	Linear Concentration Range (mg/L)	R^2	K_{NW}
n-hexanol	0 to 500	0.99	5.58
2,4-dimethly-3-pentanol	0 to 250	0.99	20.40
2-ethyl-1-hexanol	0 to 50	0.99	81.23

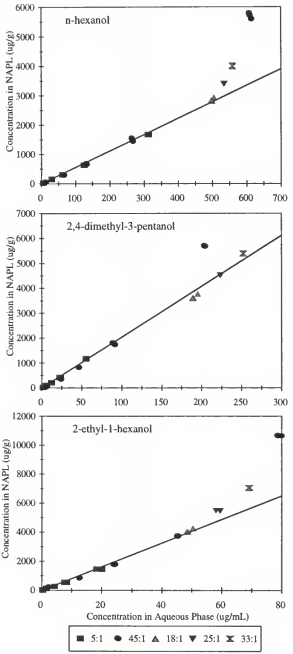

Figure 3-7. Alcohol tracer NAPL-water partitioning. Slope of line represents tracer partitioning coefficient.

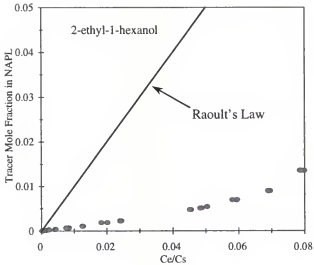

Figure 3-8. Comparison of normalized partitioning behavior of 2-ethyl-1-hexanol to ideal behavior (Raoult's law).

Table 3-2. Well flow rates and coefficient of variation.

Well	μ(Q), (Lpm)	CV(Q)*
IW-1	4.35	0.17
IW-2	7.02	0.25
IW-3	4.02	0.16
RW-2	-3.26	0.17
RW-3	-6.15	0.06
RW-4	-5.74	0.20
RW-5	-3.29	0.38
RW-6	-6.22	0.12
RW-7	-6.16	0.07

* Note: Coefficient of Variation, CV = σ/μ.

Table 3-3. Tracers used during the test, injected concentrations and duration of the injection.

Tracers		C_0 (mg/L)	Start Date & Time	t_0 (hr)
Common:	bromide as KBr	...		
	methanol	2199	08/01/98	3.8
	n-hexanol	822	15:40	
	2,4-dimethyl-3-pentanol	436		
	2-ethyl-1-hexanol	487		
Unique (IW-1):	isopropanol (IPA)	1910	08/01/98	4.7
	2-octanol	417	21:10	
Unique (IW-2):	t-butanol (TBA)	2664	08/01/98	4.7
	n-octanol	421	21:10	
Unique (IW-3):	isobutanol (IBA)	2177	08/01/98	4.7
	2,6-dimethyl-2-heptanol	417	21:10	
IFT:	iodide as KI	205	08/02/98	
	sodium dodecyl benzene sulfonate (SDBS)	48	02:30	12.5

Sample collection and analysis. Throughout the injection and displacement of the tracer solutions, samples were collected from the RWs, IWs, and MLSs at specified times in order to construct concentration BTCs. RW and IW samples were collected in 20-mL VOA vials, whereas MLS samples were stored in 5-mL vials with Teflon backed septa. After each sampling event, the sample vials were stored in an onsite refrigerator until delivered to the laboratory at UF for analysis. Analysis of alcohol tracers was conducted using either a Shimadzu 17-A or a Perkin Elmer Autosystem. Both GC's were equipped with flame ionization detectors (FID) and J. & W. Scientific DB624 (30m long, 0.53mm ID, 3um film thickness) capillary columns. Carrier gas was high purity (99.999%) nitrogen. The initial column temperature (60 °C) was held for 3 minutes, followed by ramping at 20 °C/minute to a final temperature of 200 °C. GC temperature zones were set at 150 °C for the injection ports and 220 °C for the detectors.

Analysis of the interfacial tracers (iodide and SDBS) was completed using a Shimadzu 10A-Class VP LC System. A Dionex IonPac 15cm, 4mm ID column, with same phase guard column, was incorporated in-line to a UV-VIS Detector set at a wavelength of 225nm. The mobile phase was a ternary mixture of 60% methanol, 24% water, and 8% acetonitrile containing 6mM tetrabutylammonium hydroxide (TBAH). The flow rate was regulated at a 1 mL/min.

Data analysis. Temporal moment analysis of the tracer data was limited to the common tracer suite detected at the RWs and MLS-4. Although a detailed analysis of the unique tracer data may further delineate the spatial distribution of the NAPL, partitioning behavior with the site DNAPL has not yet been investigated for the unique tracers for inclusion in this dissertation. Thus, estimates of the NAPL saturation and NAPL volume for the source area were determined from the set of common tracers measured at the RWs.

The equations outlined in section 1.3.1 were applied to the temporal moment estimates of the extrapolated tracer BTCs to determine the NAPL saturation and volume within the swept volume of each recovery well. Since the flow system at this site is not bounded by a physical barrier and required a 2:1 extraction ratio to ensure hydraulic control, the recovery wells draw in large amounts of ground water from outside the source zone. In this case, the swept volume for a single recovery well is defined as the volume of fluids delivered by the IWs, flushed through the source area, and then extracted by the RW. This is determined by modifying equation 1-11 to the following expression:

$$V_S = f_n Q_i t_n \tag{3-2}$$

where Q_t is the total injection flow rate, t_n is the mean residence time of the non-reactive tracer, and f_n is the fraction of the total mass of injected tracer recovered at the well. Thus, application of equation 3-2 at each recovery well allows estimation of the total volume swept by the injected fluids and the NAPL within this swept volume using equation 1-11.

Interfacial tracer test. An interfacial tracer test is a new method developed to measure the NAPL-water interfacial area per unit volume of porous media, a_{nw} (Annable et al., 1998a; Saripalli et al., 1997a; Saripalli et al., 1997b). This method is based on adsorption and retardation of surface-active chemicals at the immobile NAPL-water interface during tracer displacement through porous media. By measuring retardation of an interfacial tracer relative to a non-reactive tracer, the interfacial area can be estimated if the tracer adsorption isotherm is known. For interfacial tracers, the retardation factor is defined as (Saripalli et al., 1997b):

$$R_{ift} = 1 + \frac{K_i a_{nw}}{\theta_w} = \frac{t_{ift}}{t_n} \tag{3-3}$$

where K_i is the interfacial adsorption coefficient, which describes equilibrium adsorption of the tracer between the interface and the bulk solution. Since the sorption isotherm is nonlinear (function of tracer concentration), a constant K_i is approximated by using the surfactant concentration which best represents the solution monitored at a RW or MLS. This concentration is the maximum interfacial tracer concentration, C_{max}, observed at the monitoring point. This approach has shown to provide reasonable estimates of partitioning behavior (Annable et al., 1998a).

The interfacial tracer used in this study was sodium dodecyl benzene sulfonate (SDBS). The adsorption of SDBS or an anionic surfactant from dilute aqueous solutions at the NAPL-water interface can be described using Gibbs adsorption equation (Saripalli et al., 1998):

$$\Gamma = -\frac{1}{2RT}\left(\frac{d\gamma}{dC}\right)C \tag{3-4}$$

where Γ (mol/cm ^{2}) is the Gibbs surface excess of surfactant, γ (J/cm^2) is the interfacial tension between NAPL and water, C is the aqueous phase concentration (mol/mL) of surfactant, R is the universal gas constant and T (K) is temperature. Equation 3-4 is used to estimate the distribution coefficient (K_i) at the maximum tracer concentration (C_{max}) as follows (Saripalli et al., 1997b):

$$K_i = \frac{\Gamma}{C_{\max}} = -\frac{1}{2RT}\frac{d\gamma}{dC}\bigg|_{C\max} \tag{3-5}$$

where Γ is 1.446 x 10^{-10} mol/cm^2 for SDBS in PCE-water systems.

3.2.2.3. Analysis of RW data

The alcohol tracer breakthrough curves obtained at each RW are shown in Figures 3-9 and 3-10 along with the results of the exponential extrapolations on the tails to a C/C_0 of 10^{-4}. The extrapolations were performed on data in the tails that exhibited log-linear behavior. In some cases, data were ignored in the tails that appeared noisy or unreliable because of detection limitations or values below the sample analysis calibration range. Maximum C/C_0 values in the BTCs range from 0.02 to 0.25. These values are lower than typically encountered in tracer experiments because of the 2:1 extraction ratio, which diluted tracer concentrations in the RWs. One common characteristic of the BTCs at all

six RWs was the lack of separation in the BTC peaks. The only observable retardation in the partitioning tracers was in the tail data. Thus, detection limits and extrapolation techniques played a major role in the estimation of the NAPL content.

Methanol BTCs were used to estimate fluid residence times and the well swept volume (Table 3-4). The data show that RW-3 and RW-4 combined to recover approximately 50% of the injected tracer solution. Fluid residence times ranged from 14 hours at RW-4 to 39 hours at RW-5. RWs 6 and 7 had the largest swept volumes, which are a combined 48% of the total swept volume. These data indicate that the installed well pattern was not as symmetrical as the modeled design. This is mainly due to the location of IW-3, which was shifted towards RWs 3 and 4 during installation away from the center of the source area. Several of the wells and MLSs were installed slightly off of their initially designed location because of site accessibility problems due to equipment size and the location of the source area at the edge of an existing concrete pad.

The normalized first temporal moments of the partitioning tracers were corrected for the tracer pulse size and compared to the moment estimates for methanol at each location to calculate the retardation coefficients presented in Table 3-5. As expected, the retardation coefficients increased with the value of the measured partitioning coefficients. Hexanol retardation ranged from 1.01 to 1.15, which was slightly less than the values obtained for DMP (1.05 to 1.17). However, the retardation of these two tracers was below the suggested value of 1.2. Jin (1995) showed that, as retardation coefficients decrease below 1.2, the error in the saturation estimate increase rapidly. Thus, NAPL saturation estimates were determined using 2-ethyl-1-hexanol, which showed a range in retardation of 1.19 to 1.46.

The distribution in NAPL saturation and volume within the source area is shown in Table 3-6. The largest quantities of NAPL (>50% of the total) are in the swept volumes of RWs 3 and 7. These two wells are near and on opposite sides of the sump, which is the suspected point of DNAPL entry into the subsurface. The total predicted NAPL volume within the swept volume of the wells was 69 L, which gives an overall average NAPL saturation of 0.4%. Comparing this volume-averaged NAPL saturation to average discrete estimates from the soil cores (15%) suggests that the NAPL exist in thin layers which makeup approximately 3% of the vertical domain of the source area. Thus, a large portion of the flow domain appears to be uncontaminated with DNAPL.

The interfacial tracer data BTCs at the RWs are not presented because of problems with data reliability. Because the initial SDBS concentration was low (48 mg/L), dispersion in the media and dilution at the RWs reduced the concentration of SDBS at the RWs to levels difficult to quantify with current analytical equipment. However, the SDBS concentrations at some of the MLSs were reliable and permitted analysis of interfacial area at smaller scales monitored by MLSs.

3.2.2.4. Analysis of MLS data

Alcohol tracer BTCs observed at the five depths of MLS-4 are shown in Figure 3-11. Unlike the RW BTCs, a significant separation in the BTC peaks is evident indicating the presence of NAPL. The peak concentrations at these locations are also much larger than the RW data, which was expected because the MLS data are more representative of resident concentrations in the source zone, whereas RWs observe flux-averaged concentrations from the source area. The method of moments was applied to the data from MLS-4 to estimate NAPL saturations at smaller scales with depth.

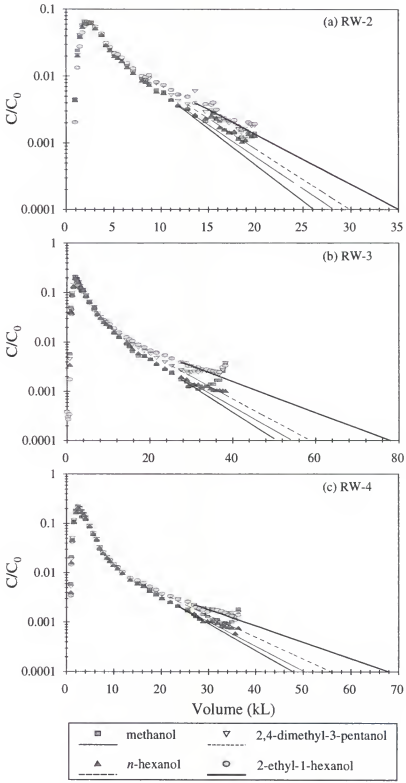

Figure 3-9. Alcohol tracer BTCs at (a) RW-2, (b) RW-3, and (c) RW-4.

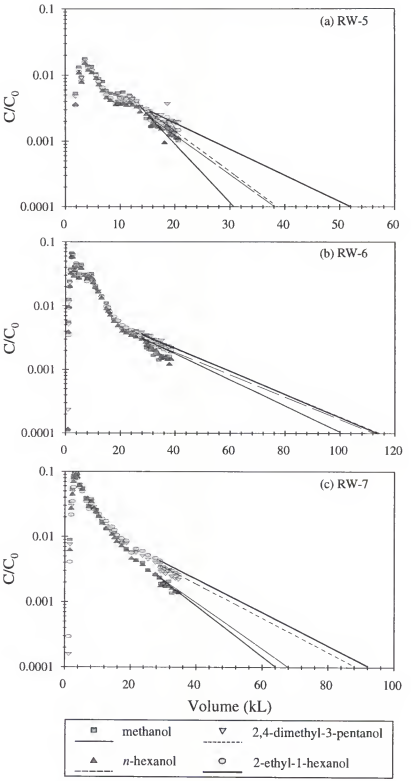

Figure 3-10. Alcohol tracer BTCs at (a) RW-5, (b) RW-6, (c) RW-7.

Table 3-4. Moment analysis results for the non-reactive tracer methanol.

Well ID	Fraction of Methanol Recovered, f_n	Methanol Residence Time, t_n (hr)	Swept Volume, V_S (L)
RW-2	0.074	22.4	1522
RW-3	0.243	14.5	3252
RW-4	0.232	14.1	3017
RW-5	0.031	39.1	1124
RW-6	0.153	33.5	4720
RW-7	0.171	23.0	3630
Total	0.903		17265

Table 3-5. Retardation coefficients relative to methanol for the three partitioning tracers.

Well ID	Retardation Coefficients, R		
	hexanol	DMP[a]	e-HEX[b]
RW-2	1.03	1.09	1.26
RW-3	1.04	1.13	1.45
RW-4	1.01	1.05	1.19
RW-5	1.15	1.17	1.46
RW-6	1.12	1.16	1.19
RW-7	1.05	1.31	1.48

[a] DMP: 2,4-dimethyl-3-pentanol
[b] e-HEX: 2-ethyl-1-hexanol

Table 3-6. Summary of NAPL saturation and volume estimates (based on e-HEX).

Well ID	NAPL Saturation, S_N (%)	NAPL Volume, V_N (L)	Fraction of Total NAPL (%)
RW-2	0.32	4.9	7.1
RW-3	0.55	18.1	26.2
RW-4	0.24	7.1	10.3
RW-5	0.57	6.4	9.3
RW-6	0.24	11.3	16.3
RW-7	0.58	21.3	30.8
Total	0.40	69.0	

At the same MLS locations, the interfacial tracer test data was processed using the method of moments and the techniques outlined in section 3.2.2.2. The SDBS and iodide BTCs at the 8.92-m (29.25-ft) depth of MLS-4 are shown in Figure 3-12. The NAPL saturation and interfacial areas at MLS-4 are summarized in Table 3-7. Also presented in the table is the ratio of interfacial area to volumetric content:

$$H_N = {a_n}/{\phi S_N} \tag{3-6}$$

This ratio was proposed by Saripalli et al. (1997b) and provides a measure of how the NAPL volume is distributed within the porous medium.

Table 3-7. Comparison of partitioning and interfacial tracer results at MLS-4.

MLS-4 Depth (m bgs)	Partitioning Tracer Test		Interfacial Tracer Test			
	R*	S_N (%)	K_i (10^{-3} cm)	R	a_n (cm^2/cm^3)	H_N (10^3 cm^{-1})
8.08	1.07	0.09	1.1	1.44	122	452
8.69	1.70	0.86	4.0	1.33	24.9	9.65
9.07	1.73	0.88	3.2	1.57	53.5	20.3
9.45	2.62	1.96	1.6	1.52	116	19.7
9.91	1.45	2.13	9.1	1.71	27.2	4.26

* Retardation coefficients are for 2-ethyl-1-hexanol except at the 32-foot depth where DMP was used.

At MLS-4 the NAPL saturation increased with depth from 0.09 to 2.13 %. The NAPL saturation measured at the bottom two samplers was around 2%, which is 5 times higher than the average saturation for the source area based on RW data. The maximum SDBS concentrations used to estimate K_i ranged from 5.5 mg/L at the bottom sampler to 47.2 mg/L at the top sampler. High values of H_N indicate that a NAPL has a large contact area and likely exist as coatings on soil. At the bottom four samplers, H_N is small indicating that the NAPL exists as patches of relatively high NAPL saturation. This

behavior was also observed in the soil core data (section 3.2.1.2). Thus, the MLS and soil core data show that the interfacial area per volume of NAPL is small. In terms of remediation, a low H_N indicates reduced efficiency because of limitations to NAPL dissolution across a relatively small interface.

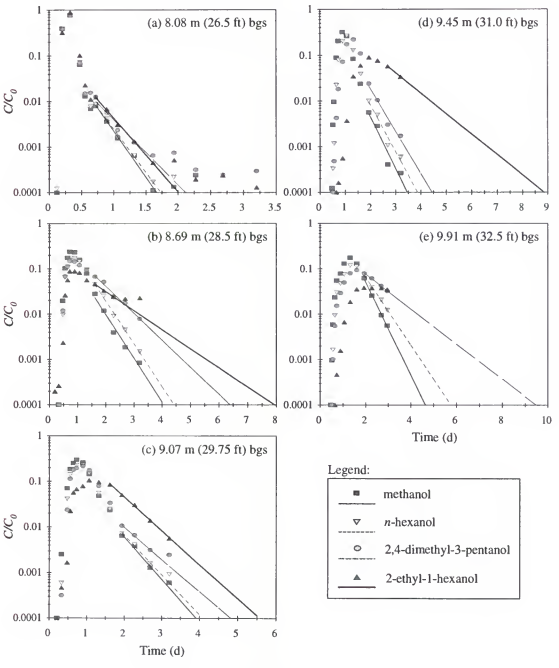

Figure 3-11. Alcohol tracer BTCs at the five depths of MLS-4.

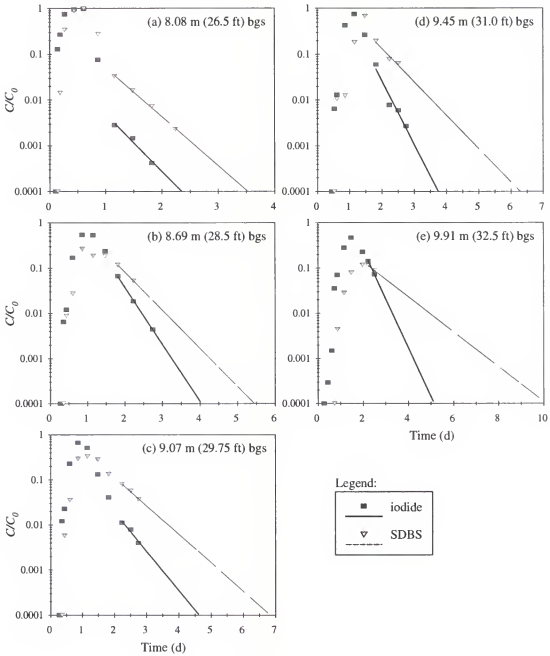

Figure 3-12. Interfacial tracer (SDBS) retardation relative to the non-reactive tracer iodide at the five depths of MLS-4.

3.2.3. Summary

In general, the data collected during site characterization suggests that the site DNAPL exists in discontinuous layers at relatively high saturations in the interval from

7.9 to 9.8 m (26 to 32 ft) bgs. Within the region of the aquifer swept by the well configuration, approximately 69 L of PCE was detected. Data from the interfacial tracer test indicates this NAPL volume has a low interfacial area, suggesting less than optimum contact of the NAPL by the PCE will occur during treatment. Based on this distribution of NAPL, a plan to focus delivery of the cosolvent solution to specified depths within the screened interval of the injection wells using packers was proposed.

3.3. Cosolvent Flushing

3.3.1. Field Methods

3.3.1.1. Cosolvent delivery

Approximately 34,000 liters of a 95% ethanol solution was delivered to the IWs during the cosolvent flood. In order to focus delivery of the cosolvent, a neoprene rubber well packer was placed in each injection well. Cosolvent was injected below the packer while potable water was injected above the packer in order to limit migration of the cosolvent solution into the aquifer above the packer. At each IW, the combined flow rate of water and cosolvent was held constant at 4.2 Lpm (1.1 gpm) for IW-1 and IW-3 and at 6.8 Lpm (1.8 gpm) for IW-2. The rate of cosolvent delivery (Q_c) to each IW was determined by the height of the packer (h) and the total flow rate per well screen length:

$$Q_c = h\frac{Q_t}{2.286\ \text{m}} \tag{3-7}$$

where Q_t is the combined flow rate of water and cosolvent to the well and 2.286 m (7.5 ft) is the screened length of the IWs. The water flow rate was the difference between the total flow rate and the cosolvent flow rate at each IW.

The height of the packer above the bottom of the well screen was initially set at 0.3 m (1 ft) in order to flush cosolvent into the region of the source area immediately below the lowest depth of detected free-phase PCE. By flooding this region with cosolvent before flushing the DNAPL-affected region, a barrier to downward mobilization of free-phase PCE was established. Thus, if free-phase mobilization of PCE from the contaminated region occurred at the cosolvent injection front, a layer of cosolvent solution was available below to solubilize the DNAPL that may have migrated from the contaminated region.

The concentration of ethanol in the cosolvent solution was ramped from 0 to 95% over 10 hours using a continuously stirred tank reactor (CSTR) that had a tank volume of 340 liters (90 gal). The gradient injection was applied in order to minimize density differences between the resident ground water and the injected cosolvent solution; thus reducing flow instability effects. After an additional 6 hours of cosolvent flushing beyond the gradient at the initial packer height, the packers were raised at a rate of approximately 15 cm (6 in) per hour to a maximum height of 1.7 m (5.5 ft) at IW-1 and IW-2 and 0.9 m (3 ft) at IW-3 (Figure 3-13). The maximum packer heights were chosen based on the location of DNAPL detected in soil cores. Seventy hours after the start of cosolvent flushing, the packers were lowered at the same rate to a final height of 30 cm (1 ft) (Figure 3-13). Water flooding over the entire well-screen interval started at approximately 3.5 days after the start of the cosolvent flood. This injection scheme placed more of the cosolvent in the lower portion of the DNAPL-affected area.

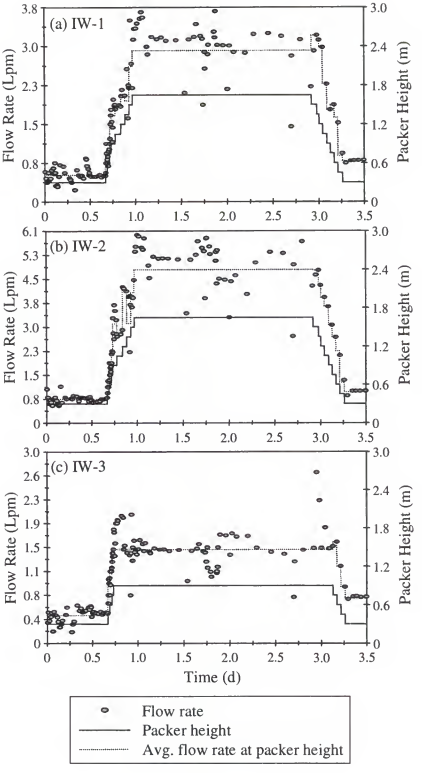

Figure 3-13. Flows rate of cosolvent solution delivered to the IWs below the specified packer height.

3.3.1.2. Sample collection and analysis

Samples were collected at the RWs and MLSs throughout the cosolvent and water floods to monitor PCE and ethanol concentrations. RW samples were collected in 20-mL VOA vials, whereas MLS samples were stored in 5-mL vials with Teflon backed septa. After each sampling event, the sample vials were stored in an onsite refrigerator until delivered to the UF laboratory for analysis. Ethanol and PCE concentrations were determined using the same GC techniques described earlier for the alcohol tracers (see section 3.2.2.2).

3.3.2. Analysis of RW Data

The initial flow rates from the RWs were similar to those applied during the tracer test. However, estimates of the contact ratio (C_R, see sect. 2.3.2.1 for definition) at the RWs during the tracer test indicated that these flow rates should be changed in order to flush regions that had the most NAPL with the most cosolvent. Thus, the flow rates at the RWs were changed at approximately two days into the cosolvent flood in order to improve cosolvent contact with the NAPL by making the C_R more uniform. The RW contact ratios from the tracer test and the flow rates during the cosolvent flood are listed in Table 3-8.

The optimal flow rates listed in Table 3-8 were determined by using equation 2-9 and setting the C_R to the average value of 317 for the total swept volume. It is important to note that using equation 2-10 to determine optimal flow rates assumes that the swept volumes are constant. However, swept volumes will change with the flow rate. Thus, changing the flow rates to the optimal values will likely make the contact ratio less variable but not equal. At the time of the flow rate change, analysis of the tracer test data

was incomplete and differed from the results in section 3.2.2.3. Thus, the new flow rates shown in Table 3-8 were not determined from the average C_R shown in Table 3-8.

Table 3-8. Optimal flow rates based on contact ratio estimates and the actual flow rates during the cosolvent flood.

Well ID	C_R (t=24 hr)	Optimal Q (Lpm)	Initial flow rate		New flow rate	
			μ (Q) (Lpm)	CV (Q)	μ (Q) (Lpm)	CV (Q)
RW-2	334	2.16	2.95	0.14	NC	
RW-3	299	7.91	5.57	0.12	3.26	0.09
RW-4	707	3.18	6.11	0.12	3.82	0.14
RW-5	107	2.84	3.14	0.16	NC	
RW-6	298	5.00	6.06	0.09	9.12	0.07
RW-7	179	9.31	5.67	0.13	8.03	0.17
Total	317	30.4	29.5		30.3	

NC: No Change

3.3.2.1. PCE dissolution

The ethanol and PCE BTCs at the 6 RWs are shown in Figure 3-14 and 3-15 (note that the range in values on the PCE and ethanol axis change with location). With the exception of RW-5 (Figure 3-15a, note that the maximum ethanol concentration at RW-5 was approximately 4.5 %), the PCE concentrations substantially increased with the arrival of ethanol at each well. At RW-5 the PCE concentrations did not increase beyond 2 mg/L (note that the step in PCE concentration at 4.75 days for RW-5 is a result of a change in analytical techniques from a GC method to a LC method). The highest PCE concentration (1300 mg/L) was observed in RW-7, which also had the largest initial volume of PCE in its swept zone predicted from the tracer test. Given that these PCE

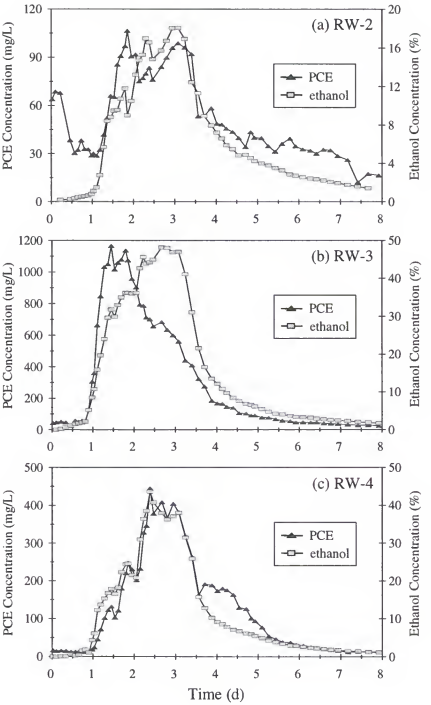

Figure 3-14. Ethanol and PCE BTCs at (a) RW-2, (b) RW-3, and (c) RW-4. Note that the scale of the PCE and etahnol axis change with location.

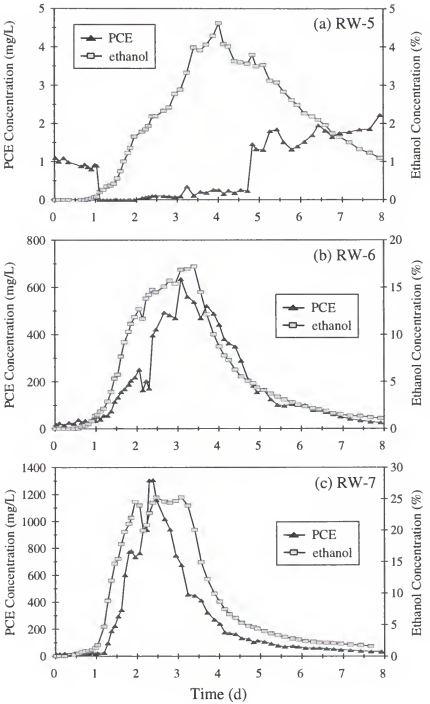

Figure 3-15. Ethanol and PCE BTCs at (a) RW-5, (b) RW-6, and (c) RW-7. Note that the scale of the PCE and etahnol axis change with location.

concentrations are diluted on average by a factor of two due to the over-extraction ratio, the depth- and flux-averaged concentrations of ethanol and PCE arriving at the RWs are likely to be twice the measured values shown in the BTCs.

At RWs 3 and 7, the PCE concentrations began to decrease prior to the start of water flooding; whereas at RWs 2, 4 and 6, the PCE concentrations decreased with the ethanol fraction indicating that continued ethanol flushing at these locations would have resulted in a larger mass of PCE recovered. By numerically integrating the PCE breakthrough curves as a function of cumulative pumped volume at each RW, the total mass of PCE extracted was 67.4 kg or 42.1 L (Table 3-9).

Table 3-9. Mass and volume of PCE extracted at the RWs during cosolvent flushing.

Well ID	Mass of PCE (kg)	Volume of PCE (L)	Fraction of Total (%)
RW-2	1.6	1.0	2.4
RW-3	17.0	10.6	25.2
RW-4	6.0	3.7	8.9
RW-5	0.04	0.02	0.06
RW-6	19.5	12.2	28.9
RW-7	23.2	14.5	34.4
Total	67.4	42.1	

3.3.2.2. Ethanol recovery

Integration of the ethanol breakthrough curves in Figures 3-14 and 3-15 estimates that 92% of the injected cosolvent was recovered 8 days after the start of cosolvent flushing (4.5 days after the start of water flooding). The distribution of the ethanol to the RWs shows that 23% of the ethanol was delivered to the swept volume of RW-7 which contained 31% of the initial NAPL (Table 3-10). The ethanol recovery at RW-7 would

have been less without the change in flow rates described in section 3.3.2. The recovery data also shows that very little (2.3%) of the injected cosolvent was captured at RW-5. Exponential extrapolations of these BTCs to an ethanol concentration of 0.01% (approximately 100 mg/L) increases the amount recovered to 97.5% (Table 3-10). Examples of extrapolated ethanol data are shown in Figure 3-16 for RWs 3 and 7. The extrapolations show that the additional time and pumped volume required to reduce the ethanol to 0.01% would have been significant. However, the estimated increase in the total pumped volume would likely be much less than 612,000 liters due to microbial degradation of ethanol once the levels fall below a tolerable level.

Table 3-10. Estimates of ethanol recovery for the raw and extrapolated data.

Well ID	Raw Data Recovery (%)	Extrapolated Recovery (%)	Additional Time with Extrapolation (days)	Additional Volume with Extrapolation (kL)
RW-2	5.9	6.4	13.4	56.8
RW-3	25.2	25.9	13.5	63.2
RW-4	17.7	18.2	11.2	61.7
RW-5	2.3	2.7	12.0	54.1
RW-6	18.3	19.6	12.6	165.0
RW-7	22.8	24.8	18.3	211.2
Total	92.2	97.5		612.1

3.3.3. Analysis of MLS Data

The ethanol and PCE breakthrough curves observed at MLS-4 are shown in Figure 3-17 for four depths. Prior to the arrival of ethanol at the MLSs, the concentration of PCE was around 70 mg/L (compared to a solubility limit of ≈ 200 mg/L). At approximately 1 day into the cosolvent flood, the arrival of ethanol increased the concentration of PCE to peak values ranging from 16,000 to 45,000 mg/L, which are 230

to 640 times larger than the background levels. The larger PCE concentration observed at the bottom two depths agrees with the tracer data that estimated larger NAPL saturations at these depths.

Since the MLSs monitored concentrations at the local scale within the source zone, the concentrations were expected to be larger than flux-averaged values observed at the RWs. The data in Figure 3-17 show that PCE concentrations within the source zone reached levels 40 to 112 times higher than the maximum PCE concentration (400 mg/L) observed at RW-4 (note that MLS-4 lies within the swept volume of RW-4, see Figure 1-9). The ethanol concentrations measured at MLS-4 were 90 to 95 %, which were approximately double the maximum value at RW-4 (45 %). These concentration differences highlight the inefficiency of flow designs such as the one used that have large dilutions at the RWs. Thus, measurement of the PCE concentrations at the MLSs provided more reliable estimates of the local solubility enhancement that can be achieved during cosolvent flushing.

3.3.4. Waste Treatment

In order to minimize cost associated with the disposal of waste containing high levels of PCE, a macro-porous polymer extraction (MPPE®) system (Figure 3-18) developed by Akzo Nobel was used to separate PCE from the extracted cosolvent solution containing ethanol, water, and dissolved PCE. This technology uses a porous polyolefin material with a proprietary extraction fluid immobilized within its structure (van der Meer and Brooks, 1998). During treatment, the waste stream was passed through a column containing MPPE® material into which the PCE preferentially partitioned. Removals of 99.99% have been demonstrated with this system (van der Meer

and Brooks, 1998). After loading with PCE, the columns were regenerated with low-pressure steam stripping. The steam vaporized the PCE from the MPPE® material and was then condensed and separated into free-phase PCE for disposal.

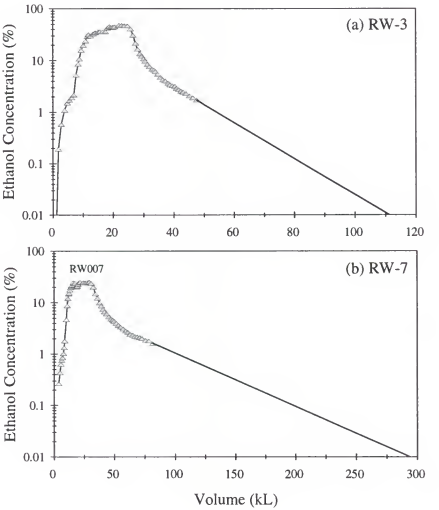

Figure 3-16. Ethanol breakthrough curves with extrapolated tails at (a) RW-3 and (b) RW-7.

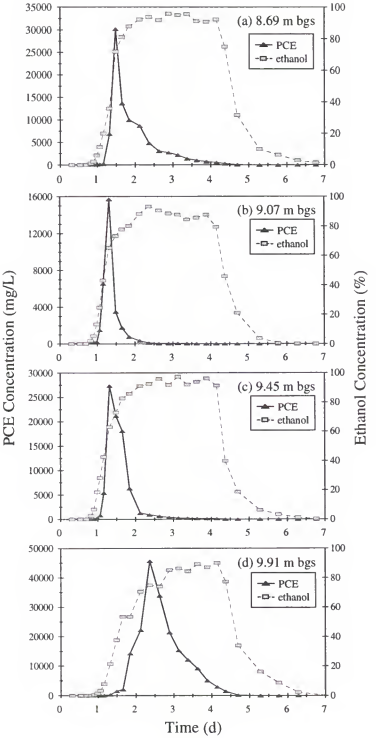

Figure 3-17. Ethanol and PCE BTCs measured at four depths of MLS-4: (a) 8.69 m, (b) 9.07 m, (c) 9.45 m, and (d) 9.91 m bgs.

Approximately 30 to 40 liters of PCE were separated from the waste stream by the MPPE® system. Compared to the initial estimate of the PCE volume from the tracer test (69 L), the PCE recovered by the MPPE® system represents a PCE removal of approximately 40 to 60 %. The treated water was stored in five 20,000-gallon tanks. Although the treated water had little or no PCE remaining, approximately 160,000 gallons were transported offsite for treatment at an industrial waste water facility because of the ethanol content.

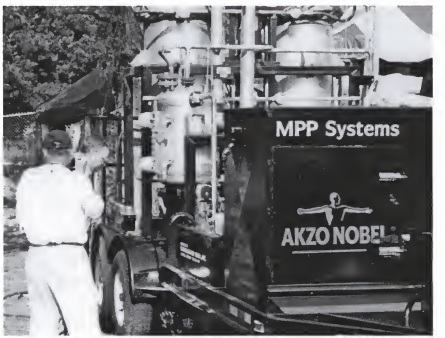

Figure 3-18. Trailer mounted macro-porous polymer extraction (MPPE®) system used to separate PCE from the waste stream.

3.4. Performance Evaluation

Soil coring and a partitioning tracer test were conducted after the cosolvent flood to evaluate the amount and distribution of PCE remaining. PCE concentrations in samples taken from the MLSs before and after cosolvent flushing are also used to evaluate the performance. Estimates of the measured effectiveness and efficiency at the scale of the RWs are also presented in this section to help evaluate spatial variability in the performance of the cosolvent flood.

3.4.1. Soil Coring

Soil cores were collected at six locations within the source area after the post-flushing partitioning tracer test. These cores were collected using the cone penetrometer technique described in section 3.2.1.1. Soils were sub-sampled into vials containing methylene chloride as in the pre-flushing cores but at larger intervals compared to the 0.1-ft spacing used previously. This larger interval was used to reduce the time and costs of the soil core analysis. Sub-samples from three of the cored locations (SPFC-2, SPFC-4, and SPFC-5) were analyzed at UF using the protocol described in section 3.2.1.1. Three other locations (SPFC-1, SPFC-3, and SPFC-6) were also cored but the sub-samples were shipped to the EPA's Kerr Lab for analysis. Data from these cores are not available. The locations of the post flushing cores relative to the wells are shown in Figure 3-19.

Plots of the vertical distribution of PCE soil concentrations at three locations are shown in Figure 3-20. These data suggest that soil concentrations indicative of free-phase PCE still remain in the 7.6 to 9.6-m bgs range. Figure 3-20a also shows a layer of PCE in a region that was not previously characterized.

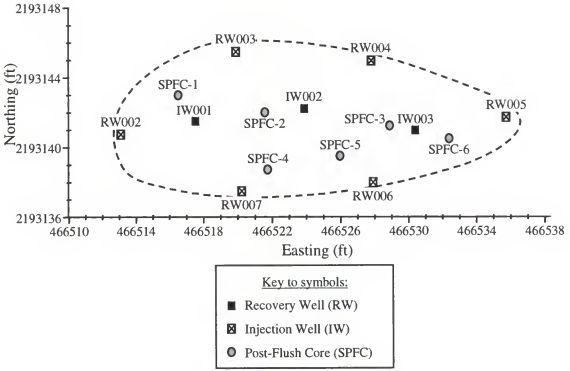

Figure 3-19. Location of the post flushing soil cores relative to the IWs and RWs.

Prior to cosolvent flushing the deepest core sample was from approximately 9.6 m bgs. Here, a soil sample from 10.4 m bgs shows that free-phase PCE exist below the zone treated during the cosolvent flood. The PCE volume represented by the data in Figure 3-20 is approximately 14 L (this value was determined using the same method that was applied to the pre-flushing cores). Comparing this PCE volume estimate to the value obtained from the pre-flush cores (38 L) provides an approximate PCE removal of 63 %.

3.4.2. Partitioning Tracer Test

3.4.2.1. Field methods

The post-flushing partitioning tracer test was conducted with a suite of five tracers delivered simultaneously to the IWs for approximately 3.6 hours (Table 3-11). In order to

compare the results from this test to the pre-flushing tracer test, flow rates were set to closely match the flow rates from the pre-flushing tracer test (Table 3-12). Sample collection and analysis methods were the same as described in section 3.2.2.2. The previously described GC method was used to analyze for the alcohol tracers, while the LC method was used to quantify the non-reactive tracer iodide.

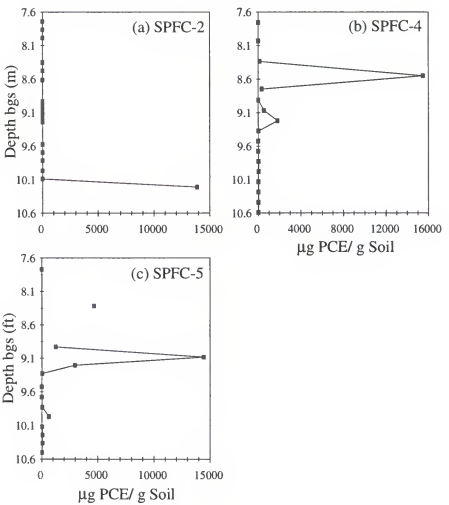

Figure 3-20. PCE concentration in soil cores collected after the cosolvent flood.

Table 3-11. Tracers and injected concentrations used during the post-flushing tracer test

Tracers		C_0 (mg/L)
Non-partitioning:	iodide as KI	116
	t-butanol (TBA)	1105
Partitioning:	*n*-hexanol	473
	2,4-dimethyl-3-pentanol	354
	2-ethyl-1-hexanol	457

Table 3-12. Average flow rate and coefficient of variation at each well.

Well	μ(Q), (gpm)	CV(Q)
IW-1	4.29	0.12
IW-2	7.06	0.07
IW-3	4.15	0.11
RW-2	-3.28	0.05
RW-3	-6.11	0.28
RW-4	-5.89	0.29
RW-5	-3.15	0.10
RW-6	-5.83	0.09
RW-7	-5.97	0.28

3.4.2.2. Analysis of EW data

During analysis of the samples, analytical interference problems were encountered which precluded quantification of the non-reactive tracers iodide and t-butanol. Thus, the three partitioning tracers were used to quantify the NAPL distribution using alternate forms of the equations presented in section 1.3.1. The average NAPL saturation (S_N) can be determined from the mean arrival time of two partitioning racers with the following (Jin et al., 1995):

$$S_N = \frac{t_2 - t_1}{\left(K_{NW,2} - 1\right)t_1 - \left(K_{NW,1} - 1\right)t_2} \tag{3-8}$$

If the retardation coefficient (R) is defined as the ratio of tracer arrival times, then equation 3-8 reduces to:

$$S_N = \frac{R-1}{K_{NW,2} - 1 - R\left(K_{NW,1} - 1\right)} \tag{3-9}$$

The partioning tracer data can also be used to determine the swept volume of a well (Jin et al., 1995):

$$V_S = \frac{Qt_1}{1 - S_N\left(1 - K_{NW,1}\right)} \tag{3-10}$$

where Q is the constant flow rate. However, the same modifications made in equation 3-2 to determine the swept volume contacted by the tracers is needed here:

$$V_S = \frac{f_1 Q_i t_1}{1 - S_N\left(1 - K_{NW,1}\right)} \tag{3-11}$$

where f_1 is the fraction of the total mass of injected tracer recovered at the well and Q_i is the total injection rate.

The tracer BTCs at RWs 3 and 7 are representative of the behavior observed at the other RWs (Figure 3-21). As in the pre-flush tracer data, tracer retardation is only observed in the BTC tails; thus making the moments and NAPL estimates sensative to the exponential extrapolations. The behavior of iodide in the BTC tail is believed a result of sample analytical problems; thus, the relative retardation of 2-ethyl-1-hexanol to *n*-hexanol was used to determine NAPL saturations and well swept volumes. Using equation (3-9) the average post-flushing NAPL saturation was 0.14% (Table 3-13). Note that this value has a larger uncertainty than the pre-flush estimate because of the reduction

in the retardation factors below 1.2 at all of the RWs except for RW-5. The total volume of NAPL remaining in the swept volume was estimated at 25.8 L. The tracer data also estimated an increase in the swept volume of 11%.

Table 3-13. NAPL satuartion and swept volume estimates for the post-flushing partitionig tracer test.

Well ID	Retardation, R		S_N	V_S	V_N
	DMP	e-HEX	(%)	(L)	(L)
RW-2	1.00	1.09	0.12	2294	2.8
RW-3	1.00	1.08	0.11	3710	4.1
RW-4	1.02	1.11	0.15	3354	4.9
RW-5	1.05	1.17	0.23	1544	3.6
RW-6	1.07	1.08	0.11	4240	4.6
RW-7	1.03	1.11	0.15	4016	5.9
Total			0.14	19157	25.8

3.4.3. Aqueous PCE Concentrations

Another technique used to evaluate the performance of the cosolvent flood is a comparison of the PCE concentrations prior to and after the cosolvent flood. Samples were collected from the MLSs immediately after they were installed and analyzed for PCE content. After all tests were completed, the MLSs were sampled on a monthly basis for three months and then each quarter thereafter. The data shows that the aqueous PCE concentrations did not significantly change due to cosolvent flushing.

3.4.4. Efficiency and Effectiveness

Based on the pre- and post-flushing estimates of the NAPL volume (V_N), the NAPL removal effectiveness (E) in the total swept volume according to equation 2-1 was 63% (Table 3-14).

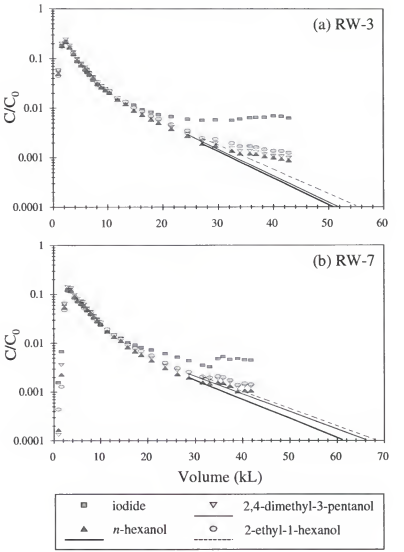

Figure 3-21. Partitioning tracer BTCs and exponential extrapolations at (a) RW-3 and (b) RW-7.

The largest removal occurred at RW-7, while the lowest was 31% at RW-4. Another estimate of the spatial removal effectiveness can be obtained by comparing the initial NAPL volume distribution to the volume of PCE extracted at each RW during cosolvent flushing (Tabel 3-15). This technique determined that 61% of the PCE was removed. Although the final values of 63% and 61% are close, the values for removal effectiveness

at each RW are not comparable, nor do they share common trends. The reason for these differences is likely caused by the change in the flow distribution during the cosolvent flood, which would have changed the swept volume at each well. Thus, the increase in flow rate at RW-6 may have caused this well to extract PCE from regions that were not in its original swept volume determined during the tracer test. Hence, effective removal greater than one was observed at RW-6. Note that the measure of effectivness in Table 3-15 is the same as the final effectiveness as determined from equation 2-4.

Table 3-14. Comparison of pre- and post-flushing NAPL volumes based on tracer tests.

Well ID	$V_{N\text{-}pre}$ (L)	$V_{N\text{-}post}$ (L)	Effectiveness (E)
RW-2	4.9	2.8	0.43
RW-3	18.1	4.1	0.77
RW-4	7.1	4.9	0.31
RW-5	6.4	3.6	0.44
RW-6	11.3	4.6	0.59
RW-7	21.3	5.9	0.72
Total	69.0	25.8	0.63

Table 3-15. Comparison of the pre-flushing NAPL distribution to the volume of PCE removed during the cosolvent flood.

Well ID	$V_{N\text{-}pre}$ (L)	Extracted V_N (L)	Effectiveness (E)
RW-2	4.9	1.0	0.20
RW-3	18.1	10.6	0.59
RW-4	7.1	3.7	0.52
RW-5	6.4	0.02	0.003
RW-6	11.3	12.2	1.08
RW-7	21.3	14.5	0.68
Total	69.0	42.1	0.61

3.4.4.1. Comparison of RW and MLS efficiency

The measure of efficiency as defined in section 2.3.2.1 was applied to the RW and MLS-4 BTCs to produce the plots in Figure 3-22. In both cases, the initial efficiency is artificially high because of the background PCE concentrations in the ground water. Once the cosolvent begins to breakthrough, the denominator (volume of cosolvent) in equation 2-7 increase, reducing the efficiency until enhanced solubilization occurs. This point is shown by the dip in the curves at the 1 to 1.5 days (Figure 3-22). The shapes of the efficiency curves in Figure 3-22 were typical of the RW and MLS locations monitored. The endpoint efficiency value is the location in the curve where the slope becomes zero because PCE and cosolvent are no longer detected in the samples. The endpoint efficiency values for the RWs are listed in Table 3-16. The listed values show that more PCE per cosolvent (0.003 L/L) was removed from RWs 6 and 7 than at the other locations. The overall efficiency for the entire cosolvent flood was 1 L of NAPL removed per 1000 L of cosolvent solution.

Table 3-16. Endpoint efficiency at the RWs.

Well ID	Endpoint Efficiency (ε)
RW-2	0.0008
RW-3	0.002
RW-4	0.001
RW-5	10^{-5}
RW-6	0.003
RW-7	0.003
Total	0.001

At the MLSs, the efficiency curves typically have a peak after the initial dip that gradually decreases as the mass is removed and cosolvent flooding continues. The peak values were typically one order of magnitude greater than the endpoint efficiencies because of the high PCE concentrations observed at the MLS. As shown in Figure 3-22, the endpoint efficiencies at the MLSs are similar to the RW efficiencies.

3.5. Costs Analysis

Although costs minimization was not an objective of the field study, cost data from the study helped identified the major cost components and ideas for reducing the cost of these components.

3.5.1. Actual Costs

The costs of the field study were categorized into three major components: design, construction, and operation (Table 3-17). For the Sages study, design costs were mostly incurred through development of a work plan that included selection of a well pattern and determining specifications for equipment and materials. The construction costs were primarily from installation of the RWs, IWs, MLSs, and fluid handling systems (tanks, piping, pumps, etc.). Costs incurred during operation of the study include the cost of the chemicals (ethanol and tracers), labor, sample analysis, and waste treatment and disposal. The total cost of the project was estimated at $440,000 (Table 3-17). The largest component of the total cost was operation (53%) followed by construction (36%) and then design (10%) (Figure 3-23a).

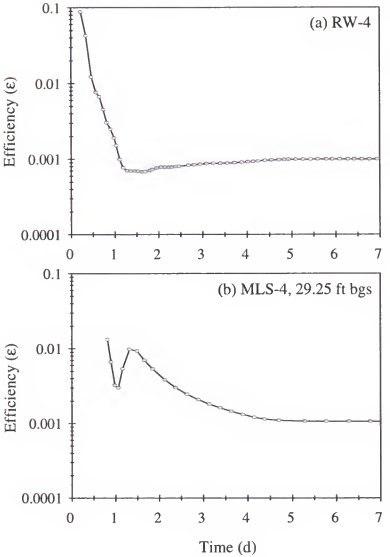

Figure 3-22. Efficiency (ε) as a function of time at (a) RW-4 and (b) the 29.25-ft depth of MLS-4.

A breakdown of the operational costs is presented in Figure 3-23b. The three largest portions of the operational cost were labor (38%), sample analysis (25%) and waste treatment and disposal (24%). The data required to evaluate a technology is typically much larger than the amount of information needed to monitor the operation of a proven remediation technology. Thus, several of the cost components can potentially be reduced.

3.5.2. Cost Optimization

Based on observations and experience gained from the Sages field study, the following design improvements are proposed for reducing the cost of implementing in situ cosolvent flushing for full scale remediation:

- Because the diameter of the IWs and RWs was 4 inches (10 cm), a large volume of soil cuttings was produced that required disposal. By reducing the well diameter to 2 inches (5 cm), the cost of installation decreases because of lower material costs and less soil for disposal as smaller augers could be used. The potential cost reduction for well installation is approximately 20%.
- A trailer-mounted injection and extraction system has been recommended to reduce construction costs by providing a reusable system easy to transport from site to site (Levine-Fricke-Recon, 1998a). The trailer would be fully equipped with pumps, hoses, connections, meters, and other appurtenances for fast setup at a site. Although this system may have a high one-time capital cost, use at several sites would reduce the cost of this component at one site by 20%.
- Reuse of ethanol recycled from the waste stream could reduce the initial amount of ethanol required at a site by 50%. Separation of ethanol from the waste stream could be accomplished by adding a distillation unit to the existing MPPE® system. Thus, after extraction of the PCE by the MPPE system, a distillation unit would concentrate the ethanol leaving a waste stream that should be cheaper to dispose of. A capital cost of $300,000 has been estimated for the distillation unit.

Table 3-17. Costs of Sages site field study.

Item	Cost	Sub-total
DESIGN		
- work plan including health & safety plan		
- modeling, well locations, system specs.		
		$46,000
CONSTRUCTION		
- Well & MLS installation		
- Drilling Subcontractor (well installation, soil coring, LFR oversite)	$29,000*	
- MLS installation (materials & labor) – UF	$20,000	
- Disposal of soil cuttings	$6,400*	
- Sample analysis (water & soil) – Savannah Lab & UF	$15,000	
- Construction Subcontractor (electrical drop, site trailer, tanks, piping, pumps, packed tower, infiltration gallery, trash disposal, etc.)	$69,300*	
- LFR labor	$20,000	
		$159,700
OPERATION		
- Chemicals (ethanol & tracers)	$18,000	
- Waste Treatment & Disposal		
- MPPE rental	$13,200*	
- IWTP (transport & disposal)	$44,000*	
- Labor (LFR and UF)	$90,000	
- Sample analysis		
- UF Laboratory	$46,000	
- Savannah Laboratory	$10,000	
- Field GC	$3,000	
- Misc. (utilities, tent, etc.)	$10,000	
		$234,200
TOTAL		$439,900

* Cost includes 10% markup.

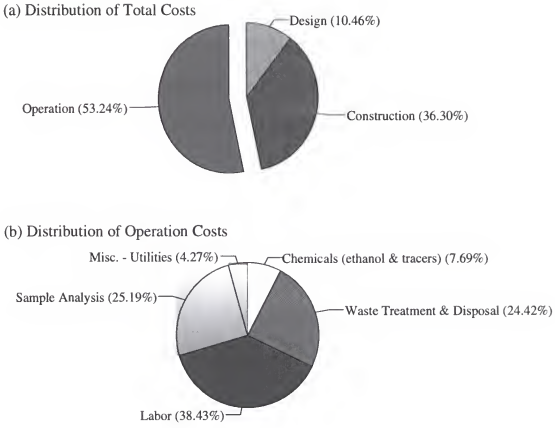

Figure 3-23. Distribution of total and operational costs for the Sages site field study.

- Optimize injection and recovery strategy by improving the well pattern design to allow a 1:1 injection:extraction ratio and still maintain hydraulic containment. This strategy would reduce the volume of wastewater extracted and increase the concentration of ethanol in the waste stream. After removal of PCE with the MPPE® system, the treated solution will have a high ethanol content that may be reinjected or supplemented with fresh ethanol prior to injection. Cost savings would come from a lower initial volume of ethanol required and from a decrease in the amount of waste required for disposal.

Another consequence of this strategy may be a reduction in the extraction efficiency of the MPPE® system due to higher ethanol concentrations. Thus, the waste stream may have to be treated by this system multiple times to reduce PCE to acceptable levels.

- Because this was a research-oriented study, a large number of samples were collected and analyzed at a high cost. The level of sampling could be reduced to the minimal set required to monitor the performance of the technology and meet regulatory requirements. Since the samples are used to produce BTCs that describe the behavior of the system, the minimum number of samples required depends on the processes observed and the hydraulics of the system. This type of information can be gained from a site-specific pilot test.
- The design cost for this study was increased several times near the beginning in order to accommodate changing goals of the study. Thus, knowledge and experience gained from this study could potentially reduce the cost of the design component by 50% ($15,000 to $20,000).

Based on these cost reduction ideas, estimates of cost per ton were generated for the Sages site (Warner, 1998). The volume of media swept at the Sages site was approximately 54 m^3, which is about 110 metric tons. In order to estimate a cost for cosolvent flushing only, the above total cost in Table 3-17 was reduced by $150,000 to account for the tracer test. By implementing the cost reduction ideas listed above, an additional $150,000 reduction in total cost could be achieved. Thus, conservative cost estimates for remediation of different ranges of soil volumes using in situ cosolvent flushing are the following:

- $1,200 to $1,500 per ton for 75 to 125 tons of soil
- $900 to 1,250 per ton for 150 to 200 tons of soil
- $800 to $1,000 per ton for 250 to 350 tons of soil

These cost ranges take into account an economy of scale typically achieved as the volume of treated media increases. For a comparison, the cost of implementing a pump and treat system at the Sages site assuming 40 years of operation would be about $2,200,000 which gives $22,000 per ton for 100 tons of soil. Thus, cosolvent flushing can reduce treatment cost by 95% and treatment time from 40 years to 1 month when compared to pump and treat.

3.6 Summary

A well configuration that placed six recovery wells around three injection wells along with a 2:1 extraction to injection ratio was used to ensure the capture of remedial fluids and tracers delivered to the DNAPL source area. As a result of this flow design, the concentration levels observed at the RWs were much lower than the concentrations measured at the MLSs during the tracer tests and cosolvent flood, indicating considerable dilution occurred at the RWs. Consequently, the volume of extracted ground water containing ethanol, PCE, and tracers was large and required considerable costs and management to treat and dispose.

Soil coring and partitioning and interfacial tracer test indicated that the DNAPL was located in thin, discontinuous layers characterized by NAPL saturations that range from 8 to 35%. Based on the tracer data from the RWs, the volume of NAPL in these

thin layers was approximately 0.4% of the total swept volume. The total predicted NAPL volume within the swept volume of the wells was 69 L.

Using packers in the IWs, delivery of the cosolvent solution (95% ethanol) was focused to regions of the swept zone showing larger initial NAPL saturations. An attempt was also made to adjust the flow rates at the RWs in order to optimize delivery of the cosolvent to the NAPL. Peak PCE concentrations extracted at the RWs (excluding RW-5) ranged from 100 to 1300 mg/L, while observations at the MLSs indicated resident concentrations within the source zone were much larger, ranging from 16,000 mg/L to 45,000 mg/L. Thus, the 2:1 extraction ratio, which draws in ground water from outside the source area, combined with the depth- and flux-averaged concentrations that arrive at the RWs to significantly reduced the levels of tracer, PCE, and ethanol measured at the RWs.

A comparison of the initial NAPL volume to the amount removed during the cosolvent flood and the amount remaining from the post-flushing tracer test shows that approximately 61 to 63% of the PCE was removed. Because the DNAPL was located in thin layers that made up a small portion of the overall flow domain, the measured removal efficiency of 1 L of PCE per 1000 L of cosolvent was low compared to its solubility in the cosolvent (200 L of PCE per 1000 L of cosolvent).

3.7 Recommendation

Evaluation of the field study was primarily conducted with information collected from the recovery wells during the tracer tests and the cosolvent flood. As an example of tracer, PCE, and ethanol behavior at smaller scales within the source zone, the data

collected from MLS-4 was presented. However, data from six other MLSs are available. Although some of the MLS locations showed very little response during the field study, data from locations other than MLS-4 may provide further insight into the processes occurring during the field study. Tracer data may provide a more detailed description of the vertical NAPL distribution. Tracer data at the MLSs may also be compared to ethanol BTCs in order to investigate the effects of fluid property contrast as in chapter 2. However, this comparison must account for the complex injection strategy used to deliver the cosolvent. As stated in the recommendations in chapter 2, modeling the hydrodynamics of cosolvent flushing using UTCHEM should provide information on the effects of flow instability in uncontained systems with a well pattern characteristic of the Sages site.

Further delineation of the DNAPL distribution may also be obtained from analysis of the unique tracer test data not presented in this chapter. The unique tracers were injected after the common set of tracers prior to the cosolvent flood. Since a unique pair of tracers was supplied to each IW, the origin of the fluids extracted at a RW can be determined. Data at the MLSs were also collected during this tracer test. However, many of the unique tracer BTCs are likely to be incomplete because the tracer test ended prior to the breakthrough of the common tracers, which were injected prior to the unique tracers.

Recommendations for future work at the Sages and other sites considering in situ cosolvent flushing are listed here:

- Additional source assessment at the Sages site is recommended to delineate the extent of the remaining DNAPL in the source area and possibly beneath

the flushed zone. Soil core data in Figure 3-20a indicates that a layer of DNAPL exists below the flushed zone at 10.4 m (34 ft) bgs.

- Implement cost reduction strategies outline in section 3.5.2; primarily by optimizing the well pattern to reduce dilution in the RWs which reduces waste and allows for reinjection of the cosolvent without the need for a distillation unit.
- Allow more time between the pre-flushing partitioning tracer test and the cosolvent flood. This extra time should be used to completely evaluate the tracer test data and allow strategies for optimizing the flow system to be developed. Modeling of the tracer test results and various remediation scenarios incorporating data from the tracer test results should be considered.

CHAPTER 4
SYNTHESIS

4.1. Technology Transferability

"Will it work at my site?" This is the most common question asked by hazardous waste site managers and owners when new technologies are introduced and begin to show promise. This question must be answered if a new technology is to be widely used and commercialized. As discussed in chapter 1, several site-specific factors control the performance of a remediation technology; primarily, complexity of the contaminant and heterogeneity of the contaminated medium. Properties of a contaminant that can make it difficult to treat are composition and distribution. For in situ treatment technologies, the ability to contact and treat the contaminant with the remedial fluids is controlled by heterogeneity in the properties of the medium, specifically permeability. Thus, to be able to answer the above question, a new technology must undergo extensive field testing to prove its performance under various site conditions.

The research presented in this dissertation examined the performance of in situ cosolvent flushing at two field sites that presented unique site conditions and challenges. Two important characteristics that differentiate these sites are: (1) DNAPL versus LNAPL, and (2) contained vs. uncontained flow system. The contaminant at Hill was a weathered multi-component LNAPL that coated most of the soil in the flushed region. Although variability in the NAPL saturation was measured, the data and observation of

the soil cores showed that the entire vertical extent of the flow domain was contaminated by NAPL to some degree. In contrast, the Sages site was contaminated with a single-component DNAPL (PCE) that migrated below the water table where it collected at high saturations in thin, discontinuous layers wherever a change in the soil structure prevented downward migration. The NAPL saturations at Hill ranged form 1 to 10%, whereas the Sages site had a much larger range in values from 0 to 35%. An important consequence of the Sages NAPL distribution is the inefficiencies associated with flushing cosolvent through a region where only a small portion in the vertical direction is contaminated. The average maximum efficiency measured at the Hill site MLSs was approximately 0.04 L of NAPL/L cosolvent. In comparison the average maximum efficiency at MLS-4 of the Sages site was 0.02 L of NAPL/L cosolvent. Thus, the more heterogeneous distribution of the NAPL at the Sages site reduced the removal efficiency in comparison to the more uniformly distributed NAPL at Hill.

The compositional complexity of the Hill NAPL makes it more difficult to remove and quantify. As described in chapter 2, selective dissolution of the NAPL by the cosolvent changes the NAPL composition by leaving behind higher molecular weight compounds with very low solubilities. Thus, estimating the NAPL mass removed via BTC integration of a constituent is inaccurate because of the changing mole fraction of the component in the NAPL. Changes in the NAPL composition have also been shown to effect the partition coefficient of the partitioning tracers. Thus, estimation of the post-flushing NAPL content and distribution are less reliable unless a technique is applied to estimate the K_{NW} for treated or washed NAPL. This issue was addressed recently by Lee

et al. (1998) in research that showed a decrease in the partition coefficients of several tracers in a NAPL (from Hill AFB) that was washed with a cosolvent solution.

Another major issue that could hinder the adaptability of this technology is cost. A breakdown of the Sages site costs revealed that the well pattern and flow specification substantially increased the amount of waste to treat and the amount of initial ethanol required. Remediation systems that do not have physical barriers to isolate the source area require hydraulic controls, which can reduce the efficiency and increase the cost of the remediation. Thus, site-specific information is required in order to optimally design a well configuration that keeps costs and waste volumes low.

4.2. Technology Application

"How many MLSs should be installed?" The value of monitoring the behavior of in situ flushing processes using a network of MLSs has been demonstrated several times throughout this work. The most beneficial use of these monitoring points has been in characterizing the distribution of the NAPL and distribution of fluid travel times. In the Hill AFB study, an extensive network of MLSs allowed observation of the link between spatial variability in performance and spatial variability in hydrodynamics and NAPL saturation. However, an extensive MLS network is not likely to be cost effective for full-scale remediation systems. Although material and installation costs for MLSs are small compared to other components, sample collection and analysis costs can make the use of MLSs prohibitive.

The number of MLSs used in a remediation system depends on the level of detail required to monitor and operate the system. In a system where the NAPL and

hydrodynamics are homogeneous, the volume-averaged information obtained from recovery wells is adequate for characterization. For systems that show slightly more heterogeneity, recovery well data may still be adequate for characterization by using a method developed by Jawitz et al. (1998b) that uses higher order moments to describe the fraction of the flow domain with NAPL in the stream tubes. As the flow domain and the NAPL distribution become more heterogeneous, more detailed information is required if flow optimization techniques such as focused flooding are to be used. Thus, a minimal set of MLSs should be located near the RWs in order to obtain volume-averaged information with depth. If more detail is required, a more expansive MLS system, like the one installed at Hill AFB, can be used along with several techniques to interpret the data from the MLSs. The first and simplest level of analysis involves using the "differential retardation" approach described earlier. This technique provides average NAPL saturations within the intervals between MLSs. Two other methods are available that provide more discrete analysis of the NAPL distribution using stochastic modeling techniques on tracer concentration snapshots (Zhang, 1997) and the tracer moments (James et al., 1997). Thus, the number of MLSs included in a design depends on the system heterogeneity and the level of detail required. Currently, flow optimization techniques are limited to focusing the delivery of the remedial fluid to specified depths in the aquifer using packers. Delineation of the NAPL saturation in the vertical direction would be the minimum requirement; thus, a minimal set of MLSs located at the RWs will provide the information needed to optimize characterization and recovery of the NAPL.

REFERENCES

Annable, M.D., Rao, P.S.C., Graham, W.D., Hatfield, K. and Wood, A.L., 1994. Use of partitioning tracers for measuring residual NAPL distribution in a contaminated aquifer: Preliminary results from a field-scale test, 2nd Tracer Workshop, Austin, TX, pp. 77-85.

Annable, M.D., Rao, P.S.C., Hatfield, K.H., Graham, W.D., Wood, A.L. and Enfield, C.G., 1998a. Partitioning tracers for measuring residual NAPL: Field-scale test results. Journal of Environmental Engineering, 124(6): 498-503.

Annable, M.D., Rao, P.S.C., Helms, A.D. and Wood, A.L., 1998b. Hydrodynamic characterization of a NAPL-contaminated remediation test cell using non-reactive tracers. Journal of Hydrologic Engineering, (in press).

Augustijn, D.C.M., 1993. Chemodynamics of complex waste mixtures: Applications to contamination and remediation of soils and aquifer media. Ph.D. Dissertation, University of Florida, Gainesville, FL, 193 pp.

Augustijn, D.C.M., Dai, D., Rao, P.S.C. and Wood, A.L., 1994a. Solvent flushing dynamics in contaminated soils. In: T. Dracos and F. Stauffer (Editors), Transport and Reactive Processes in Aquifers. A. A. Balkema, Rotterdam, The Netherlands, pp. 557-562.

Augustijn, D.C.M., Jessup, R.E., Rao, P.S.C. and Wood, A.L., 1994b. Remediation of Contaminated Soils by Solvent Flushing. Journal of Environmental Engineering, 120(1): 42-57.

Augustijn, D.C.M., Lee, L.S., Jessup, R.E., Rao, P.S.C., Annable, M.D. and Wood, A.L., 1997. Remediation of Soils and Aquifers Contaminated with Hydrophobic Organic Chemicals: Theoretical Basis for the Use of Cosolvents. In: C.H. Ward, J.A. Cherry and M.R. Scalf (Editors), Subsurface Restoration Handbook. Ann Arbor Press, Inc., Chelsea, Michigan, pp. 223-242.

Augustijn, D.C.M. and Rao, P.S.C., 1995. Enhanced Removal of Organic Contaminants by Solvent Flushing. In: D.W. Tedder and F.G. Pohland (Editors), Emerging Technologies in Hazardous Waste Management V. American Chemical Society, Washington, D.C., pp. 224-236.

Boyd, G.R. and Farley, K.J., 1992. NAPL removal from groundwater by alcohol flooding: Laboratory studies and applications. In: E.J. Calabrese and P.T. Kostecki (Editors), Hydrocarbon Contaminated Soils and Groundwater. Lewis Publishers, Boca Raton, FL.

Broholm, K. and Cherry, J.A., 1994. Enhanced dissolution of heterogeneously distibuted solvents residuals by methanol flushing: A field experiment. In: T. Dracos and F. Stauffer (Editors), Transport and Reactive Processes in Aquifers. A. A. Balkema, Rotterdam, The Netherlands, pp. 563-568.

Dai, D., 1997. Solubility and partitioning behavior of organic compounds in complex NAPL mixtures. Ph.D. Dissertation, University of Florida, Gainesville, FL, 219 pp.

Farley, K.J., Falta, R.W., Brandes, D., Milazzo, J.T. and Brame, S.E., 1993. Remediation of hydrocarbon contaminated groundwaters by alcohol flooding, Hazardous Waste Management Research Fund, Univ. of South Carolina, SC.

Fu, J.K. and Luthy, R.G., 1986a. Aromatic compound solubility in solvent/water mixtures. Journal of Environmental Engineering, 12(2): 328-345.

Fu, J.K. and Luthy, R.G., 1986b. Effect of organic solvent on sorption of aromatic solutes on to soil. Journal of Environmental Quality, 12(2): 346-366.

Gatlin, C. and Slobod, R.L., 1960. The alcohol slug process for increasing oil recovery. Transactions of AIME, 219: 46-53.

Holm, L.W. and Csaszar, A.K., 1962. Oil recovery by solvents mutually soluble in oil and water. Transactions of AIME, 225: 129.

Hunt, J.R., Sitar, N. and Udell, K.S., 1988. Nonaqueous phase liquid transport and cleanup: 1. Analysis of mechanisms. Water Resources Research, 24(8): 1247-1258.

Imhoff, P.T., Gleyzer, S.N., McBride, J.F., Vancho, L.A., Okuda, I. and Miller, C.T., 1995. Cosolvent-Enhanced Remediation of Residual Dense Nonaqueous Phase Liquids: Experimental Investigation. Environmental Science & Technology, 29(8): 1966-1976.

James, A.I., Graham, W.D., Hatfield, K., Rao, P.S.C. and Annable, M.D., 1997. Optimal estimation of residual non-aqueous phase liquid saturations using partitioning tracer concentration data. Water Resources Research, 33(12): 2621-2636.

Jawitz, J.W., Annable, M.D. and Rao, P.S.C., 1998a. Miscible fluid displacement stability in unconfined porous media: Two dimensional flow experiments and simulations. Journal of Contaminant Hydrology, 31: 211-230.

Jawitz, J.W., Annable, M.D. and Rao, P.S.C., 1998b. Characterizing the spatial distribution of non-aqueous phase contaminants using partitioning tracers and the method of moments. International Conference and Special Seminars on Groundwater Quality: Remediation and Protection, IAHS, Tubingen, Germany, 422-425.

Jin, M., 1995. A study of nonaqueous phase liquid characterization and surfactant remediation. Ph.D. Dissertation, The University of Texas at Austin, Austin, TX, 340 pp.

Jin, M., Delshad, M., Dwarakanath, V., McKinney, D.C., Pope, G.A., Sepehrnoori, K., Tilburg, C. and Jackson, R.E., 1995. Partitioning tracer test for detection, estimation, and remediation performance assessment of subsurface nonaqueous phase liquids. Water Resources Research, 31(5): 1201-1211.

Lee, C.M., Meyers, S.L., Charles L. Wright, J., Coates, J.T., Haskell, P.A. and Ronald W. Falta, J., 1998. NAPL compositional changes influence partitioning coefficients. Environmental Science and Technology, 32(22): 3574-3578.

Levine-Fricke-Recon (LFR), 1998a. Pilot test work plan former Sages dry cleaner, Levine-Fricke-Recon Inc., Tallahassee, FL.

Levine-Fricke-Recon (LFR), 1998b. Cosolvent flushing pilot study former Sages dry cleaner, Levine-Fricke-Recon Inc., Tallahassee, FL.

Luthy, R.G., Dzombak, D.A., Peters, C.A., Ali, M.A. and Roy, S.B., 1992. Solvent extraction for remediation of manufactured gas plant sites. EPRI/TR-101845, Electric Power Research Institute, Palo Alto, CA.

Luthy, R.G., Ramaswami, A., Ghoshal, S., and Merkel, W., 1993. Interfacial films in coal tar nonaqueous-phase liquid-water systems. Environmental Science and Technology, 27(13): 2914-2918.

Montgomery, J.M., Inc., 1992. Remedial Investigation Report for Operable Unit 1 for Hill Air Force Base, Utah, JMM Consulting Engineers, Inc., Salt Lake City, Utah.

Montgomery, J.M., Inc., 1993. Remedial Investigation Report Addendum for Operable Unit 1 for Hill Air Force Base, Utah, JMM Consulting Engineers, Inc., Salt Lake City, Utah.

National Research Council, 1994. Alternatives for Groundwater Cleanup. National Academy Press, Washington, D.C.

National Research Council, 1997. Innovations in Ground Water and Soil Cleanup: From Concept to Commercialization. National Academy Press, Washington, D. C.

Nelson, N.T. and Brusseau, M.L., 1996. Field study of the partitioning tracer method for detection of dense nonaqueous phase liquid in a trichloroethene-contaminated aquifer. Environmental Science & Technology, 30(9): 2859-2863.

Nkedi-Kizza, P., Rao, P.S.C. and Hornsby, A.G., 1985. Influence of organic cosolvents on sorption of hydrophobic organic chemicals by soils. Environmental Science & Technology, 19(10): 975-979.

Nkedi-Kizza, P., Rao, P.S.C. and Hornsby, A.G., 1987. Influence of organic cosolvents on leaching of hydrophobic organic chemicals through soils. Environmental Science & Technology, 21(11): 1107-1111.

Pennell, K.D., Pope, G.A. and Abriola, L.M., 1996. Influence of viscous and buoyancy forces on the mobilization of residual tetrachloroethylene during surfactant flushing. Environmental Science & Technology, 30(4): 1328-1335.

Peters, C.A. and Luthy, R.G., 1993. Coal tar dissolution in water-miscible solvents: Experimental evaluation. Environmental Science & Technology, 27(13): 2831-2843.

Peters, C.A. and Luthy, R.G., 1994. Semi-empirical thermodynamic modeling of liquid phase equilibria: Coal tar dissolution in water-miscible solvents. Environmental Science & Technology, 28(7): 1331-1340.

Pinal, R., Lee, L.S. and Rao, P.S.C., 1991. Prediction of the Solubility of Hydrophobic Compounds in Nonideal Solvent Mixtures. Chemosphere, 22(9-10): 939-951.

Pope, G.A., Jin, M., Dwarakanath, V., Rouse, B.A. and Sepehrnoori, K., 1994a. Partitioning tracer tests to characterize organic contaminants, 2nd Tracer Workshop. University of Texas, Austin, Austin, TX, pp. 77-85.

Pope, G.A., Sepehrnoori, K., Rouse, B.A., Dwarakanath, V., Jin, M., Abubakar, A. and Lim, M.H., 1994. Final Report: NAPL partitioning interwell tracer test in OU1 test cell at Hill Air Force Base, Utah, University of Texas, Austin, Austin, TX.

Powers, S.E., Abriola, L.M. and Walter J. Weber, J., 1994. An experiment investigation of nonaqueous phase liquid dissolution in saturated subsurface systems: transient mass transfer rates. Water Resources Research, 30(2): 321-332.

Rao, P.S.C., 1999. Commercialization of innovative site remediation technologies: Barriers, challanges and opportunities, 1999 Contaminated Site Remediation

Conference: Challenges Pose by Urban & Industrial Contaminants, Freemantle, Western Australia, (in press).

Rao, P.S.C., Annable, M.D., Sillan, R.K., Dai, D., Hatfield, K.H., Graham, W.D., Wood, A.L. and Enfield, C.G., 1997. Field-scale evaluation of in-situ cosolvent flushing for enhanced aquifer remediation. Water Resources Research, 33(12): 2673-2686.

Rao, P.S.C., Hornsby, A.G., Kilcrease, D.P. and Nkedi-Kizza, P., 1985. Sorption and transport of hydrophobic organic chemicals in aqueous and mixed solvent systems: Model development and preliminary evaluation. Journal of Environmental Quality, 14(3): 376-383.

Rao, P.S.C., Lee, L.S. and Wood, A.L., 1991. Solubility, sorption, and transport of hydrophobic organic chemicals in complex mixture. EPA/600/M-91/009, U.S. EPA, Ada, OK.

Rixey, W.G., Johnson, P.C., Deely, G.M., Byers, D.L. and Dortch, I.J., 1992. Mechanisms of removal of residual hydrocarbons from soils by water, solvent, and surfactant flushing. In: E.J. Calabrese and P.T. Kostecki (Editors), Hydrocarbon Contaminated Soils and Groundwater. Lewis Publishers, Boca Raton, FL, pp. Ch. 28.

Roy, S.B., Dzombak, D.A. and Ali, M.A., 1995. Assessment of in situ solvent extraction for remediation of coal tar sites: Column studies. Water Environment Research, 67(1): 4-15.

Sillan, R.K., Annable, M.D., Rao, P.S.C., Dai, D., Hatfield, K., Graham, W.D., Wood, A.L. and Enfield, C.G., 1998. Evaluation of in situ cosolvent flushing dynamics using a network of spatially distributed multilevel samplers. Water Resources Research, 34(9): 2191-2202.

Starr, R.C., Cherry, J.A. and Vales, E.S., 1992. A New Steel Sheet Piling with Sealed Joints for Groundwater Pollution Control, 45th Canadian Geotechnical Conference, Toronto, Ontario.

Starr, R.C., Cherry, J.A. and Vales, E.S., 1993. Sealable Joint Sheet Pile Cutoff Walls for Preventing and Remediating Groundwater Contamination, Technology Transfer Conference, Ontario Ministry of the Environment, Toronto, Ontario.

Taber, J.J., Kamath, I.S.K. and Reed, R.L., 1961. Mechanism of alcohol displacement of oil from porous media. Society of Petroleum Engineers Journal(September): 195-212.

U.S. Environmental Protection Agency (EPA), 1990. Solvent extraction treatment. EPA/540/2-90/021, Office of Emergency Response, Washington, D.C.

U.S. Environmental Protection Agency (EPA), 1991. Remediation of contaminated sedimants. EPA/625/6-91/028, Office of Research and Development, Washington, D.C.

Wood, A.L., 1995. Influence of cosolvents on the transport of hydrophobic organic chemicals in soils under isocratic and gradient conditions. Ph.D. Dissertation, University of Oklahoma, Norman, OK, 143 pp.

Yalkowsky, S.H. and Roseman, T., 1981. Solubilization of drugs by cosolvents. In: S.H. Yalkowsky (Editor), Techniques for Solubilization of Drugs. Marcel Dekker, Inc., New York, NY, pp. 91-134.

Zhang, Y., 1997. Spatial characterization of a hydrogeochemically heterogeneous aquifer using a three-dimensional distributed parameter extended kalman filter. Ph.D. Dissertation, University of Florida, Gainesville, FL, 219 pp.

BIOGRAPHICAL SKETCH

Randall Kari Sillan was born on April 9, 1968, in West Palm Beach, Florida. He graduated from Forest Hill High School, West Palm Beach, Florida, in 1986.

He enrolled at the University of Florida, Gainesville, Florida, in 1987, and received a Bachelor of Science degree in Mechanical Engineering in 1991.

After marrying Ms. Gloria B. Piedra in July 1992, he enrolled in the Graduate School of the University of Florida in the Department of Environmental Engineering Sciences. He received a Master of Engineering degree in 1994. His thesis topic was analysis of cone penetrometer tests in municipal solid waste landfills.

He continued his education at the University of Florida in the Department of Soil and Water Science in the College of Agriculture. He was a United States Department of Agriculture National Needs Pre-Doctoral Fellow from August 1994 through August 1997, and a Graduate Research Assistant from September 1997 through December 1998.

In December 1998, he began employment with LFR Levine-Fricke, Inc. as a Senior Project Engineer.

I certify that I have read this study and that in my opinion it conforms to acceptable standards of scholarly presentation and is fully adequate, in scope and quality, as a dissertation for the degree of Doctor of Philosophy.

P. Suresh C. Rao, Chair
Graduate Research Professor of
Soil and Water Science

I certify that I have read this study and that in my opinion it conforms to acceptable standards of scholarly presentation and is fully adequate, in scope and quality, as a dissertation for the degree of Doctor of Philosophy.

Michael D. Annable, Cochair
Associate Professor of Environmental
Engineering Sciences

I certify that I have read this study and that in my opinion it conforms to acceptable standards of scholarly presentation and is fully adequate, in scope and quality, as a dissertation for the degree of Doctor of Philosophy.

R. Dean Rhue
Professor of Soil and Water Science

I certify that I have read this study and that in my opinion it conforms to acceptable standards of scholarly presentation and is fully adequate, in scope and quality, as a dissertation for the degree of Doctor of Philosophy.

Wendy D. Graham
Associate Professor of Agricultural and
Biological Engineering

I certify that I have read this study and that in my opinion it conforms to acceptable standards of scholarly presentation and is fully adequate, in scope and quality, as a dissertation for the degree of Doctor of Philosophy.

Kirk Hatfield
Associate Professor of
Civil Engineering

This dissertation was submitted to the Graduate Faculty of the College of Agriculture and to the Graduate School and was accepted as partial fulfillment of the requirements for the degree of Doctor of Philosophy.

May 1999

Dean, College of Agriculture

Dean, Graduate School